Formulation of a Structural Model for Flutter Analysis of Low Aspect Ratio Composite Aircraft Wings

by

Timothy J. Seitz

Dissertation submitted to the Faculty of the

VIRGINIA POLYTECHNIC INSTITUTE AND STATE UNIVERSITY

in partial fulfillment of the requirements for the degree of

Doctor of Philosophy

in

Engineering Mechanics

APPROVED:

L. Meirovitch
Leonard Meirovitch

Scott L. Hendricks
Scott L. Hendricks

Liviu Librescu
Liviu Librescu

William T. Baumann
William T. Baumann

Edmund G. Henneke
Edmund G. Henneke

September 1992

Blacksburg, Virginia

FORMULATION OF A STRUCTURAL MODEL FOR FLUTTER ANALYSIS OF LOW ASPECT RATIO COMPOSITE AIRCRAFT WINGS

by

Timothy J. Seitz

Committee Chairman: L. Meirovitch

Engineering Mechanics

(ABSTRACT)

The research contributes toward a fully integrated multidisciplinary wing design synthesis by development of an appropriate structural model. The goal is to bridge the gap between highly idealized structural beam / aerodynamic strip models and the very detailed finite element and computational fluid dynamics, FEM/CFD, techniques. The former provides insufficient accuracy for flutter analysis of modern low aspect ratio composite wings. The latter is too computationally intensive for use in the inner loop of a simultaneous multidisciplinary optimization problem. The derived model provides a useful preliminary design tool as well.

ACKNOWLEDGMENTS

The author particularly wishes to acknowledge the leadership and guidance of his advisor, Dr. Leonard Meirovitch. His vision and professionalism have contributed much to this work and to the author's career. Thanks are due also to the members of the committee. Their comments and enthusiasm were essential in the day to day effort. Special thanks go to Dr. Valery Vasiliev of the Moscow Institute of Aviation Technology for inspiring my interest in composite structures. Many a blind alley were averted thanks to the discussions with co-workers with whom the author has had the privilege of sharing an office these years. Special thanks must go, of course, to the author's wife, Mary and son Daniel without whose steadfast support the opportunity to thank the others would never have arisen.

TABLE OF CONTENTS

LIST OF FIGURES

LIST OF TABLES

NOMENCLATURE

$w = w(x, y, t)$ Vertical displacement

$\psi_x = \psi_x(x, y, t)$ Shear deflection (rotation) in the x direction

$\psi_y = \psi_y(x, y, t)$ Shear deflection (rotation) in the y direction

$\phi_{i,x} = \phi_{i,x}(x, y)$ The x derivative of the ith approximating function

$X_k = X_k(x, y)$ The kth chordwise part of a family of ϕ_i

$Y_\ell = Y_\ell(y)$ The ℓth spanwise part of a family of ϕ_i

M_c The fuselage mass

I_c The fuselage pitch inertia about the fuselage mass center

x_c The location of the fuselage center of mass

R The root chord length

S The wing semispan

η_L, η_T The sweep back angle of the leading and trailing edges

$t_j = t_j(x, y)$ The height of the top of the jth layer from the plane of symmetry

x, y, z The global coordinate system with origin at the leading edge root. the y axis is out the span and x is aftward

$\epsilon_x, \epsilon_y, \epsilon_z$
$\gamma_{yz}, \gamma_{xz}, \gamma_{xy}$ Engineering strains in the global system

σ_x, σ_y
$\tau_{yz}, \tau_{xz}, \tau_{xy}$ Stresses in the global system

$1, 2$ The principle material axes of the jth layer

ϵ_1, ϵ_2
$\gamma_{23}, \gamma_{13}, \gamma_{12}$ Tensoral strains in the material system

σ_1, σ_2
$\tau_{23}, \tau_{13}\tau_{12}$ Tensoral stresses in the material system

θ_j The angle from the x axis to the material (1) axis for the jth layer

$\delta\overline{W}_{NC}$ The non-conservative virtual work

$(\ )_n, (\ )_s$ Normal and tangential quantities

$Q^j_{k\ell}$ The reduced stiffnesses in the material coordinate system for the jth layer

E^j_1, E^j_2 Young's moduli of elasticity for the jth layer

ν^j_{12}, ν^j_{21} Poisson's ratios for the jth layer

G_{23}, G_{13}, G_{12} Shear moduli for the jth layer

$[T_j]$ Transformation matrix from material to laminate axes for the jth layer

$\{\ \}^j, [\ ]^j$ Referencing the jth layer

$\hat{V}_j$ The strain energy density for layer j

V The total laminate strain energy

$\overline{Q}^j_{k\ell}$ The reduced stiffnesses in the laminate coordinate system for the jth layer

$A_{ab} = A_{ab}(x,y)$ The total laminate extensional stiffness coefficients

$D_{ab} = D_{ab}(x,y)$ The total laminate bending stiffness coefficients

T_w Total kinetic energy associated with the distributed mass of the structure

T_f Fuselage kinetic energy

$m = m(x,y)$ The distributed mass of the structure

$TE = TE(y)$
$LE = LE(y)$ The trailing and leading edges defined as linear functions of y

λ The complex eigenvalue

α The real part of λ

ω omega, the imaginary part of λ and the natural frequency

$(\ )^n$ an n term approximation

$(K_{ab})_{ij}$ The ith row and jth column of the ab sub-matrix of the stiffness matrix, K

$(H_{ab})_{ij}$ The ith row and jth column of the ab sub-matrix of the damping matrix, H

$M_{ab})_{ij}$ The ith row and jth column of the ab sub-matrix of the mass matrix, M

$\{\overline{a}\}$ the complex eigenvector

$\{\overline{a}\}^*$ The augmented eigenvector

K^*, M^* The augmented K and M matrices

q Dynamic pressure

M The Mach number

$t_N = t_N(x,y)$ The wing half thickness

γ Ratio of specific heats

U The free stream airspeed

Ω The dimensionless frequency parameter

λ_a The dimensionless dynamic pressure parameter

A Total wing area

ρ_{air} The air density

CHAPTER I

INTRODUCTION

1.1 Preliminary Remarks

Many good ideas in aerodynamics have fallen on the rocks of structural practicality. In view of this, it is becoming increasingly apparent that the marriage of these two disciplines is essential to the development of modern aircraft (refs. 1-5). Such development calls for analytical models capable of representing low aspect ratio wings and/or forward swept wings (FSW), as well as conventional high aspect ratio straight or swept back wings. The goal of the present research is to develop a suitable structural model consistent with the objectives of multidisciplinary optimization.

1.2 Literature Survey and Modeling Decisions

The problem of wing divergence has long prevented the practical implementation of the FSW concept. Recently, and particularly in the past decade, interesting structural solutions based on the anisotropy of exotic new composite materials have been presented (refs. 6-13). Active control has been proposed for the suppression of divergence and flutter instabilities (refs. 14-26) and a growing number of experimental results are appearing in the literature (refs. 27-30). The trend is toward an integrated optimization problem combining structures, aerodynamics and controls. Some investigators are beginning to define and address this problem (refs. 31-35).

Around 1980, a number of investigators came to the conclusion that the phenomenon of FSW divergence was better modeled as body freedom flutter than clamped wing divergence (refs. 36, 37), although this idea has its origins as early as 1929, (refs. 38-41). Body-freedom flutter is the unstable coupling of a flexible airplane mode and a rigid-body mode. A common such case, and the one receiving

attention here, is the coupling of flexible wing bending and rigid-body pitch.

The body-freedom flutter model is more realistic and predicts a lower speed for onset of instability. Additionally, the evidence is that composite tailoring, i.e., the practice of improving laminate performance by adjusting orthotropicity angles, predicts large increases in divergence speed while less impressive improvements in the body-freedom flutter speed are realized (ref. 42). An important point is that an equivalent increase in flutter dynamic pressure cannot be expected to accompany an increase in divergence dynamic pressure obtained by laminate rotation (ref. 43). This result provides a strong motivation for considering the benefits of combined aeroelastic tailoring and active control, particularly in the context of optimal design.

There is growing evidence that neither active control nor passive structural tailoring alone is able to provide the most efficient wing. Some of the claimed benefits of composite tailoring, used to alleviate divergence in swept forward wings, for example, are seen to be due to an idealized description of the divergence phenomenon. The application of both structural tailoring and active control is required to realize remarkable improvements in real wings.

In addition to coping with the FSW configuration, the model must also accommodate low aspect ratio wings of any sweep. A wide array of beam models for high aspect ratio wings are already available, but these not very suitable for modern delta and low aspect ratio trapezoidal wings. While the methodology developed here is equally applicable to wings of any planform, the emphasis is on low aspect ratio wings, for which suitable models are in short supply.

Weisshaar (ref. 42) uses a three-degree-of-freedom model to study the effect of including body freedoms into a FSW aeroelastic analysis. The degrees of freedom consist of fuselage pitch, plunge and a single wing bending mode. This three-degree-of-freedom model is not really adequate for studying laminated composite

wing problems, with the attendant coupling between bending and torsion. Indeed, a more sophisticated multi-mode wing model is required. Because directional stiffness, as well as low aspect ratio, must be accommodated, the elastic axis model must be replaced by a two-dimensional representation capable of accommodating fiber directional information. Some development in this direction is evident in the literature (refs. 44-47). In particular, Giles (ref. 46) provides a model that is largely suitable for the problem at hand. Using a single high-order power series to approximate displacements, Giles showed that good approximations of stresses can be obtained with analytically derived stiffness and mass terms. While this choice of functions has many advantages, they do suffer from numerical divergence, allowing terms no higher than x^4y^7. The inability to improve accuracy by adding more terms must be considered an important disadvantage. Giles also found that, while static results were reasonably well predicted, these approximate solutions did not represent the vibrational behavior of the wing very well (ref 47). This is an important drawback in the case at hand, which is concerned primarily with vibration related phenomenon.

From the preceding discussion, it is clear that an accurate representation of the important FSW characteristic of divergence must include the fuselage freedoms of pitch and plunge. The degrees of freedom associated with fuselage pitch and plunge introduce the fuselage mass and pitch inertia as discrete terms in the formulation. Chordwise flexibility and its influence on aerodynamics is also important for low aspect ratio composite wings (ref. 48).

In this study, we use a plate model to represent the wing. The model consists of an anisotropic lay-up with the different layers permitting different orthotropicity angles. The resulting laminate of generally orthotropic layers at differing layer angles is analytically equivalent to a fully anisotropic material, so that no generality is lost. The question of wing camber must be addressed also. Giles found that camber had

little influence on displacements from pressure loading, suggesting that camber is not important for aeroelastic considerations (ref. 47). Hence, the plate will be assumed to be flat, i.e., camber will not be taken into account and the lay-up will be symmetric above and below the mid-plane.

While complete freedom of choice in the lay-up may seem desirable, the more complicated strain energy expression can increase computational time substantially. Giles (refs. 46 and 47), for example, concluded that an "improved" model including nonsymmetric lay-up and airfoil camber is very computationally intensive. Hence, a compromise must be reached between modeling sophistication and reasonable computation time. Bowlus, Palazotto and Whitney (ref. 49) found that shear deformability is an important factor in the vibration of composite plates and its exclusion results in frequency estimates significantly higher than the actual ones. They also concluded that rotatory inertia has limited effect, except for very thick plates. These conclusions are also supported by the earlier work of Mindlin (ref. 51). In the text by Librescu (ref. 72) it is seen that when rotatory inertia is included, the eigenvalues appear as three sets. The two higher sets are influenced by rotatory inertia, indeed, do not appear without it. The lower set is not influenced by rotatory inertia and these are the eigenvalues of interest in this investigation. In view of this, this study includes shear flexibility but ignores rotatory inertia.

The model under consideration is a trapezoidal plate with root and tip chords parallel to the flow. There are 2k symmetrically stacked, variable thickness, generally orthotropic, laminae in the laminate (Figs. 1.1 & 1.2). The shear deformable plate assumption of Mindlin (refs. 50, 51) was used. A shear correction factor of 1.0 is used for the linear shear distribution assumption. The wing is attached to a rigid fuselage capable of pitch and plunge. This is the simplest formulation that retains the essential physical characteristics of low aspect ratio composite wings with forward or aft sweep.

It is still quite an involved formulation, as it includes three displacement variables and natural boundary conditions complicated by the sweep angles. The objective is to produce a reasonably accurate solution with as few terms as possible. To this end, the series solution uses admisible functions in the form of quasi-comparison functions to speed convergence, which is guaranteed (ref. 52). Quasi-comparison functions are defined as finite linear combinations of admissible functions capable of satisfying the natural boundary conditions as well. The formulation used in this study goes beyond any reported to date (refs. 53-55).

1.3 Outline

The model developed is applied to forward and aft swept configurations in a parametric study of the free vibration characteristics. Particular attention is given to the tailored composite forward swept wing configuration. To demonstrate the usefulness of the model and the effect of ply orientation on flutter boundaries, supersonic aerodynamic loads are added to the model. Studies are made to determine the effect on flutter speeds of various geometrical, structural and control parameters. Throughout, consideration is given to the future use of this model as part of a multidisciplinary optimization problem.

Chapter II begins with the development of the strain-displacement relations based on a Mindlin model with linear shear distribution over the thickness. Next the constitutive relation for the jth generally orthotropic layer was used to develop a strain energy function for the entire laminate.

In Chapter III, the governing partial differential equations of motion are derived by means of the extended Hamilton principle. The kinetic energy consists of two parts, one associated with a rigid fuselage and the other associated with the wing distributed mass. The nonconservative virtual work arises from the aerodynamic forces. Piston theory aerodynamics is seen to be highly appropriate for use with this

wing model. The complete boundary value problem, consisting of the differential equations and boundary conditions, is derived from this variational principle.

In Chapter IV, the eigenvalue problem is derived directly from the variational principle. This formulation has the advantage over conventional formulations of the eigenvalue problem in that the natural boundary conditions are included automatically, thus permitting the use of admissible functions instead of comparison functions. More importantly, it permits the use of quasi-comparison functions. Such functions were shown to lead to rapid numerial convergence in the past and demonstrate the same characteristic in this study.

In Chapter V, parametric studies are presented. Numerical results were obtained by means of a computer program developed based on the theory presented in this dissertation. The computer program was used to investigate the effect on flutter speed of the variation of wing sweep, material distribution and other relevant parameters.

Finally, Chapter VI contains a discussion and conclusions of the research carried out, as well as ideas for further work.

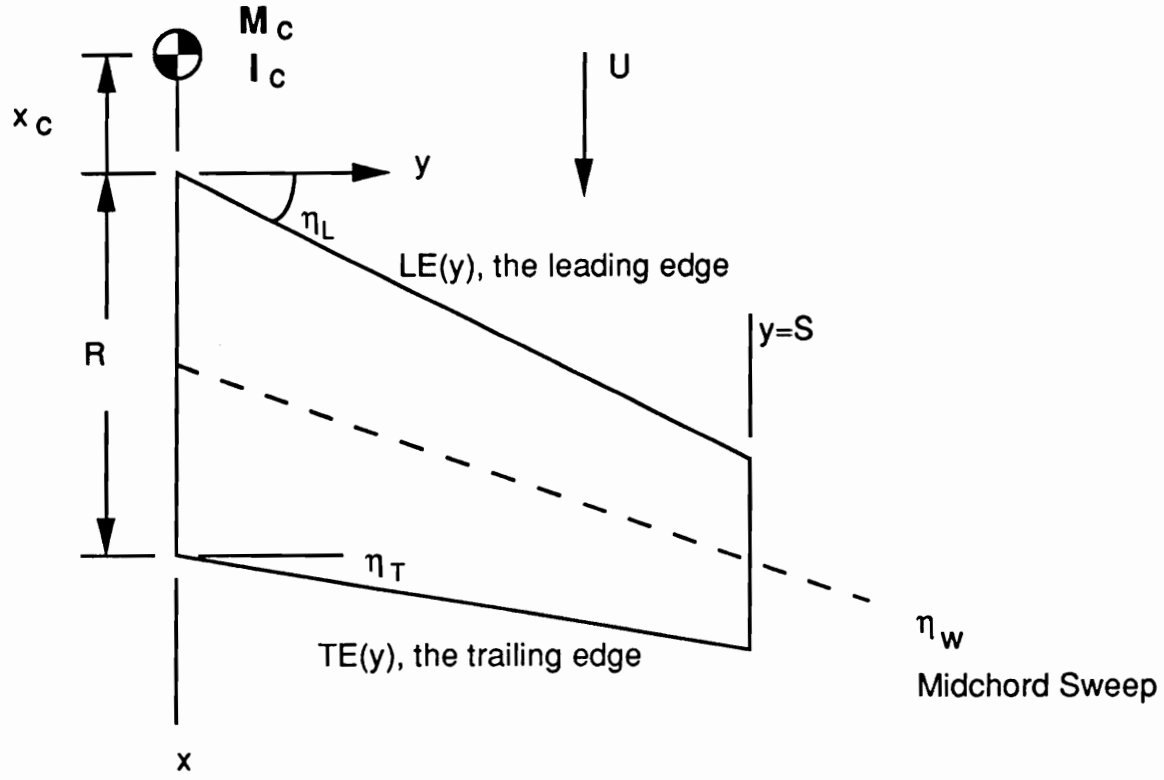

FIGURE 1.1 - Planform Nomenclature

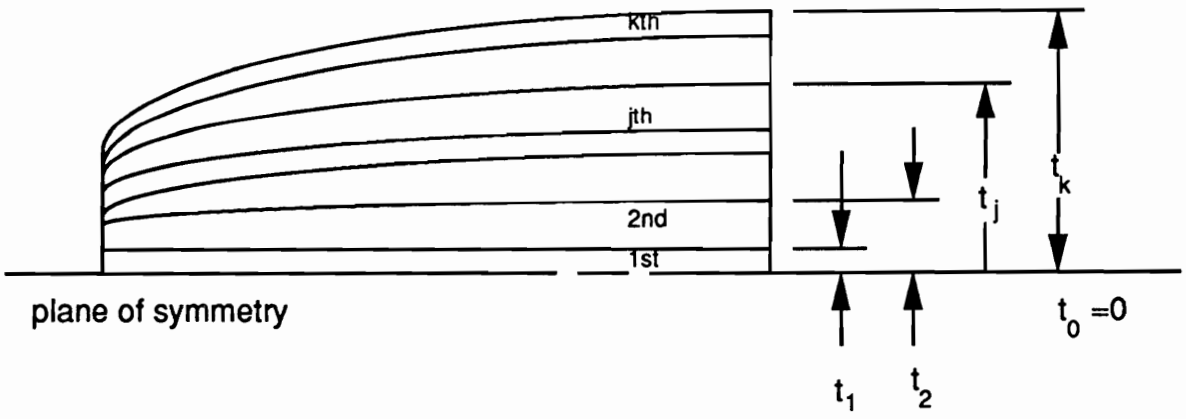

FIGURE 1.2 - Laminate Nomenclature

CHAPTER II

DEVELOPMENT OF THE STRAIN ENERGY FUNCTION

2.1 Strain-Displacement Relations

The mathematical model consists of a trapezoidal, anisotropic plate of variable thickness and capable of shear deformations. By considering the case of generally orthotropic layers, in the sense that the principal material directions are not aligned with the body axes, a result indistinguishable from an anisotropic lay-up is achieved. The material remains inherently orthotropic, however, with all the attendant advantages of practical realization in manufacturing, (ref. 56).

A fundamental objective is to avoid unnecessary complications of the structural model, which is achieved by assuming a symmetric lay-up of generally orthotropic layers. In essence, a Mindlin plate is considered that differs from the classical Kirchoff plate theory in that the assumption of line segments remaining perpendicular to the middle plane is dropped. Shear deformation is assumed to be a function of z, in this case linear for a linear shear deformation assumption. The admission of shear deformations into the problem necessitates the introduction of two new displacement variables, ψ_x and ψ_y, which represent the angular rotations of the perpendicular line segments in the x and y directions, respectively. The definition of the assumed displacement field follows from these and other plate assumptions. Let u_0, v_0 and w_0 be the midplane deflections in the x, y and z directions. Then, the displacement of a typical point in the domain of the plate is (ref. 57)

$$u = u_0 + z\psi_x, \qquad \psi_x = \psi_x(x, y) \tag{2.1a}$$

$$v = v_0 + z\psi_y, \qquad \psi_y = \psi_y(x, y) \tag{2.1b}$$

$$w = w_0, \qquad w = w(x, y) \tag{2.1c}$$

The lay-up is symmetric and will not be subjected to in-plane loads. In view of this, it is reasonable to assume that u_0 and v_0 are zero. Then, the strain-displacement relations assume the simple form (ref. 58)

$$\epsilon_x = z\psi_{x,x}, \quad \epsilon_y = z\psi_{y,y}, \quad \epsilon_z = 0 \tag{2.2a,b,c}$$

$$\gamma_{yz} = \psi_y + w_{,y}, \quad \gamma_{xz} = \psi_x + w_{,x}, \quad \gamma_{xy} = z\left(\psi_{x,y} + \psi_{y,x}\right) \tag{2.2d,e,f}$$

where the shear strains are recognized as engineering shear strains. Moreover, the symbols "$,x$" and "$,y$" in the subscripts denote derivatives with respect to x and y, respectively.

2.2 Constitutive Relations

Consider the jth generally orthotropic layer with principal axes 1 and 2. The constitutive equations for this layer take the form (ref. 58)

$$\begin{bmatrix} \sigma_1 \\ \sigma_2 \\ \tau_{23} \\ \tau_{13} \\ \tau_{12} \end{bmatrix}^j = [Q]^j \begin{bmatrix} \epsilon_1 \\ \epsilon_2 \\ \gamma_{23} \\ \gamma_{13} \\ \gamma_{12} \end{bmatrix}^j \tag{2.3a}$$

where

$$[Q]^j = \begin{bmatrix} Q^j_{11} & Q^j_{12} & 0 & 0 & 0 \\ Q^j_{12} & Q^j_{22} & 0 & 0 & 0 \\ 0 & 0 & Q^j_{44} & 0 & 0 \\ 0 & 0 & 0 & Q^j_{55} & 0 \\ 0 & 0 & 0 & 0 & Q^j_{66} \end{bmatrix} \tag{2.3b}$$

The elements of $[Q]^j$ are related to material properties of the jth layer by

$$Q^j_{11} = \frac{E^j_1}{1 - \nu^j_{12}\nu^j_{21}}, \quad Q^j_{12} = \frac{\nu^j_{12}E^j_2}{1 - \nu^j_{12}\nu^j_{21}}, \quad Q^j_{22} = \frac{E^j_2}{1 - \nu^j_{12}\nu^j_{21}} \tag{2.4a,b,c}$$

$$Q^j_{44} = G^j_{23}, \quad Q^j_{55} = G^j_{13}, \quad Q^j_{66} = G^j_{12} \tag{2.4d,e,f}$$

where E_i, G_{im} and ν_{im} are Young's moduli, shear moduli and Poisson's ratios, respectively. Next, the constitutive equations for the jth layer are transformed to the plate coordinates x and y. The stress tensor transformation is (ref. 59)

$$\sigma'_{im} = a_{ir}a_{ms}\sigma_{rs} \tag{2.5a}$$

and the linear strain tensor transformation is

$$\ell'_{im} = a_{ir}a_{ms}\ell_{rs} \tag{2.5b}$$

where the transformation tensor is based on the angle θ_j from the plate axis x to the material axis $(1)_j$, and

$$a^j_{im} = \begin{bmatrix} \cos\theta_j & -\sin\theta_j & 0 \\ \sin\theta_j & \cos\theta_j & 0 \\ 0 & 0 & 1 \end{bmatrix} \tag{2.6}$$

where the superscript refers to the jth layer transformation tensor. We recall the difference in definition the of tensoral shearing strain versus the engineering shearing strain, or

$$\gamma_{im} = 2\ell_{im} \qquad for\ i \neq m \tag{2.7a}$$

$$\gamma_{im} = \ell_{im} \qquad for\ i = m \tag{2.7b}$$

In light of eqn. (2.6), an expansion of eqn. (2.4) leads to the stress transformation for the jth layer

$$\begin{bmatrix} \sigma_x \\ \sigma_y \\ \tau_{yz} \\ \tau_{xz} \\ \tau_{xy} \end{bmatrix}^j = \begin{bmatrix} \cos^2\theta_j & \sin^2\theta_j & 0 & 0 & -\sin 2\theta_j \\ \sin^2\theta_j & \cos^2\theta_j & 0 & 0 & \sin 2\theta_j \\ 0 & 0 & \cos\theta_j & \sin\theta_j & 0 \\ 0 & 0 & -\sin\theta_j & \cos\theta_j & 0 \\ \frac{1}{2}\sin 2\theta_j & -\frac{1}{2}\sin 2\theta_j & 0 & 0 & \cos 2\theta_j \end{bmatrix} \begin{bmatrix} \sigma_1 \\ \sigma_2 \\ \tau_{23} \\ \tau_{13} \\ \tau_{12} \end{bmatrix}^j \tag{2.8}$$

Similarly, using eqns. (2.5b), (2.6) and (2.7), we obtain the engineering strain transformation

$$\begin{bmatrix} \epsilon_x \\ \epsilon_y \\ \frac{\gamma_{yz}}{2} \\ \frac{\gamma_{xz}}{2} \\ \frac{\gamma_{xy}}{2} \end{bmatrix}^j = \begin{bmatrix} \cos^2\theta_j & \sin^2\theta_j & 0 & 0 & -\sin 2\theta_j \\ \sin^2\theta_j & \cos^2\theta_j & 0 & 0 & \sin 2\theta_j \\ 0 & 0 & \cos\theta_j & \sin\theta_j & 0 \\ 0 & 0 & -\sin\theta_j & \cos\theta_j & 0 \\ \frac{1}{2}\sin 2\theta_j & -\frac{1}{2}\sin 2\theta_j & 0 & 0 & \cos 2\theta_j \end{bmatrix} \begin{bmatrix} \epsilon_1 \\ \epsilon_2 \\ \frac{\gamma_{23}}{2} \\ \frac{\gamma_{13}}{2} \\ \frac{\gamma_{12}}{2} \end{bmatrix}^j \tag{2.9}$$

Denoting the transformation matrix in eqns. (2.8) and (2.9) by $[T_j]^{-1}$, then

$$[T_j] = \begin{bmatrix} \cos^2\theta_j & \sin^2\theta_j & 0 & 0 & \sin 2\theta_j \\ \sin^2\theta_j & \cos^2\theta_j & 0 & 0 & -\sin 2\theta_j \\ 0 & 0 & \cos\theta_j & -\sin\theta_j & 0 \\ 0 & 0 & \sin\theta_j & \cos\theta_j & 0 \\ -\frac{1}{2}\sin 2\theta_j & \frac{1}{2}\sin 2\theta_j & 0 & 0 & \cos 2\theta_j \end{bmatrix} \tag{2.10}$$

A similar development for only three components of stress and strain is carried out in (ref. 56). Introducing the transformation matrix

$$[R] = \begin{bmatrix} 1 & 0 & 0 & 0 & 0 \\ 0 & 1 & 0 & 0 & 0 \\ 0 & 0 & 2 & 0 & 0 \\ 0 & 0 & 0 & 2 & 0 \\ 0 & 0 & 0 & 0 & 2 \end{bmatrix} \tag{2.11}$$

we can represent the engineering strains in the form

$$\begin{bmatrix} \epsilon_x \\ \epsilon_y \\ \gamma_{yx} \\ \gamma_{xz} \\ \gamma_{xy} \end{bmatrix} = [R] \begin{bmatrix} \epsilon_x \\ \epsilon_y \\ \frac{\gamma_{yz}}{2} \\ \frac{\gamma_{xz}}{2} \\ \frac{\gamma_{xy}}{2} \end{bmatrix}, \quad \begin{bmatrix} \epsilon_1 \\ \epsilon_2 \\ \gamma_{23} \\ \gamma_{13} \\ \gamma_{12} \end{bmatrix} = [R] \begin{bmatrix} \epsilon_1 \\ \epsilon_2 \\ \frac{\gamma_{23}}{2} \\ \frac{\gamma_{13}}{2} \\ \frac{\gamma_{12}}{2} \end{bmatrix} \tag{2.12a, b}$$

Then, combining eqns. (2.3), (2.8), (2.9) and (2.12), we can write the jth layer

constitutive relationship as follows:

$$\begin{bmatrix} \sigma_x \\ \sigma_y \\ \tau_{yz} \\ \tau_{xz} \\ \tau_{xy} \end{bmatrix}^j = [T_j]^{-1}\,[Q_j]\,[R]\,[T_j]\,[R]^{-1} \begin{bmatrix} \epsilon_x \\ \epsilon_y \\ \gamma_{yz} \\ \gamma_{xz} \\ \gamma_{xy} \end{bmatrix}^j \tag{2.13}$$

Conveniently,

$$[R]\,[T_j]\,[R]^{-1} = [T_j]^{-T} \tag{2.14}$$

so that

$$\begin{bmatrix} \sigma_x \\ \sigma_y \\ \tau_{yz} \\ \tau_{xz} \\ \tau_{xy} \end{bmatrix}^j = \left[\overline{Q}_j\right] \begin{bmatrix} \epsilon_x \\ \epsilon_y \\ \gamma_{yz} \\ \gamma_{xz} \\ \gamma_{xy} \end{bmatrix}^j \tag{2.15}$$

where

$$\left[\overline{Q}_j\right] = [T_j]^{-1}\,[Q_j]\,[T_j]^{-T} \tag{2.16}$$

in which $[\,]^{-T}$ denotes the inverse transpose.

2.3 Total Laminate Strain Energy

The total laminate strain energy will be used in Chapter III in conjunction with the variational principle yielding the boundary value problem. The laminate consists of $2k$ symmetrically stacked layers of variable thickness. Each layer height, t_j, is a continuous function of x and y. Figure 1.2 shows the laminate nomenclature. First, we consider the strain energy density for a single layer j and its counterpart below the midplane, or

$$\hat{V}_j = \int_{t_{j-1}}^{t_j} \sum_{i=1}^{5} \sigma_i^j \epsilon_i^j dz \tag{2.17}$$

where $i = x, y, yz, xz, xy$. Summation over all the layers and integrating over the domain of the plate leads to the total strain energy

$$V = \int_0^S \int_{LE}^{TE} \left\{ \sum_{j=1}^{k} \left[\int_{t_{j-1}}^{t_j} \sum_{i=1}^{5} \sigma_i^j \epsilon_i^j dz \right] \right\} dx dy \tag{2.18}$$

Substituting the strain-displacement relations, eqns. (2.2), and the constitutive relations, eqn. (2.15), into eqn. (2.18) and integrating over the layer thicknesses, we obtain the total strain energy expression

$$
\begin{aligned}
V = \int_0^S \int_{LE}^{TE} \sum_{j=1}^{k} \Big\{ & \frac{1}{3}\left(t_j^3 - t_{j-1}^3\right) \Big[\psi_{x,x}^2 \overline{Q}_{11}^j + \psi_{y,y}^2 \overline{Q}_{22}^j + \psi_{x,y}^2 \overline{Q}_{66}^j \\
& + \psi_{y,x}^2 \overline{Q}_{66}^j + \psi_{x,x}\psi_{y,y}\left(\overline{Q}_{12}^j + \overline{Q}_{21}^J\right) + \psi_{x,x}\psi_{x,y}\left(\overline{Q}_{16}^j + \overline{Q}_{61}^j\right) \\
& + \psi_{x,x}\psi_{y,x}\left(\overline{Q}_{16}^j + \overline{Q}_{61}^j\right) + \psi_{y,y}\psi_{x,y}\left(\overline{Q}_{26}^j + \overline{Q}_{62}^j\right) + \psi_{y,y}\psi_{y,x} \\
& \cdot \left(\overline{Q}_{26}^j + \overline{Q}_{62}^j\right) + 2\psi_{x,y}\psi_{y,x}\overline{Q}_{66}^j \Big] + \left(t_j - t_{j-1}\right) \Big[\psi_x^2 \overline{Q}_{55}^j + \psi_y^2 \overline{Q}_{44}^j \\
& + w_{,x}^2 \overline{Q}_{55}^j + w_{,y}^2 \overline{Q}_{44}^j + \psi_x\psi_y\left(\overline{Q}_{45}^j + \overline{Q}_{54}^j\right) + 2\psi_x w_{,x}\overline{Q}_{55}^j + \psi_x w_{,y} \\
& \cdot \left(\overline{Q}_{45}^j + \overline{Q}_{54}^j\right) + \psi_y w_{,x}\left(\overline{Q}_{45}^j + \overline{Q}_{54}^j\right) + 2\psi_y w_{,y}\overline{Q}_{44}^j \\
& + w_{,x}w_{,y}\left(\overline{Q}_{45}^j + \overline{Q}_{45}^j\right) \Big] \Big\}\, dxdy
\end{aligned}
\tag{2.19}
$$

Collecting terms and taking advantage of the symmetry of $\overline{Q}$, eqn. (2.19) can be expressed more compactly as

$$
\begin{aligned}
V = \int_0^S \int_{LE}^{TE} \sum_{j=1}^{k} \Big\{ & \frac{1}{3}\left(t_j^3 - t_{j-1}^3\right) \Big[\psi_{x,x}^2 \overline{Q}_{11}^j + \psi_{y,y}^2 \overline{Q}_{22}^j \\
& + \left(\psi_{x,y} + \psi_{y,x}\right)^2 \overline{Q}_{66}^j + 2\psi_{x,x}\psi_{y,y}\overline{Q}_{12}^j + 2\psi_{x,x}\left(\psi_{x,y} + \psi_{y,x}\right)\overline{Q}_{16}^j \\
& + 2\psi_{y,y}\left(\psi_{x,y} + \psi_{y,x}\right)\overline{Q}_{26}^j \Big] + \left(t_j - t_{j-1}\right) \Big[\left(\psi_x + w_{,x}\right)^2 \overline{Q}_{55}^j \\
& + \left(\psi_y + w_{,y}\right)^2 \overline{Q}_{44}^j + 2\left(\psi_x + w_{,x}\right)\left(\psi_y + w_{,y}\right)\overline{Q}_{45}^j \Big] \Big\}\, dxdy
\end{aligned}
\tag{2.20}
$$

It must be recognized here that $t_j = t_j(x, y)$. The summation can be eliminated from the strain energy expression by considering the total laminate extensional and bending stiffness coefficients A_{ab} and D_{ab} defined as (ref. 56)

$$
A_{ab} = \sum_{j=1}^{k} \left(t_j - t_{j-1}\right)\overline{Q}_{ab}^j, \quad D_{ab} = \frac{1}{3}\sum_{j=1}^{k}\left(t_j^3 - t_{j-1}^3\right)\overline{Q}_{ab}^j \tag{2.21a,b}
$$

and we observe that, because the thickness of the various layers is variable, $A_{ab} = A_{ab}(x, y)$ and $D_{ab} = D_{ab}(x, y)$. Using eqns. (2.21), the total laminate strain energy

can now be expressed in the compact form

$$V = \int_0^S \int_{LE}^{TE} \left\langle \begin{bmatrix} \psi_{x,x} \\ \psi_{x,y} \\ \psi_{x,y} + \psi_{y,x} \end{bmatrix}^T \begin{bmatrix} D_{11} & D_{12} & D_{16} \\ D_{12} & D_{22} & D_{26} \\ D_{16} & D_{26} & D_{66} \end{bmatrix} \begin{bmatrix} \psi_{x,x} \\ \psi_{y,y} \\ \psi_{x,y} + \psi_{y,x} \end{bmatrix} \right.$$
$$\left. + \begin{bmatrix} \psi_y + w_{,y} \\ \psi_x + w_{,x} \end{bmatrix}^T \begin{bmatrix} A_{44} & A_{45} \\ A_{45} & A_{55} \end{bmatrix} \begin{bmatrix} \psi_y + w_{,y} \\ \psi_x + w_{,x} \end{bmatrix} \right\rangle dx dy \tag{2.22}$$

CHAPTER III

DERIVATION OF THE EQUATIONS OF MOTION

3.1 Consideration of the Wing Root Boundary

The mathematical model considered consists of a rigid fuselage free to pitch and plunge attached to a flexible wing. The fuselage plunge and pitch increase the number of degrees of freedom of the flexible wing model by two. The wing root, attached to the rigid fuselage, is constrained to be straight, resulting in the only geometric boundary conditions for this problem.

Aircraft, particularly in the predesign stage, are commonly assumed to have symmetric mass and stiffness distributions with respect to a vertical plane through the centerline of the fuselage. This divides the modes into two classes, symmetric and antisymmetric. Wing stores and uneven fuel loading tend to destroy this symmetry. The effects are not within the confines of this study, so that they will be ignored. The symmetrical structural model for the airplane includes the important body-freedom flutter as well as wing bending-torsion. The antisymmetric counterpart includes such responses as wing rock.

The symmetric case precludes fuselage rolling motion, so that the airplane responds as a rigid body only in pitch and plunge. The choice of a symmetric model along with the decision to have a rigid wing root, dictate certain conditions at the wing root, $y = 0$. The displacement $w(x, 0)$ is a linear function of x, so that $w_{,xx}$ and $w_{,y}$ are zero along $y = 0$. The shear deformation variable ψ_x is constant along $y = 0$, so that the derivative of ψ_x with respect to x is zero. Symmetry requires that ψ_y and $\psi_{x,y}$ be zero along the $y = 0$ boundary. Figure 3.1 illustrates these conditions. Among these, only $w_{,xx} = 0$ and $\psi_{x,x} = 0$ represent the minimum geometric boundary conditions

along the wing root consistent with the system order. They are the only geometric boundary conditions present in this problem. Elastic deformation of the wing root is prevented while rigid-body displacement is allowed. All approximating functions in a discretized approximate solution must satisfy these geometric and symmetry constraints; in fact, this is the manner in which they will be included.

The variations in the kinetic and potential energy expressions and the nonconservative virtual work follow in the next three subsections. This prepares the way for use of the extended Hamilton principle. Hamilton's principle is a formulation of problems of dynamics for holonomic conservative systems whereby all the equations of motion are derived by rendering stationary a scalar integral. A generalization of Hamilton's principle permitting the inclusion of nonconservative forces is known as the extended Hamilton principle.

3.2.1 Variation in the Potential Energy

The strain energy density for the jth plate laminate was derived in section 2.3 and is expressed as eqn. (2.17). The potential energy of the system is entirely due to the plate strain energy, as there are no external conservative forces acting upon the system. The total potential energy is given by eqn. (2.22). Then, the variation in the total potential energy is simply

$$\begin{aligned}\delta V = 2\int_0^S \int_{LE}^{TE} \Bigg\{ &\begin{bmatrix} \delta\psi_y + \delta w_{,y} \\ \delta\psi_x + \delta w_{,x} \end{bmatrix}^T \begin{bmatrix} A_{44} & A_{45} \\ A_{45} & A_{55} \end{bmatrix} \begin{bmatrix} \psi_y + w_{,y} \\ \psi_x + w_{,x} \end{bmatrix} \\ &+ \begin{bmatrix} \delta\psi_{x,x} \\ \delta\psi_{x,y} \\ \delta\psi_{x,y} + \delta\psi_{y,x} \end{bmatrix}^T \begin{bmatrix} D_{11} & D_{12} & D_{16} \\ D_{12} & D_{22} & D_{26} \\ D_{16} & D_{26} & D_{66} \end{bmatrix} \begin{bmatrix} \psi_{x,x} \\ \psi_{y,y} \\ \psi_{x,y} + \psi_{y,x} \end{bmatrix} \Bigg\} dxdy \end{aligned} \tag{3.1}$$

Integrating eqn. (3.1) by parts with respect to x and y, we obtain

$$\delta V = 2\int_0^S \int_{LE}^{TE} \left\{ \begin{bmatrix} \psi_y + w_{,y} \\ \psi_x + w_{,x} \end{bmatrix}^T \begin{bmatrix} A_{44} & A_{45} \\ A_{45} & A_{55} \end{bmatrix} \begin{bmatrix} \delta\psi_y \\ \delta\psi_x \end{bmatrix} \right.$$

$$
\begin{aligned}
&- \delta w \begin{bmatrix} \partial/\partial y \\ \partial/\partial x \end{bmatrix}^T \left[\begin{bmatrix} A_{44} & A_{45} \\ A_{45} & A_{55} \end{bmatrix} \begin{bmatrix} \psi_y + w_{,y} \\ \psi_x + w_{,x} \end{bmatrix} \right] \\
&- \begin{bmatrix} \delta\psi_x \\ \delta\psi_y \end{bmatrix}^T \left[\begin{bmatrix} \partial/\partial x & 0 \\ 0 & \partial/\partial y \\ \partial/\partial y & \partial/\partial x \end{bmatrix}^T \left[\begin{bmatrix} D_{11} & D_{12} & D_{16} \\ D_{12} & D_{22} & D_{26} \\ D_{16} & D_{26} & D_{66} \end{bmatrix} \begin{bmatrix} \psi_{x,x} \\ \psi_{y,y} \\ \psi_{x,y} + \psi_{y,x} \end{bmatrix} \right] \right] \Bigg\} dxdy \\
&+ 2 \int_0^S \Bigg\{ \begin{bmatrix} 0 \\ \delta w \end{bmatrix}^T \left[\begin{bmatrix} A_{44} & A_{45} \\ A_{45} & A_{55} \end{bmatrix} \begin{bmatrix} \psi_y + w_{,y} \\ \psi_x + w_{,x} \end{bmatrix} \right] \\
&+ \begin{bmatrix} \delta\psi_x \\ 0 \\ \delta\psi_y \end{bmatrix}^T \left[\begin{bmatrix} D_{11} & D_{12} & D_{16} \\ D_{12} & D_{22} & D_{26} \\ D_{16} & D_{26} & D_{66} \end{bmatrix} \begin{bmatrix} \psi_{x,x} \\ \psi_{y,y} \\ \psi_{x,y} + \psi_{y,x} \end{bmatrix} \right] \Bigg\} \Bigg|_{LE}^{TE} dy \\
&+ 2 \int_{LE}^{TE} \Bigg\{ \begin{bmatrix} \delta w \\ 0 \end{bmatrix}^T \left[\begin{bmatrix} A_{44} & A_{45} \\ A_{45} & A_{55} \end{bmatrix} \begin{bmatrix} \psi_y + w_{,y} \\ \psi_x + w_{,x} \end{bmatrix} \right] \\
&+ \begin{bmatrix} 0 \\ \delta\psi_y \\ \delta\psi_x \end{bmatrix}^T \left[\begin{bmatrix} D_{11} & D_{12} & D_{16} \\ D_{12} & D_{22} & D_{26} \\ D_{16} & D_{26} & D_{66} \end{bmatrix} \begin{bmatrix} \psi_{x,x} \\ \psi_{y,y} \\ \psi_{x,y} + \psi_{y,x} \end{bmatrix} \right] \Bigg\} \Bigg|_0^S dx
\end{aligned} \tag{3.2}
$$

Note that the terms evaluated along the boundaries lead to the natural boundary conditions.

3.2.2 Variation in the Kinetic Energy

The kinetic energy contains contributions from two sources, the wing and the fuselage. The wing is regarded as a plate, so that the kinetic energy takes the form

$$
T_w = \frac{1}{2} \int_0^S \int_{LE}^{TE} m(x,y)\, \dot{w}^2(x,y,t)\, dxdy \tag{3.3}
$$

where

$$
m = m(x,y) = 2 \sum_{j=1}^{k} (t_j - t_{j-1})\, \rho^j \tag{3.4}
$$

The kinetic energy associated with the fuselage, regarded as rigid, is

$$
T_f = \frac{1}{2R} \int_{LE}^{TE} \left\{ M_c \left[\dot{w} + (x_c - x)\, \dot{w}_{,x} \right]^2 + I_c \dot{w}_{,x}^2 \right\} dx \Big|_{y=0} \tag{3.5}
$$

where M_c is the mass, I_c is the pitch inertia and x_c is the distance from the origin of the x, y, z system to the center of mass. The total kinetic energy is the sum of the two

contributions. Hence, taking the variation in the total kinetic energy and integrating over time from t_1 to t_2, we obtain

$$\begin{aligned}
\int_{t_1}^{t_2} \delta T dt = & \int_{t_1}^{t_2} \int_0^S \int_{LE}^{TE} m\dot{w}\delta\dot{w} dx dy dt + \frac{M_c}{R} \int_{t_1}^{t_2} \int_{LE}^{TE} (\dot{w} + (x_c - x)\dot{w}_{,x}) \\
& \cdot \delta\dot{w} dx dt \Big|_{y=0} + \frac{M_c}{R} \int_{t_1}^{t_2} \int_{LE}^{TE} (x_c - x)(\dot{w} + (x_c - x)\dot{w}_{,x}) \delta\dot{w}_{,x} dx dt \Big|_{y=0} \\
& + \frac{I_c}{R} \int_{t_1}^{t_2} \int_{LE}^{TE} \dot{w}_{,x} \delta\dot{w}_{,x} dx dt \Big|_{y=0} \\
= & \int_0^S \int_{LE}^{TE} m\dot{w}\delta w \Big|_{t_1}^{t_2} dx dy - \int_{t_1}^{t_2} \int_0^S \int_{LE}^{TE} \frac{\partial}{\partial t}(m\dot{w})\, \delta w dx dy dt \\
& + \frac{M_c}{R} \int_{LE}^{TE} \left\{ \left[(\dot{w} + (x_c - x)\dot{w}_{,x}) \delta w \Big|_{t_1}^{t_2} - \int_{t_1}^{t_2} \left[\frac{\partial}{\partial t}(\dot{w} + (x_c - x)\dot{w}_{,x}) \delta w \right. \right. \right. \\
& + \frac{\partial}{\partial t}(\dot{w} + (x_c - x)\dot{w}_{,x})(x_c - x)\delta w_{,x} + \frac{I_c}{M_c} \frac{\partial}{\partial t}(\dot{w}_{,x}) \delta w_{,x} \Big] dt \\
& + \left[(x_c - x)(\dot{w} + (x_c - x)\dot{w}_{,x}) + \frac{I_c}{M_c} \dot{w}_{,x} \right] \delta w_{,x} \Big|_{t_1}^{t_2} \Big\} dx \Big|_{y=0}
\end{aligned} \tag{3.6}$$

By definition of the varied path, the variation of the displacement variables is zero at the end points t_1 and t_2, so that the first and third terms in eqn (3.6) are zero. The last term can be eliminated entirely by another integration by parts with respect to x and observing that the variation of w is zero at t_1 and t_2, or

$$\begin{aligned}
& \frac{M_c}{R} \int_{LE}^{TE} \left[(x_c - x)(\dot{w} + (x_c - x)\dot{w}_{,x}) + \frac{I_c}{M_c} \dot{w}_{,x} \right] \frac{\partial}{\partial x} \partial w \Big|_{t_1}^{t_2} \Big|_{y=0} \\
& = \frac{1}{R} \left[M_c (x_c - x)(\dot{w} + (x_c - x)\dot{w}_{,x}) + I_c \dot{w}_{,x} \right] \delta w \Big|_{LE}^{TE} \Big|_{t_1}^{t_2} \Big|_{y=0} \\
& \quad - \frac{1}{R} \int_{LE}^{TE} \frac{\partial}{\partial x} \left[M_c (x_c - x)(\dot{w} + (x_c - x)\dot{w}_{,x}) \right. \\
& \quad \left. + I_c \dot{w}_{,x} \right] \delta w dx \Big|_{t_1}^{t_2} \Big|_{y=0}
\end{aligned} \tag{3.7}$$

Finally, the fifth term is integrated by parts with respect to x yielding

$$\begin{aligned}
& -\frac{1}{R} \int_{t_1}^{t_2} \int_{LE}^{TE} \frac{\partial}{\partial t} \left[M_c (\dot{w} + (x_c - x)\dot{w}_{,x})(x_c - x) + I_c \dot{w}_{,x} \right] \frac{\partial}{\partial x} \delta w \Big|_{y=0} dx dt \\
& = \frac{-1}{R} \int_{t_1}^{t_2} \frac{\partial}{\partial t} \left[M_c (\dot{w} + (x_c - x)\dot{w}_{,x})(x_c - x) + I_c \dot{w}_{,x} \right] \delta w dt \Big|_{LE}^{TE} \Big|_{y=0}
\end{aligned}$$

$$+\frac{1}{R}\int_{t_1}^{t_2}\int_{LE}^{TE}\frac{\partial^2}{\partial x\partial t}\left[M_c\left(\dot{w}+\left(x_c-x\right)\dot{w}_{,x}\right)\left(x_c-x\right)\right.$$
$$\left.+I_c\dot{w}_{,x}\right]\delta w dx dt\Big|_{y=0} \tag{3.8}$$

Combining eqns. (3.6-3.8), we obtain

$$\int_{t_1}^{t_2}\delta T dt=\int_{t_1}^{t_2}\Big\langle-\int_0^S\int_{LE}^{TE}\frac{\partial}{\partial t}\left(m\dot{w}\right)\delta w dx dy+\frac{1}{R}\int_{LE}^{TE}\Big\{\frac{\partial^2}{\partial x\partial t}\left[M_c\left(\dot{w}\right.\right.$$
$$\left.+\left(x_c-x\right)\dot{w}_{,x}\right)\left(x_c-x\right)+I_{cg}\dot{w}_{,x}\Big]-M_c\frac{\partial}{\partial t}\left(\dot{w}+\left(x_c\right.\right.$$
$$\left.\left.-\ x\right)\dot{w}_{,x}\right)\Big\}\delta w dx\Big|_{y=0}-\frac{1}{R}\frac{\partial}{\partial t}\left[M_c\left(\dot{w}+\left(x_c-x\right)\dot{w}_{,x}\right)\left(x_c-x\right)\right.$$
$$\left.+I_c\dot{w}_{,x}\right]\delta w\Big|_{LE}^{TE}\Big|_{y=0}\Big\rangle dt \tag{3.9}$$

3.3 Virtual Work of the Nonconservative Forces

Under consideration is a wing in the form of a trapezoidal planform, and in particular one characterized by low aspect ratio and/or forward swept configuration. The most important speed regime for such a wing is undoubtedly supersonic. The main reason for including the aerodynamics is to demonstrate the usefulness of the structural model. A complete investigation of a wing would require appropriate aerodynamic theories for subsonic, transonic, supersonic and perhaps hypersonic speed regimes.

The usefulness of this model can be demonstrated with supersonic aerodynamics chosen for appropriateness and relative ease of application. The supersonic regime lends itself to simpler aerodynamic theories for the loads. For large Mach numbers, $M^2 >> 1$, there is a weak memory effect, in addition to weak three-dimensional effects (ref. 62). This opens up the prospect of a point-function relation between the pressure difference $p_u - p_\ell$ and the displacement w of the wing, which makes it both convenient and useful when considering eventual inclusion of this model into an optimization routine. The structural model is suitable for wings of any aspect ratio.

Piston theory will be used to demonstrate this model, although it must be understood that, because it is a strip theory, it is not as suitable for very low aspect ratios as more sophisticated theories.

Piston theory has been shown to match experimental results quite well in the case of Mach numbers greater than about 2.5 and the product of Mach and thickness ratio considerably smaller than unity. Piston theory has zero memory and the loads generated at a given point depend only on aerodynamic derivatives at that point and time. This latter property allows the writing of an explicit aerodynamic operator operating on the vertical displacement of the wing (ref. 55) in the form

$$A_{11} = -\frac{4q}{M}\left[1 + \frac{\gamma+1}{2}M\frac{d}{dx}t_N\right]\left(\frac{\partial}{\partial x} + \frac{1}{U}\frac{\partial}{\partial t}\right) \tag{3.10}$$

A derivation of eqn. (3.10) follows.

Piston theory begins with the physical argument that at high Mach numbers the pressure on an airfoil surface is that of a one-dimensional piston moving with equivalent velocity into otherwise undisturbed ideal gas. The undisturbed pressure, density and sonic speed are denoted by p_∞, ρ_∞ and a_∞, respectively. The argument was originally put forward by Hayes and Lighthill (refs. 65 and 73) and was later systematically developed by Landahl (ref. 63) and Ashley and Zartarian, (ref. 64).

For simple waves and no entropy changes, the pressure on the piston face is (ref. 65)

$$\frac{p}{p_\infty} = \left[1 + \left(\frac{\gamma-1}{2}\right)\left(\frac{v}{a_\infty}\right)\right]^{2\gamma/(\gamma-1)} \tag{3.11}$$

where v is the piston velocity. A binomial expansion of eqn. (3.11) for the case in which $[(\gamma-1)/2]\,v/a_\infty << 1$ yields,

$$\frac{p}{p_\infty} = 1 + \gamma\left(\frac{v}{a_\infty}\right) + \frac{1}{4}\gamma(\gamma+1)\left(\frac{v}{a_\infty}\right)^2 + \frac{1}{12}\gamma(\gamma+1)\left(\frac{v}{a_\infty}\right)^3 \ldots \tag{3.12}$$

Let $Z(x,y,t)$ be the position of an airfoil surface. The normal fluid velocity then depends on the surface inclination with respect to the free stream and any time

dependence of Z

$$v = \frac{\partial Z}{\partial t} + U\frac{\partial Z}{\partial x} \tag{3.13}$$

Supersonic airfoils in general and this model in particular are symmetrical structures about the midplane. Thus, the equation describing both surfaces for Z measured away from the midplane is the same. Let $Z_s(x,y)$ define this contour and $Z_0(x,y,t)$ define motion due to oscillation, and note that Z is defined outward from the midplane, so that the sign of Z_0 differs for the two surfaces, as illustrated in Fig. 3.2. The full equations of both surfaces are then

$$Z_u(x,y,t) = Z_s(x,y) + Z_0(x,y,t) \tag{3.14a}$$

$$Z_\ell(x,y,t) = Z_s(x,y) - Z_0(x,y,t) \tag{3.14b}$$

where the subscript u denotes the upper surface of the airfoil and ℓ the lower one. The effective piston velocity can be written as

$$v_u = v_s + v_o = U\frac{\partial Z_s}{\partial x} + \left(\frac{\partial Z_o}{\partial t} + U\frac{\partial Z_o}{\partial x}\right) \tag{3.15a}$$

$$v_\ell = v_s - v_o = U\frac{\partial Z_s}{\partial x} - \left(\frac{\partial Z_o}{\partial t} + U\frac{\partial Z_o}{\partial x}\right) \tag{3.15b}$$

Substituting eqns (3.15) into eqn. (3.12) and retaining the first three terms in the series, we obtain

$$\begin{aligned}\frac{\Delta p}{p_\infty} = &\frac{p_u - p_\ell}{p_\infty} = \left(\frac{2\gamma}{a_\infty}\right) w_0 + \left(\frac{\gamma(\gamma+1)}{a_\infty^2}\right) w_s w_0 \\ &= \left(\frac{2\gamma}{a_\infty}\right)\left[1 + \frac{\gamma+1}{2}M\frac{\partial Z_s}{\partial x}\right]\left(\frac{\partial Z_o}{\partial t} + U\frac{\partial Z_o}{\partial x}\right)\end{aligned} \tag{3.16}$$

At this point, Z_s is identified as $t_N(x,y)$, the wing half thickness, and Z_0 as the wing deflection $w(x,y,t)$. For incompressible dynamic pressure

$$q = \frac{\gamma}{2}p_\infty M^2 \tag{3.17}$$

so that, introducing a change of sign due to the downstream direction of the coordinate x, we obtain

$$\Delta p = \frac{-4q}{M}\left[1 + \frac{\gamma+1}{2}M\frac{dt_N}{dx}\right]\left(\frac{\partial}{\partial x} + \frac{1}{U}\frac{\partial}{\partial t}\right)w \tag{3.18}$$

which verifies eqn. (3.10).

The nonconservative virtual work is due to the aerodynamic forces just derived. The distributed force, eqn. (3.18), is multiplied by the corresponding virtual displacement to yield the nonconservative virtual work density. Note that the aerodynamic forces act only through the virtual displacement δw, and not through $\delta\psi_x$ and/or $\delta\psi_y$. The integral over time of the nonconservative virtual work is simply

$$\int_{t_1}^{t_2}\delta\overline{W}_{NC}dt = \frac{-4q}{M}\int_{t_1}^{t_2}\int_0^S\int_{LE}^{TE}\left[1 + \frac{\gamma+1}{2}M\frac{dt_N}{dx}\right]\left(w_{,x} + \frac{1}{U}\dot{w}\right)\delta w dx dy dt \tag{3.19}$$

3.4 The Extended Hamilton Principle and the Boundary Value Problem

The extended Hamilton principle can be written in the form (ref. 60)

$$\int_{t_1}^{t_2}\left(\delta T - \delta V + \delta\overline{W}_{NC}\right)dt = 0 \tag{3.20}$$

Substituting eqns. (3.2) (3.9) and (3.19) into (3.20), we obtain

$$\begin{aligned}
0 = \int_{t_1}^{t_2}\Bigg[\int_0^S\int_{LE}^{TE}\Bigg(&\Bigg\{2\frac{\partial}{\partial x}\left[\left(\psi_x + w_{,x}\right)A_{55} + \left(\psi_y + w_{,y}\right)A_{45}\right] + 2\frac{\partial}{\partial y}\left[\left(\psi_x + w_{,x}\right)A_{45}\right.\\
&\left. + \left(\psi_y + w_{,y}\right)A_{44}\right] - \frac{\partial}{\partial t}\left(m\dot{w}\right) - \frac{4q}{M}\left(1 - \frac{\gamma+1}{2}M\frac{dt_N}{dx}\right)\left(w_{,x} + \frac{1}{U}\dot{w}\right)\Bigg\}\delta w\\
&+ 2\Bigg\{\frac{\partial}{\partial x}\left[\psi_{x,x}D_{11} + \psi_{y,y}D_{12} + \left(\psi_{x,y} + \psi_{y,x}\right)D_{16}\right] + \frac{\partial}{\partial y}\left[\psi_{x,x}D_{16} + \psi_{y,y}D_{26}\right.\\
&\left. + \left(\psi_{x,y} + \psi_{y,x}\right)D_{66}\right] - \left[\left(\psi_x + w_{,x}\right)A_{55} + \left(\psi_y + w_{,y}\right)A_{45}\right]\Bigg\}\delta\psi_x\\
&+ 2\Bigg\{\frac{\partial}{\partial y}\left[\psi_{x,x}D_{12} + \psi_{y,y}D_{22} + \left(\psi_{x,y} + \psi_{y,x}\right)D_{26}\right] + \frac{\partial}{\partial x}\left[\psi_{x,x}D_{16} + \psi_{y,y}D_{26}\right.\\
&\left. + \left(\psi_{x,y} + \psi_{y,x}\right)D_{66}\right] - \left[\left(\psi_x + w_{,x}\right)A_{45} + \left(\psi_y + w_{,y}\right)A_{44}\right]\Bigg\}\delta\psi_y\Bigg)dx dy\\
&- 2\int_0^S\left\{\left[\left(\psi_x + w_{,x}\right)A_{55} + \left(\psi_y + w_{,y}\right)A_{45}\right]\delta w + \left[\psi_{x,x}D_{11} + \psi_{y,y}D_{12}\right.\right.
\end{aligned}$$

$$+\left(\psi_{x,y}+\psi_{y,x}\right)D_{16}\right]\delta\psi_x+\left[\psi_{x,x}D_{16}+\psi_{y,y}D_{26}+\left(\psi_{x,y}+\psi_{y,x}\right)D_{66}\right]\delta\psi_y\Big\}\Big|_{LE}^{TE}dy$$

$$+\int_{LE}^{TE}\left(\left\{\frac{1}{R}\frac{\partial^2}{\partial x\partial t}\left[M_c\left(\dot{w}+\left(x_c-x\right)\dot{w}_{,x}\right)\left(x_c-x\right)+I_c\dot{w}_{,x}\right]-\frac{M_c}{R}\frac{\partial}{\partial t}\left[\dot{w}\right.\right.\right.$$

$$\left.\left.\left.+\left(x_c-x\right)\dot{w}_{,x}\right]\Big|_{y=0}-2\left[\left(\psi_x+w_{,x}\right)A_{45}+\left(\psi_y+w_{,y}\right)A_{44}\right]\Big|_o^S\right\}\delta w\right.$$

$$-2\left[\psi_{x,x}D_{16}+\psi_{y,y}D_{26}+\left(\psi_{x,y}+\psi_{y,x}\right)D_{66}\right]\Big|_o^S\delta\psi_x$$

$$\left.-2\left[\psi_{x,x}D_{12}+\psi_{y,y}D_{22}+\left(\psi_{x,y}+\psi_{y,x}\right)D_{26}\right]\Big|_o^S\delta\psi_y\right)dx$$

$$-\frac{1}{R}\frac{\partial}{\partial t}\left[M_c\left(\dot{w}+\left(x_c-x\right)\dot{w}_{,x}\right)\left(x_c-x\right)+I_c\dot{w}_{,x}\right]\delta w\Big|_{LE}^{TE}\Big|_{y=0}\Bigg]dt \tag{3.21}$$

The virtual displacements are arbitrary except that they must be compatible with the system constraints. Following the usual steps (ref. 71), eqn. (3.21) can be satisfied for all δw, $\delta\psi_x$ and $\delta\psi_y$ provided

$$\frac{\partial}{\partial x}\left[\left(\psi_x+w_{,x}\right)A_{55}+\left(\psi_y+w_{,y}\right)A_{45}\right]+\frac{\partial}{\partial y}\left[\left(\psi_x+w_{,x}\right)A_{45}+\left(\psi_y+w_{,y}\right)A_{44}\right]$$

$$-\frac{1}{2}\frac{\partial}{\partial t}\left(m\dot{w}\right)-\frac{2q}{M}\left[1+\frac{\gamma+1}{2}M\frac{dt_N}{dx}\right]\left(w_{,x}+\frac{1}{U}\dot{w}\right)=0$$

$$0<y<S,\qquad LE<x<TE \tag{3.22}$$

$$\frac{\partial}{\partial x}\left[\psi_{x,x}D_{11}+\psi_{y,y}D_{12}+\left(\psi_{x,y}+\psi_{y,x}\right)D_{16}\right]+\frac{\partial}{\partial y}\left[\psi_{x,x}D_{16}+\psi_{y,y}D_{26}\right.$$

$$\left.+\left(\psi_{x,y}+\psi_{y,x}\right)D_{66}\right]-\left[\left(\psi_x+w_{,x}\right)A_{55}+\left(\psi_y+w_{,y}\right)A_{45}\right]=0$$

$$0<y<S,\qquad LE<x<TE \tag{3.23}$$

$$\frac{\partial}{\partial x}\left[\psi_{x,x}D_{16}+\psi_{y,y}D_{26}+\left(\psi_{x,y}+\psi_{y,x}\right)D_{66}\right]+\frac{\partial}{\partial y}\left[\psi_{x,x}D_{12}+\psi_{y,y}D_{22}\right.$$

$$\left.+\left(\psi_{x,y}+\psi_{y,x}\right)D_{26}\right]-\left[\left(\psi_x+w_{,x}\right)A_{45}+\left(\psi_y+w_{,y}\right)A_{44}\right]=0$$

$$0<y<S,\qquad LE<x<TE \tag{3.24}$$

$$\left(\psi_x+w_{,x}\right)A_{55}+\left(\psi_y+w_{,y}\right)A_{45}=0\qquad 0<y<S,\qquad x=TE,LE \tag{3.25}$$

$$\psi_{x,x}D_{11}+\psi_{y,y}D_{12}+\left(\psi_{x,y}+\psi_{y,x}\right)D_{16}=0\qquad 0<y<S\qquad x=TE,LE \tag{3.26}$$

$$\psi_{x,x} D_{16} + \psi_{y,y} D_{26} + (\psi_{x,y} + \psi_{y,x}) D_{66} = 0 \qquad 0 < y < S \qquad x = TE, LE \quad (3.27)$$

$$(\psi_x + w_{,x}) A_{45} + (\psi_y + w_{,y}) A_{44} = 0 \qquad LE < x < TE, \qquad y = S \quad (3.28)$$

$$\psi_{x,x} D_{16} + \psi_{y,y} D_{26} + (\psi_{x,y} + \psi_{y,x}) D_{66} = 0 \qquad LE < x < TE, \qquad y = S, 0 \quad (3.29)$$

$$\psi_{x,x} D_{12} + \psi_{y,y} D_{22} + (\psi_{x,y} + \psi_{y,x}) D_{26} = 0 \qquad LE < x < TE, \qquad y = S, 0 \quad (3.30)$$

$$\frac{1}{2R} \frac{\partial^2}{\partial x \partial t} \left[M_c \left(\dot{w} + (x_c - x) \dot{w}_{,x} \right) (x_c - x) + I_c \dot{w}_{,x} \right] - \frac{M_c}{2R} \frac{\partial}{\partial t} \left[\dot{w} + (x_c - x) \dot{w}_{,x} \right] + (\psi_x + w_{,x}) A_{45} + (\psi_y + w_{,y}) A_{44} = 0 \qquad LE < x < TE, \qquad y = 0 \quad (3.31)$$

$$\frac{1}{2R} \frac{\partial}{\partial t} \left[M_c \left(\dot{w} + (x_c - x) \dot{w}_{,x} \right) (x_c - x) + I_c \dot{w}_{,x} \right] = 0 \quad y = 0, \quad x = TE, \quad LE \quad (3.32)$$

Equations (3.22-3.32) define the boundary value problem for the system, in which eqns. (3.22-3.24) are recognized as the differential equations and eqns. (3.25-3.32) as the natural boundary conditions. The extended Hamilton principle, eqn. (3.21), can be rewritten in terms of the left hand expressions of the equations defining the boundary value problem in the compact form

$$\begin{aligned} 0 = \int_{t_1}^{t_2} \Bigg\{ & \int_0^S \int_{LE}^{TE} \left[(3.22)\, \delta w + (3.23)\, \delta \psi_x + (3.24)\, \delta \psi_y \right] dx dy - \int_0^S \left[(3.25)\, \delta w \right. \\ & \left. + (3.26)\, \delta \psi_x + (3.27)\, \delta \psi_y \right] \Big|_{LE}^{TE} dy - \int_{LE}^{TE} \left[(3.28)\, \delta w + (3.29)\, \delta \psi_x \right. \\ & \left. + (3.30)\, \delta \psi_y \right] \Big|_{y=S} dx + \int_{LE}^{TE} \left[(3.31)\, \delta w + (3.29)\, \delta \psi_x + (3.30)\, \delta \psi_y \right] \Big|_{y=0} dx \\ & - (3.32) \Big|_{LE}^{TE} \Big|_{y=0} \Bigg\} dt \end{aligned} \quad (3.33)$$

It is clear that Hamilton's principle provides a complete picture of the system dynamics, including the equations of motion and the natural boundary conditions.

Next, one additional point must be made before this boundary value problem formulation can be regarded as complete. This point relates to the shape of the

boundaries. The cartesian coordinates x, y are the natural choice for a rectangular plate. In the problem at hand, the plate is trapezoidal, so that it is more appropriate to express the boundary conditions in terms of the normal and tangential coordinates n, s. Hence, at the leading and trailing edge the boundary conditions are more suitably expressed as

$$(\psi_n + w_{,n})\, A_{nn} + (\psi_s + w_{,s})\, A_{ns} = 0 \quad \text{(free edges)} \tag{3.34}$$

$$\psi_{n,n} D_{n,n} + \psi_{s,s} D_{ns} + (\psi_{n,s} + \psi_{s,n})\, D_{nz} = 0 \quad \text{(free edges)} \tag{3.35}$$

$$\psi_{n,n} D_{n,z} + \psi_{s,s} D_{s,z} + (\psi_{n,s} + \psi_{s,n})\, D_{zz} = 0 \quad \text{(free edges)} \tag{3.36}$$

Physically, these three boundary conditions require shear force, bending moment and twisting moment to be independently zero along the free edges. The displacement variables ψ_n and ψ_s and the unit vectors can be represented in terms of ψ_x, ψ_y and the sweep angle η. The derivatives are directional derivatives and the $[A]$ and $[D]$ matrices are rotated by η using eqn. (2.16). These directional derivatives and transformations are carried out and substituted into eqns. (3.34-3.36). The results are shear, moment and twisting terms for free edges swept by an angle η. After simplification, the natural boundary conditions at the leading and trailing edge are

$$(\psi_x + w_{,x})\,(A_{55}\cos\eta - A_{45}\sin\eta) + (\psi_y + w_{,y})\,(A_{45}\cos\eta - A_{44}\sin\eta) = 0$$
$$x = LE, TE \tag{3.37}$$

$$\psi_{x,x}\left(D_{11}\cos^2\eta + D_{12}\sin^2\eta - 2D_{16}\sin\eta\cos\eta\right) + \psi_{y,y}\left(D_{12}\cos^2\eta + D_{22}\sin^2\eta - 2D_{26}\sin\eta\cos\eta\right) + (\psi_{x,y} + \psi_{y,x})\left(D_{16}\cos^2\eta + D_{26}\sin^2\eta - 2D_{66}\sin\eta\cos\eta\right) = 0 \qquad x = LE, TE \tag{3.38}$$

$$\psi_{x,x}\left[(D_{11} - D_{12})\sin\eta\cos\eta + D_{16}\left(\cos^2\eta - \sin^2\eta\right)\right] + \psi_{y,y}\left[(D_{12} - D_{22}) \cdot \sin\eta\cos\eta + D_{26}\left(\cos^2\eta - \sin^2\eta\right)\right] + (\psi_{x,y} + \psi_{y,x})\left[(D_{16} - D_{26})\sin\eta\cos\eta + D_{66}\left(\cos^2\eta - \sin^2\eta\right)\right] = 0 \qquad x = LE, TE \tag{3.39}$$

Clearly, when $\eta = 0$, eqns. (3.25-3.27) at $y = S$ are recovered and when $\eta = 90°$ eqns. (3.28-3.30) are recovered.

The boundary value problem can be summarized as follows: the equations of motion are expressed as eqns. (3.22 - 3.24) and the natural boundary conditions are expressed as eqns. (3.28-3.30) and (3.37-3.39). The system is clearly of sixth order consisting of three second-order partial differential equations and three natural boundary conditions on each boundary. The y=0 boundary has the only geometric boundary conditions for this boundary value problem. The natural boundary conditions at y=0 specified by eqns. (3.29) and (3.30) are replaced by two geometric boundary conditions required for the rigid fuselage condition. The geometric boundary conditions are

$$w_{,xx} = 0, \qquad y = 0 \tag{3.40}$$

$$\psi_{x,x} = 0, \qquad y = 0 \tag{3.41}$$

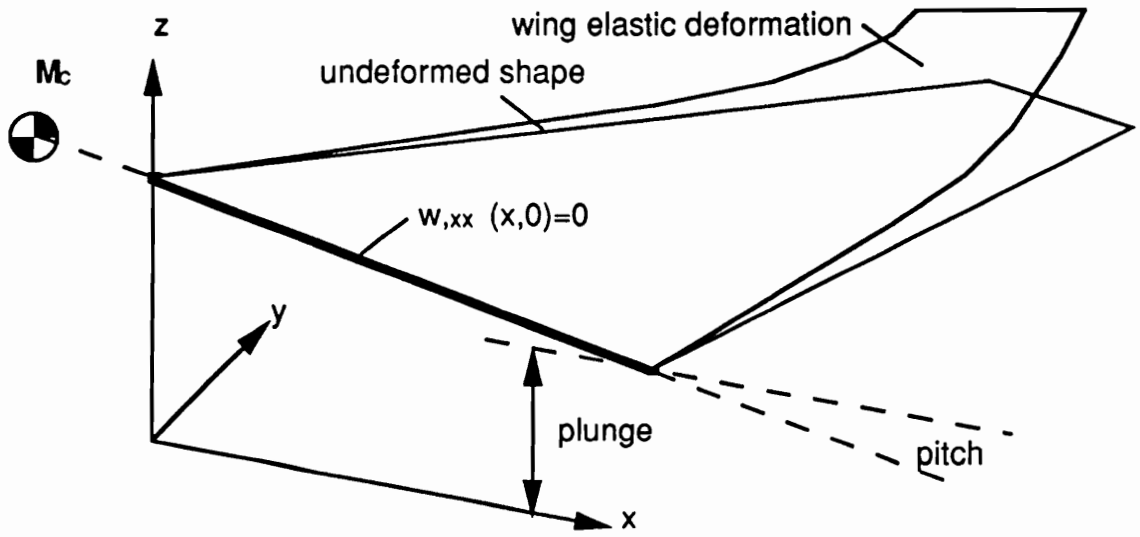

FIGURE 3.1a - Wing Root Deflection Boundary Conditions

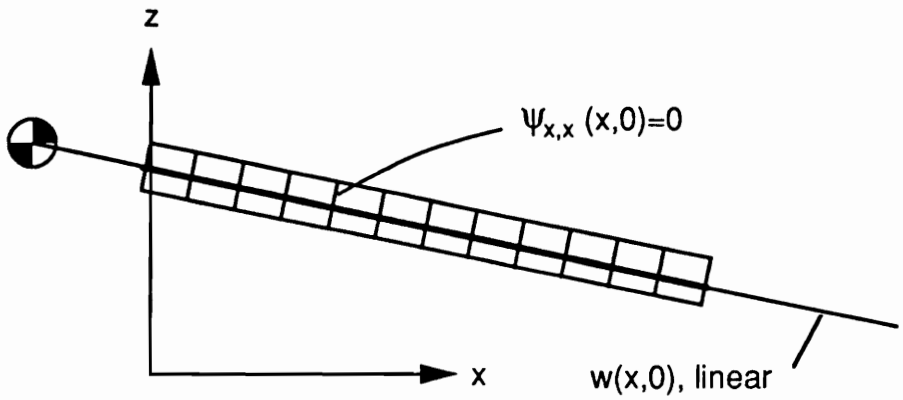

FIGURE 3.1b - Wing Root Shear Boundary Conditions

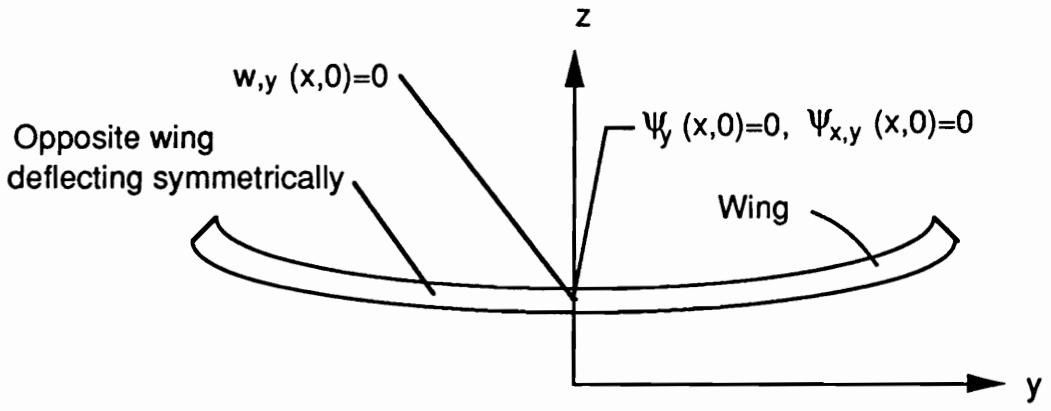

FIGURE 3.1c - Wing Root Geometry - Symmetry Conditions

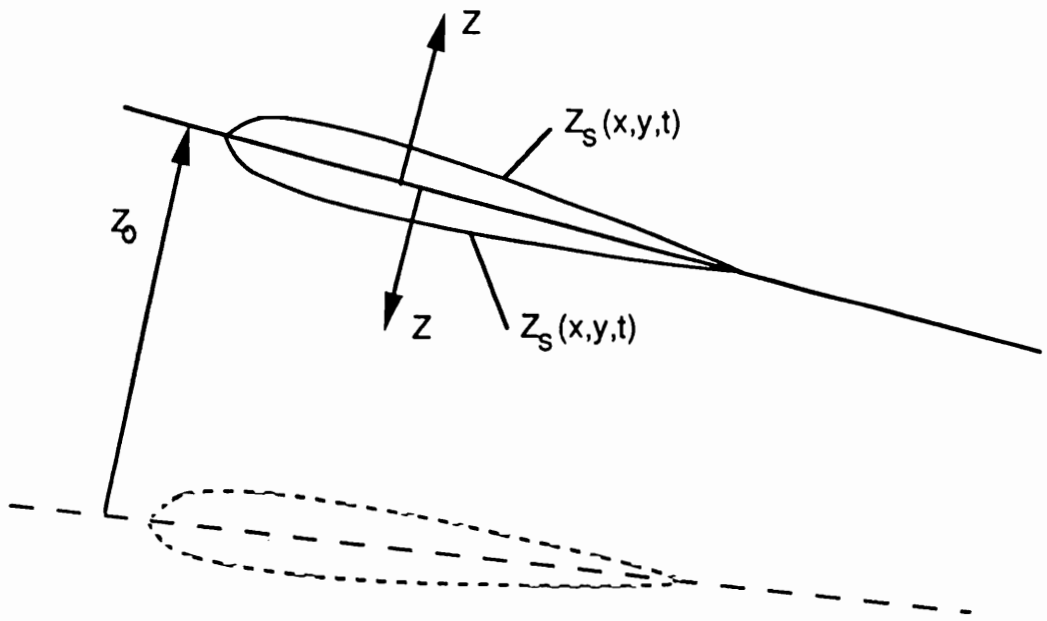

FIGURE 3.2 Surface Location Z(x,y,t) for a Symmetrical Airfoil

CHAPTER IV

THE EIGENVALUE PROBLEM

4.1 The Algebraic Eigenvalue Problem

Typically, the differential eigenvalue problem is obtained from the boundary value problem by assuming that the time and spatial variables are separable. The result is a differential eigenvalue problem in terms of the spatial variables and the parameter λ. The dependence on time has been removed. The differential eigenvalue problem consists of the corresponding differential equations and boundary conditions. For a non-self-adjoint system, no closed-form solution can be expected, so that one must be content with an approximate solution. This involves discretization in space, which for non-self-adjoint systems can be carried out by the Galerkin's version of the weighted residuals method. According to this method, the solution minimizes the error in the differential equations, with the boundary conditions being satisfied by requiring that the approximating functions satisfy all the boundary conditions. Such approximating functions are known as comparison functions (ref. 71). The net result of the discretization process is to replace the differential eigenvalue problem by an algebraic one.

The requirement for comparison functions can be relaxed by integrating certain integrals by parts a sufficient number of times to take into account all the natural boundary conditions. As a result, it is possible to produce an approximate solution in terms of admissible functions, which need satisfy only the geometric boundary conditions, instead of comparison functions. This formulation has been demonstrated to have poor convergence characteristics. In the following, a procedure possessing the best features of both approaches is described.

It is here proposed to derive the algebraic eigenvalue problem directly from the extended Hamilton principle. Because eqn. (3.33) contains all the natural boundary conditions, an approximate solution need satisfy only the geometric boundary conditions, i.e., it can be in terms of admissible functions. Such functions are significantly more plentiful than comparison functions, especially for this problem.

To derive the differential eigenvalue problem, we assume a solution of the boundary value problem in the form

$$w(x,y,t) = w(x,y)\,e^{\lambda t}, \quad \psi_x(x,y,t) = \psi_x(x,y)\,e^{\lambda t}, \quad \psi_y(x,y,t) = \psi_y(x,y)\,e^{\lambda t} \tag{4.1}$$

where λ is in general a complex quantity, $\lambda = \alpha + i\omega$. Introducing eqns. (4.1) into eqn. (3.33) and dividing through by exp λt, we can write

$$\begin{aligned}
&\int_0^S \int_{LE}^{TE} [f_1 \delta w + (3.23)\,\delta\psi_x + (3.24)\,\delta\psi_y]\,dx dy \\
&\quad - \int_0^S [(3.25)\,\delta w + (3.26)\,\delta\psi_x + (3.27)\,\delta\psi_y]\Big|_{LE}^{TE} dy \\
&\quad + \int_{LE}^{TE} [f_2 \delta w + (3.29)\,\delta\psi_x + (3.30)\,\delta\psi_y]\Big|_{y=0} dx \\
&\quad - \int_{LE}^{TE} [(3.28)\,\delta w + (3.29)\,\delta\psi_x + (3.30)\,\delta\psi_y]\Big|_{y=S} dx - f_3\Big|_{LE}^{TE}\Big|_{y=0} = 0
\end{aligned} \tag{4.2}$$

in which

$$\begin{aligned}
f_1 =& \frac{\partial}{\partial x}[(\psi_x + w_{,x})\,A_{55} + (\psi_y + w_{,y})\,A_{45}] + \frac{\partial}{\partial y}[(\psi_x + w_{,x})\,A_{45} \\
&+ (\psi_y + w_{,y})\,A_{44}] - \frac{1}{2} m w \lambda^2 - \frac{2q}{M}\left[1 + \frac{\gamma+1}{2} M \frac{d}{dx} t_N\right]\left(w_{,x} + \frac{1}{U} w\lambda\right) = 0 \\
f_2 =& -\frac{1}{R}\left\{M_c\,[w + (x_c - x)\,w_{,x}] - \frac{1}{2}\left[M_c\,(x_c - x)^2 + I_c\right] w_{,xx}\right\}\lambda^2 \\
&+ (\psi_x + w_{,x})\,A_{45} + (\psi_y + w_{,y})\,A_{44}, \quad y = 0 \\
f_3 =& \frac{1}{2R}\left\{M_c\,(x_c - x)\,w + \left[M_c\,(x_c - x)^2 + I_c\right] w_{,x}\right\}\lambda^2, \\
&x = LE,\ TE, \qquad y = 0
\end{aligned} \tag{4.3}$$

Equation (4.2) can be used to derive the differential eigenvalue problem for a trapezoidal plate with $2k$ symmetrically stacked, variable thickness, generally orthotropic laminae with all the natural boundary conditions included. We do not propose to derive the differential eigenvalue problem, as no closed-form solution is possible. Instead, we propose to use eqn. (4.2) to derive the algebraic eigenvalue problem.

Let us assume that the various displacements appearing in eqn. (4.2) can be expressed as linear combinations of trial functions of the form

$$w^n = \sum_{i=1}^{n} a_i \phi_i \ , \quad \psi_x^n = \sum_{i=n+1}^{2n} a_i \phi_i \ , \quad \psi_y^n = \sum_{i=2n+1}^{3n} a_i \phi_i \ , \tag{4.4}$$

$$\int_0^S \int_{LE}^{TE} \begin{bmatrix} 1 \\ 1 \\ 1 \end{bmatrix} \left[\left[\begin{bmatrix} f_4 & f_7 & f_{10} \\ f_5 & f_8 & f_{11} \\ f_6 & f_9 & f_{12} \end{bmatrix} + \lambda \begin{bmatrix} f_{13} & 0 & 0 \\ 0 & 0 & 0 \\ 0 & 0 & 0 \end{bmatrix} \right.\right.$$

$$\left.\left. + \lambda^2 \begin{bmatrix} f_{14} & 0 & 0 \\ 0 & 0 & 0 \\ 0 & 0 & 0 \end{bmatrix} \right] \right] \begin{bmatrix} \sum_{j=1}^{n} \delta a_j \phi_j \\ \sum_{j=n+1}^{2n} \delta a_j \phi_j \\ \sum_{j=2n+1}^{3n} \delta a_j \phi_j \end{bmatrix} dx dy$$

$$- \int_0^S \begin{bmatrix} 1 \\ 1 \\ 1 \end{bmatrix} \begin{bmatrix} f_{15} & 0 & 0 \\ f_{16} & f_{18} & f_{20} \\ f_{17} & f_{19} & f_{21} \end{bmatrix} \begin{bmatrix} \sum_{j=1}^{n} \delta a_j \phi_j \\ \sum_{j=n+1}^{2n} \delta a_j \phi_j \\ \sum_{j=2n+1}^{3n} \delta a_j \phi_j \end{bmatrix} \Bigg|_{LE}^{TE} dy$$

$$+ \int_{LE}^{TE} \begin{bmatrix} 1 \\ 1 \\ 1 \end{bmatrix} \left[\begin{bmatrix} f_{22} & 0 & 0 \\ f_{23} & f_{25} & f_{27} \\ f_{24} & f_{26} & f_{28} \end{bmatrix} \right.$$

$$+\lambda^2 \begin{bmatrix} f_{29} & 0 & 0 \\ 0 & 0 & 0 \\ 0 & 0 & 0 \end{bmatrix} \Bigg] \begin{bmatrix} \sum_{j=1}^{n} \delta a_j \phi_j \\ \sum_{j=n+1}^{2n} \delta a_j \phi_j \\ \sum_{j=2n+1}^{3n} \delta a_j \phi_j \end{bmatrix} \Bigg|_{y=0} dx$$

$$- \int_{LE}^{TE} \begin{bmatrix} 1 \\ 1 \\ 1 \end{bmatrix} \begin{bmatrix} f_{30} & 0 & 0 \\ f_{31} & f_{25} & f_{27} \\ f_{32} & f_{26} & f_{28} \end{bmatrix} \begin{bmatrix} \sum_{j=1}^{n} \delta a_j \phi_j \\ \sum_{j=n+1}^{2n} \delta a_j \phi_j \\ \sum_{j=2n+1}^{3n} \delta a_j \phi_j \end{bmatrix} \Bigg|_{y=S} dx$$

$$- \lambda^2 \begin{bmatrix} 1 \\ 1 \\ 1 \end{bmatrix} \begin{bmatrix} f_{33} & 0 & 0 \\ 0 & 0 & 0 \\ 0 & 0 & 0 \end{bmatrix} \begin{bmatrix} \sum_{j=1}^{n} \delta a_j \phi_j \\ \sum_{j=n+1}^{2n} \delta a_j \phi_j \\ \sum_{j=2n+1}^{3n} \delta a_j \phi_j \end{bmatrix} \Bigg|_{LE}^{TE} \Bigg|_{y=0} = 0 \qquad (4.5)$$

The various terms in eqn. (4.5) reflect the separation of each eqn. (4.2) term into dependence on w, ψ_x, ψ_y, λ and λ^2. The terms in eqn. (4.5) follow as:

$$f_4 = \sum_{j=1}^{n} \left\{ \frac{\partial}{\partial x} \left(\phi_{i,x} A_{55} + \phi_{i,y} A_{45} \right) + \frac{\partial}{\partial y} \left(\phi_{i,x} A_{45} + \phi_{i,y} A_{44} \right) - \frac{2q}{M} \left[1 + \frac{\gamma + 1}{2} M \frac{d}{dx} t_N \right] \phi_{i,x} \right\} a_i$$

$$f_5 = \sum_{i=n+1}^{2n} \left\{ \frac{\partial}{\partial x} \left(\phi_i A_{55} \right) + \frac{\partial}{\partial y} \left(\phi_i A_{45} \right) \right\} a_i$$

$$f_6 = \sum_{i=2n+1}^{3n} \left\{ \frac{\partial}{\partial x} \left(\phi_i A_{45} \right) + \frac{\partial}{\partial y} \left(\phi_i A_{44} \right) \right\} a_i$$

$$f_7 = \sum_{j=1}^{n} \left\{ -\phi_{i,x} A_{55} - \phi_{i,y} A_{45} \right\} a_i$$

$$f_8 = \sum_{i=n+1}^{2n} \left\{ -\phi_i A_{55} + \frac{\partial}{\partial x} \left(\phi_{i,x} D_{11} + \phi_{i,y} D_{16} \right) + \frac{\partial}{\partial y} \left(\phi_{i,x} D_{16} + \phi_{i,y} D_{66} \right) \right\} a_i$$

$$f_9 = \sum_{i=2n+1}^{3n} \left\{ -\phi_i A_{45} + \frac{\partial}{\partial x}\left(\phi_{i,x} D_{16} + \phi_{i,y} D_{12}\right) + \frac{\partial}{\partial y}\left(\phi_{i,x} D_{66} + \phi_{i,y} D_{26}\right) \right\} a_i$$

$$f_{10} = \sum_{i=1}^{n} \left\{ -\phi_{i,x} A_{45} - \phi_{i,y} A_{44} \right\} a_i$$

$$f_{11} = \sum_{i=n+1}^{2n} \left\{ -\phi_i A_{45} + \frac{\partial}{\partial x}\left(\phi_{i,x} D_{16} + \phi_{i,y} D_{66}\right) + \frac{\partial}{\partial y}\left(\phi_{i,x} D_{12} + \phi_{i,y} D_{26}\right) \right\} a_i$$

$$f_{12} = \sum_{i=2n+1}^{3n} \left\{ -\phi_i A_{44} + \frac{\partial}{\partial x}\left(\phi_{i,x} D_{66} + \phi_{i,y} D_{26}\right) + \frac{\partial}{\partial y}\left(\phi_{i,x} D_{26} + \phi_{i,y} D_{22}\right) \right\} a_i$$

$$f_{13} = \sum_{i=1}^{n} \left\{ -\frac{2q}{M}\left[1 + \frac{\gamma+1}{2} M \frac{d}{dx} t_N\right] \frac{1}{U} \phi_i \right\} a_i$$

$$f_{14} = \sum_{i=1}^{n} \left\{ -\frac{1}{2} m \phi_i \right\} a_i$$

$$f_{15} = \sum_{i=1}^{n} \left\{ A_{55} \phi_{i,x} + A_{45} \phi_{i,y} \right\} a_i$$

$$f_{16} = \sum_{i=n+1}^{2n} \left\{ A_{55} \phi_i \right\} a_i$$

$$f_{17} = \sum_{i=2n+1}^{3n} \left\{ A_{45} \phi_i \right\} a_i$$

$$f_{18} = \sum_{i=n+1}^{2n} \left\{ \phi_{i,x} D_{11} + \phi_{i,y} D_{16} \right\} a_i$$

$$f_{19} = \sum_{i=2n+1}^{3n} \left\{ \phi_{i,x} D_{16} + \phi_{i,y} D_{12} \right\} a_i$$

$$f_{20} = \sum_{i=n+1}^{2n} \left\{ \phi_{i,x} D_{16} + \phi_{i,y} D_{66} \right\} a_i$$

$$f_{21} = \sum_{i=2n+1}^{3n} \left\{ \phi_{i,x} D_{66} + \phi_{i,y} D_{26} \right\} a_i$$

$$f_{22} = \sum_{i=1}^{n} \left\{ \phi_{i,x} A_{45} + \phi_{i,y} A_{44} \right\} a_i$$

$$f_{23} = \sum_{i=n+1}^{2n} \left\{ \phi_i A_{45} \right\} a_i$$

$$f_{24} = \sum_{i=2n+1}^{3n} \{\phi_i A_{44}\} a_i$$

$$f_{25} = \sum_{i=n+1}^{2n} \{\phi_{i,y} D_{66} + \phi_{i,x} D_{16}\} a_i$$

$$f_{26} = \sum_{i=2n+1}^{3n} \{\phi_{i,y} D_{26} + \phi_{i,x} D_{66}\} a_i$$

$$f_{27} = \sum_{i=n+1}^{2n} \{\phi_{i,y} D_{26} + \phi_{i,x} D_{12}\} a_i$$

$$f_{28} = \sum_{i=2n+1}^{3n} \{\phi_{i,y} D_{22} + \phi_{i,x} D_{26}\} a_i$$

$$f_{29} = \sum_{i=1}^{n} -\frac{1}{R} \left\{ M_c \left[\phi_i + (x_c - x)\, \phi_{i,x}\right] - \frac{1}{2} \left[M_c (x_c - x)^2 + I_c\right] \phi_{i,xx} \right\} a_i$$

$$f_{30} = \sum_{i=1}^{n} \{\phi_{i,x} A_{45} + \phi_{i,y} A_{44}\} a_i$$

$$f_{31} = \sum_{i=n+1}^{2n} \{\phi_i A_{45}\} a_i$$

$$f_{32} = \sum_{i=2n+1}^{3n} \{\phi_i A_{44}\} a_i$$

$$f_{33} = \sum_{i=1}^{n} \frac{1}{2R} \left\{ M_c (x_c - x)\, \phi_i + \left[M_c (x_c - x)^2 + I_c\right] \phi_{i,x} \right\} a_i$$

Since the variations, δa_j, are arbitrary and independent, their coefficients are independently zero. Equation (4.5), then, leads to a set of $3n$ equations in λ and the $3n$ unknown values of a_j. This is the algebraic eigenvalue problem

$$\left[[K] + \lambda [H] + \lambda^2 [M]\right] [a] = 0 \tag{4.6}$$

where

$$[K] = \begin{bmatrix} K_{11} & K_{12} & K_{13} \\ K_{21} & K_{22} & K_{23} \\ K_{31} & K_{32} & K_{33} \end{bmatrix}, [H] = \begin{bmatrix} H_{11} & 0 & 0 \\ 0 & 0 & 0 \\ 0 & 0 & 0 \end{bmatrix}, [M] = \begin{bmatrix} M_{11} & 0 & 0 \\ 0 & 0 & 0 \\ 0 & 0 & 0 \end{bmatrix} \tag{4.7}$$

For $i = 1$ to n and $j = 1$ to n the following can be formed by making use of expressions f_4^*, f_{15}^*, f_{22}^* and f_{30}^* corresponding to the expressions in braces in f_4, f_{15}, f_{22} and f_{30}.

$$(K_{11})_{ij} = \int_0^S \int_{LE}^{TE} f_4^* \phi_j dx dy - \int_0^S f_{15}^* \phi_j \Big|_{LE}^{TE} dy + \int_{LE}^{TE} f_{22}^* \phi_j \Big|_{y=0} dx - \int_{LE}^{TE} f_{30}^* \phi_j \Big|_{y=S} dx \tag{4.8a}$$

Similarly for all combinations of $i, j = 1$ to n, $n+1$ to $2n$, and $2n+1$ to $3n$, the following are formed, where i, j are from 1 to n

$$(K_{12})_{ij} = \int_0^S \int_{LE}^{TE} f_7^* \phi_j dx dy \tag{4.8b}$$

$$(K_{13})_{ij} = \int_0^S \int_{LE}^{TE} f_{10}^* \phi_j dx dy \tag{4.8c}$$

$$(K_{21})_{ij} = \int_0^S \int_{LE}^{TE} f_5^* \phi_j dx dy - \int_0^S f_{16}^* \phi_j \Big|_{LE}^{TE} dy + \int_{LE}^{TE} f_{23}^* \phi_j \Big|_{y=0} dx - \int_{LE}^{TE} f_{31}^* \phi_j \Big|_{y=S} dx \tag{4.8d}$$

$$(K_{22})_{ij} = \int_0^S \int_{LE}^{TE} f_8^* \phi_j dx dy - \int_0^S f_{18}^* \phi_j \Big|_{LE}^{TE} dy - \int_{LE}^{TE} f_{25}^* \phi_j \Big|_0^S dx \tag{4.8e}$$

$$(K_{23})_{ij} = \int_0^S \int_{LE}^{TE} f_{11}^* \phi_j dx dy - \int_0^S f_{20}^* \phi_j \Big|_{LE}^{TE} dy - \int_{LE}^{TE} f_{27}^* \phi_j \Big|_0^S dx \tag{4.8f}$$

$$(K_{31})_{ij} = \int_0^S \int_{LE}^{TE} f_6^* \phi_j dx dy - \int_0^S f_{17}^* \phi_j \Big|_{LE}^{TE} dy + \int_{LE}^{TE} f_{24}^* \phi_j \Big|_{y=0} dx - \int_{LE}^{TE} f_{32}^* \phi_j \Big|_{y=S} dx \tag{4.8g}$$

$$(K_{32})_{ij} = \int_0^S \int_{LE}^{TE} f_9^* \phi_j dx dy - \int_0^S f_{19}^* \phi_j \Big|_{LE}^{TE} dy - \int_{LE}^{TE} f_{26}^* \phi_j \Big|_0^S dx \tag{4.8h}$$

$$(K_{33})_{ij} = \int_0^S \int_{LE}^{TE} f_{12}^* \phi_j dx dy - \int_0^S f_{21}^* \phi_j \Big|_{LE}^{TE} dy - \int_{LE}^{TE} f_{28}^* \phi_j \Big|_0^S dx \tag{4.8i}$$

$$(H_{11})_{ij} = \int_0^S \int_{LE}^{TE} f_{13}^* \phi_j dx dy \tag{4.8j}$$

$$(M_{11})_{ij} = \int_0^S \int_{LE}^{TE} f_{14}^* \phi_j dx dy + \int_{LE}^{TE} f_{29}^* \phi_j \Big|_{y=0} dx - f_{33}^* \Big|_{LE}^{TE} \Big|_{y=0} \tag{4.8k}$$

Equations (4.8) have been derived by discretizing the extended Hamilton's principle in the form of eqn. (3.33). Equation (3.33), in turn, depends on variations in the strain energy and kinetic energy expressions, which have been integrated by parts as is required for deriving the boundary value problem. We can derive the algebraic eigenvalue problem directly from eqn. (3.20) by considering variations in the strain energy and kinetic energy expressions, eqns. (3.1) and (3.6). Proceeding as before, the algebraic eigenvalue problem can be formed for which the equations for $(K_{ab})_{ij}$, $(H_{11})_{ij}$ and $(M_{11})_{ij}$ become

$$(K_{11})_{ij} = -\int_0^S \int_{LE}^{TE} \Big\{ \phi_{i,x}\phi_{j,x}A_{55} + (\phi_{i,y}\phi_{j,x} + \phi_{i,x}\phi_{j,y})\, A_{45} + \phi_{i,y}\phi_{j,y}A_{44} + \frac{2q}{M}\left[1 + \frac{\gamma+1}{2}M\frac{d}{dx}t_N\right]\phi_{i,x}\phi_j \Big\}\, dxdy \tag{4.9a}$$

$$(K_{12})_{ij} = (K_{21})_{ji} = -\int_0^S \int_{LE}^{TE} \{\phi_{i,x}\phi_j A_{55} + \phi_{i,y}\phi_j A_{45}\}\, dxdy \tag{4.9b}$$

$$(K_{13})_{ij} = (K_{31})_{ji} = -\int_0^S \int_{LE}^{TE} \{\phi_{i,x}\phi_j A_{45} + \phi_{i,y}\phi_j A_{44}\}\, dxdy \tag{4.9c}$$

$$(K_{22})_{ij} = -\int_0^S \int_{LE}^{TE} \{\phi_i\phi_j A_{55} + \phi_{i,x}\phi_{j,x}D_{11} + \phi_{i,y}\phi_{j,y}D_{66} + (\phi_{i,y}\phi_{j,x} + \phi_{i,x}\phi_{j,y})\, D_{16}\}\, dxdy \tag{4.9d}$$

$$(K_{23})_{ij} = (K_{32})_{ji} = -\int_0^S \int_{LE}^{TE} \{\phi_i\phi_j A_{45} + \phi_{i,x}\phi_{j,x}D_{16} + \phi_{i,y}\phi_{j,x}D_{66} + \phi_{i,x}\phi_{j,y}D_{12} + \phi_{i,y}\phi_{j,y}D_{26}\}\, dxdy \tag{4.9e}$$

$$(K_{33})_{ij} = -\int_0^S \int_{LE}^{TE} \{\phi_i\phi_j A_{44} + \phi_{i,x}\phi_{j,x}D_{66} + \phi_{i,y}\phi_{j,y}D_{22} + (\phi_{i,y}\phi_{j,x} + \phi_{i,x}\phi_{j,y})\, D_{26}\}\, dxdy \tag{4.9f}$$

$$(H_{11})_{ij} = -\int_0^S \int_{LE}^{TE} \frac{2q}{UM}\left[1 + \frac{1+\gamma}{2}M\frac{d}{dx}t_N\right]\phi_i\phi_j dxdy \tag{4.9g}$$

$$(M_{11})_{ij} = -\frac{1}{2}\int_0^S \int_{LE}^{TE} m(x,y)\phi_i\phi_j dxdy$$
$$-\frac{1}{R}\int_{LE}^{TE}\left\{M_c\phi_i\phi_j + \frac{1}{2}\left[I_c + M_c\left(x_c - x\right)^2\right]\phi_{i,x}\phi_{j,x}\right\}\Big|_{y=0} dx$$
$$-\frac{M_c}{2R}\left(x_c - x\right)\phi_i\phi_j\Big|_{LE}^{TE}\Big|_{y=0} \qquad (4.9h)$$

The system is non-self-adjoint due to the presence of H_{11} and the nonconservative virtual work portion of K_{11}.

The form of the eigenvalue problem, eqn. (4.6) is not convenient for numerical solution. For a numerical solution, the second-order problem must be transformed into a first-order form, which can be expressed as follows:

$$[K^*]\,[\overline{a}^*] = \lambda\,[M^*]\,[\overline{a}^*] \qquad (4.10)$$

where

$$[\overline{a}^*] = \left[\overline{a}^T \vdots \lambda\overline{a}^T\right]^T \qquad (4.11a)$$

$$[K^*] = \begin{bmatrix} O & \vdots & I \\ \cdots & \cdots & \cdots \\ -K & \vdots & -H \end{bmatrix} \qquad (4.11b)$$

$$[M^*] = \begin{bmatrix} I & \vdots & O \\ \cdots & \cdots & \cdots \\ O & \vdots & M \end{bmatrix} \qquad (4.11c)$$

The solution of eqn. (4.10) is in general complex.

The eigenvalue problem for the corresponding self-adjoint system is

$$\left[\left[\hat{K}\right] + \lambda^2\,[M]\right][a] = 0 \qquad (4.12)$$

where

$$\left[\hat{K}\right] = \begin{bmatrix} \hat{K}_{11} & K_{12} & K_{13} \\ K_{21} & K_{22} & K_{23} \\ K_{31} & K_{32} & K_{33} \end{bmatrix} \qquad (4.13)$$

$$\hat{K}_{11} = -\int_0^S \int_{LE}^{TE} \left\{\phi_{i,x}\phi_{j,x}A_{55} + \left(\phi_{i,y}\phi_{j,x} + \phi_{i,x}\phi_{j,y}\right)A_{45} + \phi_{i,y}\phi_{j,y}A_{44}\right\} dxdy \qquad (4.14)$$

The matrix $\left[\hat{K}\right]$ is derived from a scalar potential function, so that it is symmetric, or

$$\left[\hat{K}_{ab}\right]_{ij} = \left[\hat{K}_{ba}\right]_{ji} \qquad a = 1,2,3; \quad b = 1,2,3 \tag{4.15}$$

In contrast with the eigenvalue problem for non-self-adjoint systems, eqn. (4.12) can be solved directly and its solution is real.

4.2 Admissible Functions: A Quasi-comparison Function Approach

The algebraic eigenvalue problem, eqns. (4.10) has been formulated in terms of a series approximation of the displacement variables. The formulation is such that the approximating functions may come from the large class of admissible functions. These functions need satisfy only the geometric boundary conditions and be sufficiently differentiable so that the integrals in eqns. (4.8) or (4.9) are defined. Indeed, considerable effort was made to avoid a solution requiring comparison functions as approximating functions. Comparison functions must satisfy all the boundary conditions and as such are a small subset of the class of admissible functions.

The problem under consideration includes natural boundary conditions, and rapid convergence depends on satisfaction of these boundary condtions. Exact satisfaction is very difficult, so that we seek an approximate satisfaction only, in the same manner as for the interior points. To this end, we choose admissible functions in such a way that finite linear combinations of them are capable of satisfying the natural boundary conditions exactly. This ensures that the boundary conditions will be solved approximately to any degree of accuracy desired, along with the differential equations. Admissible functions possessing this property are known as quasi-comparison functions (ref. 52). The set of quasi-comparison functions is a subset of the admissible functions and, in turn, contain the comparison functions as a subset.

A goal of this structural model is minimum calculation time, which requires rapid convergence. The quasi-comparison functions are selected from several families of functions, so that what is lacking in one family is compensated by another. Quasi-comparison functions selected in this manner can be shown to lead to very rapid convergence, even outpacing comparison functions chosen from a single family. Examples of this are contained in the paper by Meirovitch and Kwak, (ref. 52).

A set of two-dimensional functions in x and y must be selected for use in approximating the displacement field. Because the motion includes the possibility of rigid-body pitch and plunge in addition to flexible deformation, the two rigid-body shape functions are chosen as

$$\phi_1(x,y) = 1, \qquad \phi_2(x,y) = \frac{x}{R} \tag{4.16}$$

where R is the root chord length. The remaining $n-2$ functions are chosen from more than one family of functions. Meirovitch and Kwak, (ref. 52), demonstrated convincingly that selection from more than one family was more important than an attempt to pick functions that are similar to the expected eigenfunctions. Their paper showed that even very unusual choices of sets of functions lead to rapid convergence, provided that the several families are such that all the boundary conditions can be satisfied with a finite number of terms. A good choice might be a family of functions that crosses the nominal plane a correct number of times combined with some other family complementing these functions. Plate admissible functions constructed as products of uniform beam shape functions in the x and y directions appear as good candidates for quasi-comparison functions. Effort in that direction has revealed two shortcomings. The beam functions contain hyperbolic trigonometric functions, which lead to numerical difficulties if a sufficient number of terms are used. Secondly, a beam function contains four terms so that a two-dimensional function consisting of

the product of two of these functions has sixteen terms. Equations (4.9) require the integration of terms such as $\phi_i\phi_j$ which is now seen to have 256 terms. Any gain due to the quality of the approximating functions is lost in the complexity of evaluating them.

As shown in ref. 61, there is no urgency to approximate the mode shapes closely with each function. To do so is to ignore a basic premise of the method, namely, that the functions work together to produce an accurate approximation. Another, and far simpler selection, is a set of products of simple trigonometric series. The functions $\phi(i)$, $i = 3,4,\ldots,$ $(n+2)/2$, which are half of those remaining in an n function approximation, are such functions, or

$$\phi_i = X_k(x)Y_\ell(y); \qquad i = 3,4,\ldots,\frac{n+2}{2} \tag{4.17}$$

The spanwise functions $Y_\ell(y)$ are appropriate segments of a sine function chosen such that there is an appropriate number of zero crossings. Multiplication by y/S ensures the satisfaction of geometric boundary conditions and symmetry conditions at $y = 0$, so that we choose

$$Y_\ell(y) = \frac{y}{S}\sin\left[\frac{(2\ell-1)\pi}{2S}y\right], \qquad \ell = 1,2,3\ldots \quad 0 \le y \le S \tag{4.18}$$

The chordwise functions $X_k(x)$ are also segments of a sine function chosen to appropriately cross zero, or

$$X_k(x) = \sin\left[\pi\left(k+\frac{1}{2}\right)\frac{x}{R}\right]; \qquad k = 1,2,3\ldots \quad 0 \le x \le R \tag{4.19}$$

Equation (4.19) does not account for wing sweep, however, and when the variable limits of x are incorporated, X_k becomes a function of x and y. Furthermore, because there are no geometric boundary conditions along the leading and trailing edges, the first two $X_k(x)$ should be constant displacement and constant slope. This reflects the

possibility of plate modes with curvature in the y direction only, so that

$$X_k(x,y) = 1.0,\ k = 1,\ LE \leq x \leq TE \tag{4.20a}$$

$$X_k(x,y) = \frac{x}{R},\ k = 2,\ LE \leq x \leq TE \tag{4.20b}$$

$$X_k(x,y) = \sin\left\{\frac{3\pi}{4} + \pi\left(k - \frac{3}{2}\right)\left[\frac{x - y\tan\eta_L}{R - y(\tan\eta_L - \tan\eta_T)}\right]\right\}$$
$$k = 3,4,5\ldots\quad LE \leq x \leq TE \tag{4.20c}$$

The functions described by eqns. (4.18 and 4.19) are shown in Fig. 4.1 and 4.2. They bear some resemblance to beam free-free and cantilever modes, respectively.

Another family of ϕ_i for $(n+4)/2 \leq i \leq n$ is to be selected. Simple power series appear as good candidates, as they complement the trigonometric functions. As mentioned in the introduction, power series by themselves tend to experience numerical difficulties when a large number of terms is included. Giles (ref. 46) reported numerical problems with two-dimensional power series above x^4y^7. For integer exponents beginning with zero, x^4y^7 is the 40th term in the series. Another family, the sine functions, are included plus the two rigid-body modes, so that 82 terms can be used before the prospect of power series numerical difficulties arises. Also, more rapid convergence is to be expected, so that adequate accuracy can be anticipated with significantly fewer than 82 terms. This is shown to be the case in Chapter V.

The two-dimensional power series to be used has the form given by eqn. (4.17). The $Y_\ell(y)$ functions are zero at $y = 0$ and are equal to 1 at $y = S$, the semispan. The exponent begins at 2 and increases by increments of 0.5, or

$$Y_\ell(y) = \left(\frac{y}{S}\right)^{\left(\frac{\ell+3}{2}\right)},\quad \ell = 1,2,3,\ldots \qquad 0 \leq y \leq S \tag{4.21}$$

The X_k functions are also power series, except that they alternate direction between the leading edge and the trailing edge. The wing sweep requires shifting and scaling

as before, resulting in X_k becoming functions of x and y, so that

$$X_k(x,y) = \left\{ \frac{\frac{R}{2}\left[1+(-1)^k\right] - (-1)^k x + \frac{1}{2}\left[1+(-1)^k\right](\tan\eta_T - \tan\eta_L)\, y}{R + (\tan\eta_T - \tan\eta_L)\, y} \right\}^{\mathrm{INT}\left(\frac{k+3}{2}\right)}$$
$$k = 1,2,3\ldots \qquad LE \le x \le TE \tag{4.22}$$

where INT( ) implies truncation to the corresponding integer value. Graphs of these $X_k(x,y)$ and $Y_\ell(y)$ appear as Figures 4.3 and 4.4.

Selection of the approximating functions as combinations of chordwise and spanwise functions from several families as the number n of terms increases is somewhat complicated. The order of selection within a given family affects the accuracy for a given number n of terms and hence the rate of convergence. The admissible functions are more simply expressed in terms of certain constants, which themselves depend on the function position in the n series of functions. The order of selection within a given family is indicated by the choice of KI and LI (or KJ and LJ) which depend on i and j. Because the low aspect ratio case is important, the chordwise and spanwise functions are combined such that the number of each considered is about equal for a given number of terms and a given family of functions. This implies that spanwise and chordwise modes are about equally important for the representation of low aspect ratio wings. The entries in TABLE 4.1 show the order of selection of spanwise and chordwise functions within a given family. The table values correspond to i beginning at 1 for a given family of functions.

The algebraic eigenvalue problem is assembled inside a double loop from 1 to n. For a given i or j, subtracting 2 for the trigonomentric series or $(n+2)/2$ for the power series gives the corresponding value found in TABLE 4.1 which now begins at 1 for each new family of functions. From this value KI and LI (or KJ and LJ), may be found. In terms of i,

TABLE 4.1 Function Selection Order

		Spanwise Functions, $Y_\ell(y)$						
	LI	1	2	3	4	5	6	7
	KI							
Chordwise	1	1	3	6	10	15	21	28
Functions	2	2	5	9	14	20	27	
$X_k(x,y)$	3	4	8	13	19	26		
	4	7	12	18	25			
	5	11	17	24				
	6	16	23					
	7	22						

$$\begin{aligned} LI =& i - 2 - \left(\text{DIAG}^2 - \text{DIAG}\right)/2\,, \qquad i = 3,4,\ldots,\frac{n+2}{2} \\ =& \left(2i - 2 - n - \text{DIAG}^2 + \text{DIAG}\right)/2\,, \qquad i = \frac{n+4}{2},\ldots,n \end{aligned} \tag{4.23}$$

$$KI = \text{DIAG} + 1 - LI\,, \qquad i = 3,4,\ldots,n \tag{4.24}$$

where DIAG is the number of the diagonal of TABLE 4.1 and is determined as:

$$\begin{aligned} \text{DIAG} =& \text{NINT}\sqrt{2i-4}\,, \qquad i = 3,4,\ldots,\frac{n+2}{2} \\ =& \text{NINT}\sqrt{2i-n-2}\,, \qquad i = \frac{n+4}{2},\ldots,n \end{aligned} \tag{4.25}$$

where $NINT(\ )$ implies the nearest integer. A similar process exists for J. For each pass through the double i,j loop, each value of $(K_{ab})_{ij}$, $(M_{11})_{ij}$ and $(H_{11})_{ij}$ is evaluated for each i,j pair inside the i,j loop.

The complete set of two-dimensional approximating functions in terms of i through LI and KI is

$$\phi_1 = 1, \qquad \phi_2 = \frac{x}{R} \tag{4.26a,b}$$

$$\phi_i = \frac{y}{S}\sin AIy, \qquad i = 3,4,\ldots,\frac{n+2}{2}, \quad KI = 1 \tag{4.27a}$$

$$\phi_i = \frac{xy}{RS}\sin AIy, \qquad i = 3,4,\ldots,\frac{n+2}{2}, \quad KI = 2 \tag{4.27b}$$

$$\phi_i = \frac{y}{S}\sin(AIy)\sin\frac{B + xCI + y\ DI}{R + yEA}$$
$$i = 3,4,\ldots,\frac{n+2}{2}, \qquad KI \geq 3 \tag{4.27c}$$

$$\phi_i = \left(\frac{y}{S}\right)^{NI} \qquad i = \frac{n+4}{2},\ldots,n, \quad KI = 1 \tag{4.28a}$$

$$\phi_i = \frac{x}{R}\left(\frac{y}{S}\right)^{NI} \qquad i = \frac{n+4}{2}\ldots,n, \quad KI = 2 \tag{4.28b}$$

$$\phi_i = MI\ y^{NI}\left[\frac{1}{2}(1 - QI) + QI\frac{x + yP}{R + y\ EA}\right]^{SI}$$
$$i = \frac{n+4}{2},\ldots,n, \quad KI \geq 3 \tag{4.28c}$$

where

$$B = \frac{3R\pi}{4}, \quad EA = \tan\eta_T - \tan\eta_L, \quad P = -\tan\eta_L \tag{4.29a,b,c}$$

$$AI = \frac{(2LI - 1)\,\pi}{2S}, \quad CI = \pi\left(KI - \frac{3}{2}\right), \quad DI = \pi\left[\frac{3}{4}EA + \left(KI - \frac{3}{2}\right)P\right] \tag{4.29d,e,f}$$

$$MI = \left(\frac{1}{S}\right)^{NI}, \quad NI = \left(\frac{LI + 3}{2}\right), \quad QI = -(-1)^{KI}, \quad SI = INT\left(\frac{KI + 1}{2}\right) \tag{4.29g,h,i,j}$$

Similar series are used for $j = 1,2,\ldots,n$ so that eqns. (4.26-4.25) have their counterparts in j.

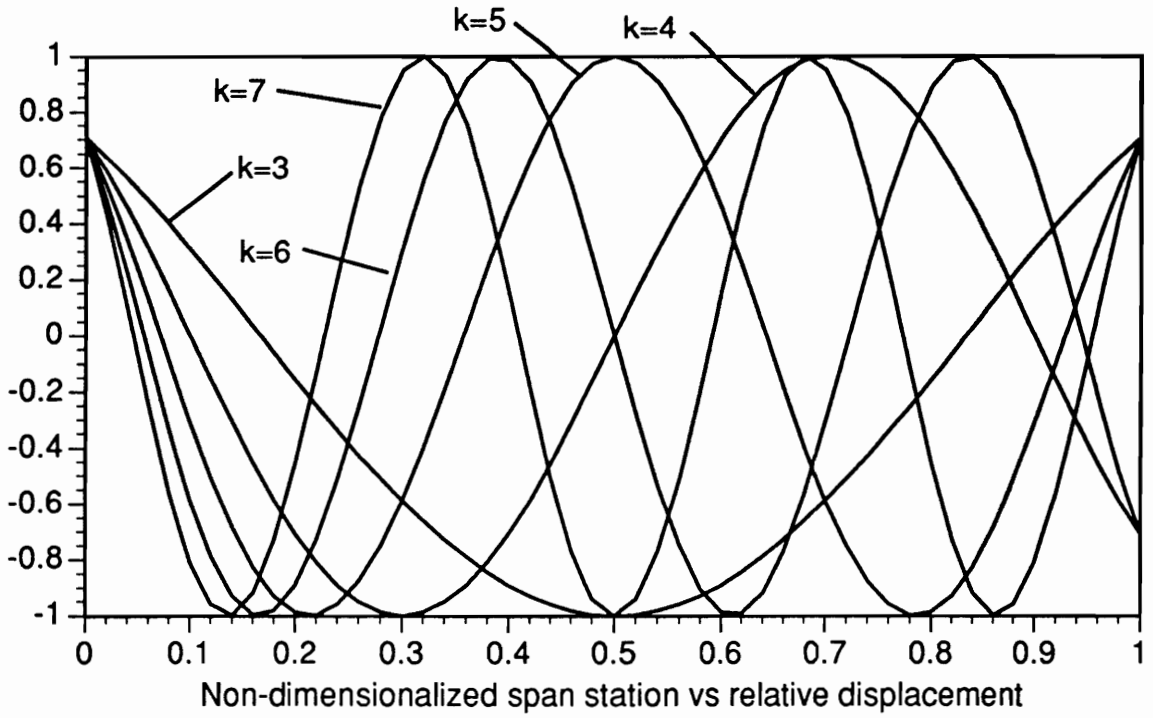

FIGURE 4.1 - $X_k(x)$ - the Sine Series

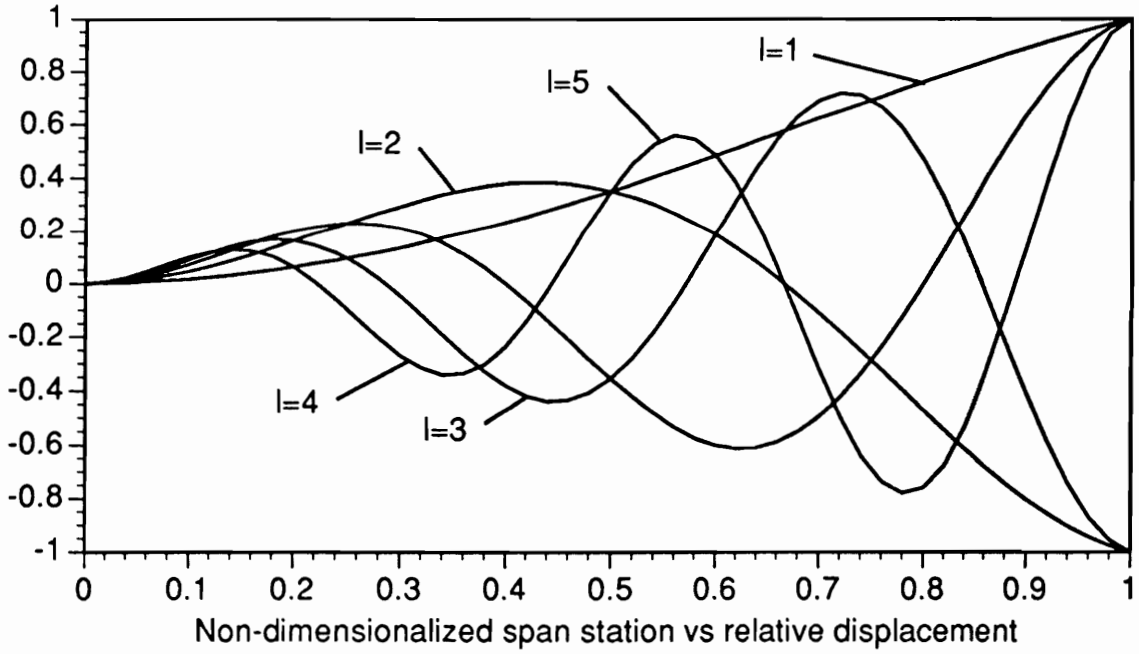

FIGURE 4.2 - $Y_l(y)$ - the Sine Series

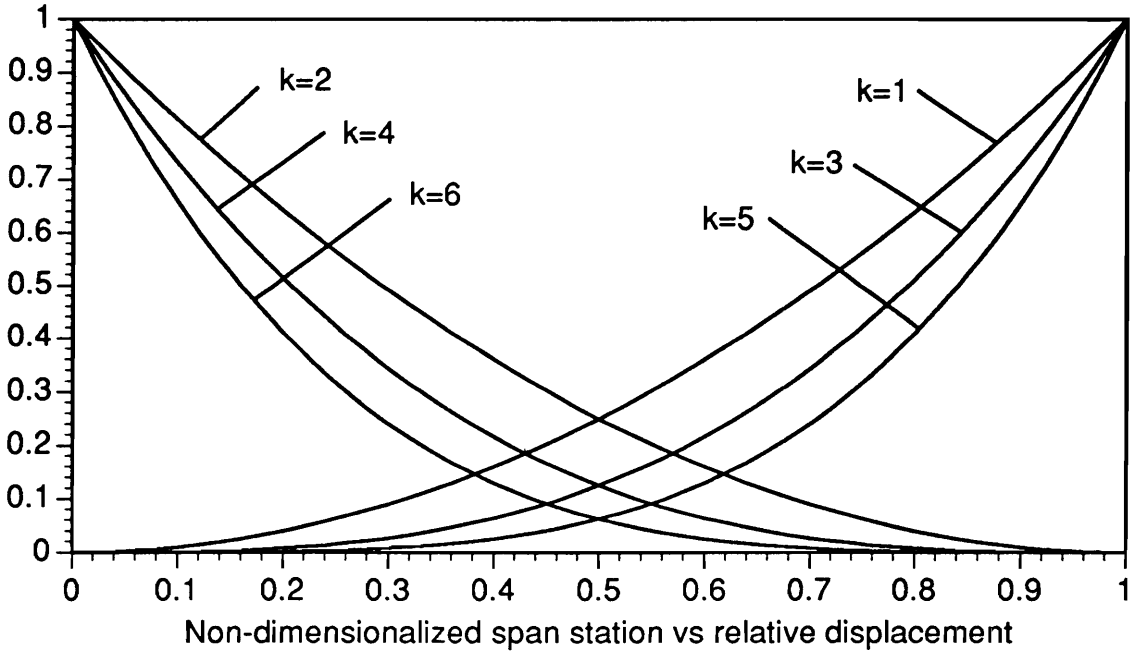

FIGURE 4.3 - $X_k(x,y)$ - the Power Series

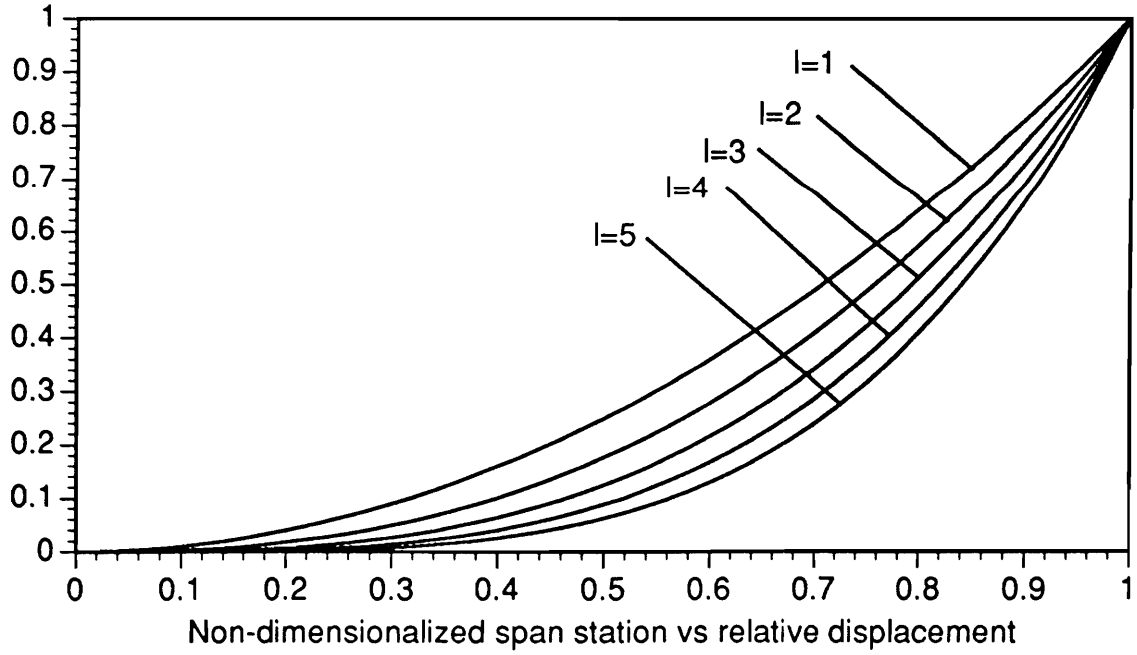

FIGURE 4.4 - $Y_l(y)$ - the Power Series

CHAPTER V

NUMERICAL RESULTS

In presenting numerical results, it is useful to define several dimensionless quantities. The frequency can be nondimensionalized as follows:

$$\Omega = \omega A \left[\frac{\rho_{\text{ref}}}{E_{\text{ref}} t_{\text{ref}}^2} \right]^{1/2} \tag{5.1}$$

Similarly, a speed parameter can be defined that yields the dimensionless dynamic pressure

$$\lambda_a = \frac{2qA^2}{E_{\text{ref}} t_{\text{ref}}^4} = \frac{\rho_{\text{air}} U^2 A^2}{E_{\text{ref}} t_{\text{ref}}^4} \tag{5.2}$$

The quantities $(\ )_{\text{ref}}$ are reference values. The quantities E_{ref} and ρ_{ref} are E_2 and ρ for the main structural material, t_{ref} is the total thickness at the wing root and leading edge intersection. Other dimensionless parameters are those conventionally used for wing geometry, such as the taper ratio TR and the aspect ratio AR. The former is the tip chord divided by the root chord and the latter is the square of the total span divided by the total wing area. Next, two parameters associated with the distribution of a tailoring ply are introduced. The parameter CSKEW specifies a linear thickness distribution from a value of -1 corresponding to the maximum thickness of the layer at the trailing edge to a value 1 corresponding to the maximum thickness at the leading edge. The nominal thickness value for the tailoring layer corresponds to CSKEW = 0. The parameter SSKEW is specified in the same way, with the limits applying in the spanwise direction from the wing root to the wing tip. The distribution of these two parameters is such that the total mass of the layer and the external shape of the wing remain constant. Moreover, the fact that CSKEW can take negative values does not imply that the layer thicknesses become negative.

Figure 5.1 shows a rectangular wing, with the middle layer being regarded as the tailoring layer. In Fig. 5.1a, the tailoring layer is at its nominal thickness distribution corresponding to both CSKEW and SSKEW equal to zero. In Fig. 5.1b, a condition corresponding to SSKEW approaching 1 is depicted with the tailoring plies being most heavily distributed near the wing tip. Figures 5.1c and 5.1d correspond respectively to CSKEW = 1 and CSKEW = −1.

5.1 Convergence and Accuracy

The analytical model derived in Chapter IV is solved numerically by means of a computer program. Parametric studies of both the free vibration and the flutter problems are discussed in Sections 5.2 and 5.3. First, the convergence and accuracy of the present model is considered.

The convergence of the free vibration eigenvalues of an anisotropic low aspect ratio wing is considered in Fig. 5.2. This nominal wing is designated AN1 in TABLE 5.1. The convergence rate of the first five nonzero eigenvalues is depicted as the frequency parameter Ω versus the number of terms in the approximating series. The first two eigenvalues have zero value and correspond to rigid-body modes, which converge immediately; they are not shown in Fig. 5.2. It should be pointed out here that a linear combination of admissible functions must possess a minimum number of terms before it qualifies as a quasi-comparison function. The number must be such as to permit satisfaction of all natural boundary conditions. As soon as this number of terms has been reached, convergence of the computed eigenvalues to the actual ones is relatively rapid.

The two flutter mechanisms of most concern are the bending-torsion mode and the body-freedom mode. The body-freedom flutter mode occurs instead of the divergence mode when pitch freedom is introduced. Reasonably accurate representations of the pitch mode and the first two flexible modes, as well as fairly accurate representation

of the third flexible mode, are required to capture these two mechanisms. The indications from Fig. 5.2 are that 20 terms are sufficient for this purpose, certainly for establishing a trend.

Convergence of the flutter dynamic pressure parameter for a forward swept variant of AN1 is shown in Fig. 5.3. The flutter mechanism acting is body-freedom flutter. Reasonable convergence has been achieved with 20 terms.

Computational costs are depicted in Fig. 5.4 showing CPU in seconds versus the number of terms for three solutions. It is clear that the basic problem formulation and associated numerical integrations constitute the bulk of the computing costs. Graph 3 of Fig. 5.4 makes clear that neither the aerodynamic terms nor the eigensolutions add excessively to the total cost.

Fig. 5.5 shows three frequencies corresponding to an isotropic plate of aspect ratio 5; the computed values are compared with the exact values given in Table 11.4 of Ref. 66. The plate is 1/2 inch steel and is fixed on a short side (see PL1 of Table 6.1). The remaining three edges are free. The clamped condition is simulated with the present model by taking very large values for fuselage mass and pitch inertia. The results are quite acceptable. As expected from the discussion of quasi-comparison functions in Section 4.3, the matching is poor for small numbers of terms but begins to converge quite rapidly when a certain critical number of terms is reached.

The accuracy of the flutter analysis is checked through a comparison with results obtained in ref. 67 by Rossettos and Tong, which is one of the few works available on the flutter of a plate with free edges in the supersonic region. Their model consists of a single layer, constant thickness, square composite plate clamped at one edge and subjected to supersonic flow on the upper surface. The aerodynamics is based on a variant of the piston theory that converges to eqn. (3.10) for sufficiently high Mach numbers and with flow over both surfaces. Comparison is for a square composite

plate, PL2 of TABLE 5.1, with a fiber orientation of 24°. The model derived here predicted on the average flutter speeds 6% higher than those of Ref. 67.

5.2 Free Vibration Results

Several trial wings were developed to demonstrate various characteristics of fluttering wings; they are listed in TABLE 5.1. The anisotropic wing AN1 is very general and is considered representative of actual modern fighter aircraft. The F-16, developed by General Dynamics, is a single engine, single pilot, light-weight air combat aircraft. The AN1 wing, while not identical to the F-16 wing, shares many characteristics with it. References 68 and 69 contain several anisotropic composite variants of the present F-16 aluminum structure. The nominal AN1 wing is unswept. However with a 17° aft sweep, the AN1 is quite similar to these variants and as such is considered a realistic structure. The layup, in addition to being described in TABLE 5.1, is also depicted in Fig. 5.6.

The fifth and outermost layer is the layer used for tailoring. Its thickness is chosen such that the layer comprises 30% of the skin. During parametric studies, the core thickness distribution is varied to accommodate the tailoring variations. This allows the skin weight and the external shape to remain constant during variation of the material distribution. The result is more nearly independent, single variable parametric studies.

The AN1 wing is realistic and contains already some tailoring in its nominal form. The OR1 wing is a similar but strictly orthotropic structure. It is described in TABLE 5.1. It also contains a tailoring layer that renders the layup anisotropic if its filament angle departs from the nominal value of 0°.

A larger aspect ratio isotropic wing is also included for comparison to more conventional wing results. It is designated IS1 and includes an orthotropic tailoring layer as well. Finally there are two rectangular plates, designated PL1 and PL2,

which were used in Section 5.1 for convergence and accuracy studies.

The interest in the free vibration case is mainly for its relation to the flutter results. The two flutter mechanisms, body-freedom and bending-torsion, dictate that we concentrate on the pitch mode and the first two flexible modes, although the first few flexible modes above these will also have some influence. The rigid-body modes, pitch and plunge, are input directly as admissible functions, so that their convergence is not an issue. The convergence of the flexible mode shapes and frequencies was discussed in Section 5.1.

Representative mode shapes are depicted for the following example. An orthotropic plate, PL3 of TABLE 5.1, is analyzed and its free vibration mode shapes are plotted in Figs. 5.7-5.13. Even for an aspect ratio of 4, the importance of the chordwise flexibility is evident in the 3rd flexible mode and is dominant in the 5th flexible mode. The significance of slight differences in the mode shapes is demonstrated in Figs. 5.14 and 5.15. These figures are comparable to Figs. 5.9 and 5.10, except that the former pair are for a 20° forward sweep of the tailoring layer. While the difference in the mode shapes is slight, the change in bending-torsion frequency ratio is significant and results in a large flutter dynamic pressure increase.

The location of the wing with respect to the center of mass of the airplane has an effect on the wing frequencies. Figure 5.16 shows the frequency parameter variation with the fuselage mass center position for the AN1 wing. This wing is critical in bending-torsion flutter, so that the separation of those two frequencies is paramount. Figure 5.16 tempts one to speculate that the ideal mass center position for AN1 is just ahead of the midchord. This case is considered in Section 5.3.

For body-freedom flutter, the most critical parameter is geometrical. If the wing is not swept forward or nearly so then this flutter mechanism cannot arise. Work by Weisshaar (refs. 27, 42, 43) and Miller (ref. 70) and others demonstrate a surprising

influence of a tailoring layer swept just a few degrees off nominal. Body-freedom flutter can be eliminated, or pushed up to significantly higher speeds, if a percentage of the spanwise plies are reoriented 10° forward. Two factors are at work in this case and both are free vibration matters. When an orthotropic layer for which $E_1 >> E_2$ is reoriented, bending begins to occur in the direction normal to E_1. The result is an effective rotation of the elastic axis in the direction opposite to the reorientation of the tailoring ply. The other factor at work is the necessary reduction of spanwise bending stiffness that must accompany the reorienting of plies away from the midchord. This second factor eventually overpowers the first, so that ply reorientations are most effective when they are small.

Figure 5.17 shows the frequency parameter of the first flexible mode varying with the sweep angle of a tailoring layer. The results for three wings are shown. An interesting phenomenon is observed in Fig. 5.17 for the low aspect ratio wing. This wing has its highest bending stiffness associated with a significantly aft swept tailoring layer, $\theta = 10°$. The implication is that tailoring plies might not be as effective for low aspect ratio wings. This trend, shown to be true in the next section, was not previously discovered due to inherent limitations of the one-dimensional models commonly used.

Much has been said about the benefits of using the anisotropicity of a composite layup to tailor the response of a wing. Such discussion has been limited almost entirely to ply orientation. The dominant use of one-dimensional structural models has forced this limitation on the current investigation. One can easily suppose that distribution of the tailoring material in both the spanwise and chordwise directions might significantly affect the response. These trends are readily investigated with the current plate model through the parameters CSKEW and SSKEW introduced earlier. To this end, we consider the AN1 wing with the tailoring layer set to the nominal

sweep of zero. As ply distribution is varied from a concentration near the trailing edge to the leading edge, there is a change in frequency of the natural modes. The associated frequency parameters increase by 8%, 6% and 3%, respectively, for the first three flexible modes. The bending-torsion separation increases by 5%. For a similar spanwise variation from wing tip concentration to wing root, frequencies again vary. In this case, the increases are 34%, 14% and 12%, respectively, for the first three flexible modes. For bending-torsion separation, the change is slight at 2.5%. This reflects the increase in bending stiffness, which occurs when material is shifted near the wing root. Clearly, the two-dimensional nature of this material distribution has an effect on the free vibration outcome. It seems reasonable to expect that the flutter response will also be affected, allowing a refinement of the concept of tailoring with composites.

5.3 Flutter Analysis Results

Two flutter mechanisms are of primary concern for a symmetric model of a wing with forward or aft sweep. The first is the classical bending-torsion flutter that can occur for a wing of any sweep when the frequencies of these two modes begin to coalesce as the speed increases. The AN1 wing described in TABLE 5.1 is a tailored anisotropic wing in its nominal form. Figure 5.18 contains two graphs depicting bending-torsion flutter for the AN1 wing with 30% of forward sweep and half the nominal core thickness. The upper graph shows α, the real part of the eigenvalue, plotted versus the dynamic pressure. For negative values, this quantity corresponds to aerodynamic damping. The lower graph is Ω vs q, the imaginary part of the eigenvalue plotted versus the dynamic pressure. The classical separation response of the two modes is seen in the α versus λ_a plot of Fig. 5.18. One mode, the torsion mode, turns downward toward a very stable condition just as the bending mode heads for instability. In the Ω versus λ_a plot the two frequencies are seen to coalesce as

the instability approaches. Complete coalescence does not occur when the fuselage is capable of rigid-body motions. The rigid-body pitch frequency is seen to assume a nonzero value, which rises as the speed increases. Without the tailored layup of AN1, the pitch and bending modes would surely combine to cause body-freedom flutter before the bending-torsion coupling could arise. Recall that bending-torsion flutter is unlikely at any speed for this angle of forward sweep. It is seen then that the same tailoring which eliminates body-freedom flutter by apparent aft sweeping of the elastic axis also makes bending-torsion flutter possible. A trade-off is implied and caution must be exercised when contemplating a tailored composite design solution.

The OR1 wing with a 30° forward sweep is considered next to examine the characteristics of body-freedom flutter. Because OR1 is orthotropic and the sweep is forward, the flutter mode will be body-freedom flutter, or divergence if clamped. The bending-torsion case occurs at a much higher speed or may not occur at all for this large angle of forward sweep. The α versus λ_a and Ω versus λ_a plots for this case are shown in Fig. 5.19. The pitch mode is characteristically very lightly damped and moves toward instability as the bending mode moves away from the imaginary axis. The pitch and bending frequencies coalesce now with increasing dynamic pressure rather than separating as in the previous example.

Weisshaar (ref. 42) et al have reported a trend in the ratio $\Omega_{\text{flutter}}/\Omega_{\text{fundamental}}$ for the two flutter mechanisms just presented. In a particular case in Ref. 42, the ratio is equal to 0.26 for a body-freedom flutter and to 3.40 for a bending-torsion flutter. Figures 5.18 and 5.19 confirm this trend with ratios of 0.42 and 2.64, respectively.

In Section 5.2, the effect of the fuselage mass center position on the bending-torsion frequency separation was considered. Some authors have considered fuselage rigid-body motions in their work and have found that the mass center position affects the flutter speed significantly. Miller (ref. 70) argues that the fuselage mass center

position changes the phasing between the bending and pitch modes. This is analogous to the widely held concept of using mass ballast to alter the phasing between bending and torsion modes to control bending-torsion flutter. "When the wing is undergoing a natural bending motion, a pitching moment is created about the aircraft center of mass because the wing center of mass is either forward or aft of the aircraft center of mass. In free vibration modes, angular momentum must be equal to zero. Thus the fuselage pitches in such a way that a moment is produced which opposes that of the wing bending motion, resulting in zero angular momentum." (Miller et al, ref. 70).

In Fig. 5.20, λ_{ac} is plotted versus the fuselage mass center position for the AN1 wing. In the previous section, frequency separation was identified as a mechanism whereby the mass center position affects the flutter speed. Phase adjustment has now also been considered to be involved. These combine to place the optimum mass center location for this wing at 30% of the chord location. The mass center position is clearly a factor in determining the flutter dynamic pressure, but cannot be accounted for without the fuselage rigid-body motions being included in this model.

The effect of wing sweep on flutter dynamic pressure is considered next. The orthotropic wing OR1 is depicted in Fig. 5.21 for midchord sweep angles between 40° and −40°. In addition to the two mechanisms discussed throughout this chapter, the clamped bending-torsion and clamped divergence cases are also plotted for comparison. A number of sources confirm the implications of Fig. 5.21, i.e., forward swept wings are prone to divergence or body-freedom flutter while aft swept wings are prone to bending-torsion flutter.

The effect of tailoring plies, particularly on divergence or body-freedom flutter has received a great deal of attention. Figure 5.22 shows the flutter dynamic pressure versus the tailoring ply angle for three wings. In all three cases, body-freedom flutter is critical and small negative ply angles are expected to be effective. There

is an implication in Fig. 5.17 that the low aspect ratio wing does not realize much benefit, because its maximum bending stiffness occurs for a somewhat more aft swept configuration than the other higher aspect ratio cases. This fact, demonstrated in Fig. 5.22, has important design implications for the design of low aspect ratio wings. If the model used does not account for low aspect ratios, then this phenomenon will be entirely missed.

Figure 5.22 shows the interesting and somewhat surprising result that flutter dynamic pressure is strongly affected by very small changes in the layer orientation in the vicinity of 0°. Blair (ref. 27) states that "It is difficult to appreciate that such a small change in fiber orientation can so drastically affect aeroelastic performance of a physical system." Reference 27 verifies this statement experimentally.

Virtually all the analytical and experimental work on tailoring forward swept wings to date does not consider low aspect ratio wings. It seems that this area deserves further investigation.

Finally, we wish to consider the distribution of tailoring plies over the wing planform. The present model is ideally suited to investigation of parameters such as layer thicknesses, which are free to vary in both chordwise and spanwise directions. Such distribution investigations are likely to result in lower structural weight or higher flutter speeds, so that they must be included in any search for an optimal wing design. The present model can be used to conduct such investigations with ease. The parameters CSKEW and SSKEW are used to accomplish this. The results are impressive. In the chordwise direction, a flutter dynamic pressure increase of 25% or decrease of 25% is observed, depending on whether the leading or trailing edge is favored for material placement, respectively. Similarly, in the spanwise direction, the flutter dynamic pressure increases 29% if the wing root is favored, but drops 35% if the plies are concentrated near the tip. These results are for an OR1 wing of aspect

ratio 6 and a forward sweep angle of 20°. The tailoring layer is as described in TABLE 5.1 and is swept 10° forward of the midchord line. These new results go a long way toward justifying this more sophisticated model.

TABLE 5.1: NOMINAL EXAMPLE WINGS

DESIGNATION:		AN1	OR1	IS1	PL1	PL2	PL3
Layer Materials		1C/4GE	1C/4GE	1C/1A/1GE	1S	1R	1C/4GE
Tailoring Layer		5	5	3	—	—	5
Total Wing Area in^2		40320.	40320.	40320.	4204.8	20000.	40320.
Taper Ratio		.3333	.3333	.3333	1.0	1.0	1.0
Aspect Ratio		3.0	3.0	8.0	5.0	2.0	4.0
Midchord Sweepback (deg)		0.0	0.0	-20.0	0.0	0.0	0.0
Non-Wing Aircraft Weight (lbs)		18000.	18000.	18000.	∞	∞	18000.
Non-Wing Aircraft Pitch Inertia (lb-in-sec^2)		5.0E7	5.0E7	5.0E7	∞	∞	5.0E7
Non-Wing Aircraft CG As percent Root Chord		0.46	-0.35	-.25	—	—	-.25
Total Fuel Weight (lbs)		1200.	1200.	1200.	0.0	0.0	1200.
Total Non-Skin Wing Structural Weight (lbs)		1000.	1000.	1000.	0.0	0.0	1000.
Thickness	LE,ROOT	3.284	2.500	5.000	0.25	.7122	5.0
of the	TE,ROOT	.682	2.500	5.000	0.25	.7122	5.0
1st Layer	LE,TIP	1.006	1.000	2.000	0.25	.7122	2.0
Thickness	LE,ROOT	.0595	.0500	.210	—	—	.0500
of the	TE,ROOT	.0455	.0500	.210	—	—	.0500
2nd Layer	LE,TIP	.0405	.0300	.126	—	—	.0300
Thickness	LE,ROOT	.0475	.0500	.0500	—	—	.0500
of the	TE,ROOT	0595	.0500	.0500	—	—	.0500
3rd Layer	LE,TIP	.0350	.0300	.0300	—	—	.0300
Thickness	LE,ROOT	.0440	.0500	—	—	—	.0500
of the	TE,ROOT	.0300	.0500	—	—	—	.0500
4th Layer	LE,TIP	.0370	.0300	—	—	—	.0300
Thickness	LE,ROOT	.0649	.0600	—	—	—	.0600
of the	TE,ROOT	.0581	.0600	—	—	—	.0600
5th Layer	LE,TIP	.0484	.0360	—	—	—	.0360
Layer Orientation from Midchord (Deg. AFT)		-/-17/38 -52/0/-	-/-45/45 0/0/-	-/-/0	—	0	-/-45/45 0/0/-

TABLE 5.2 NOMINAL MATERIALS

		Low Stiffness Core "C"	Aluminum "A"	Steel "S"	Graphite Epoxy "GE"	Composite Per (Ref. 124) "R"
E_1	lb-in^2	100.	1.03E7	3.0E7	2.1E7	2.1E7
E_2	lb-in^2	100.	1.03E7	3.0E7	1.7E6	1.5E6
ν_{21}		.3	.334	.3	.017	.01714
ν_{12}		.3	.334	.3	.210	.24
G_{23}	lb-in^2	30.	3.8E6	1.15E7	6.5E5	5.46E5
G_{13}	lb-in^2	30.	3.8E6	1.15E7	6.5E5	5.46E5
G_{12}	lb-in^2	30.	3.8E6	1.15E7	6.5E5	5.46E5
ρ	lb-in^{-3}	.00116	.098	.283	.054	.054

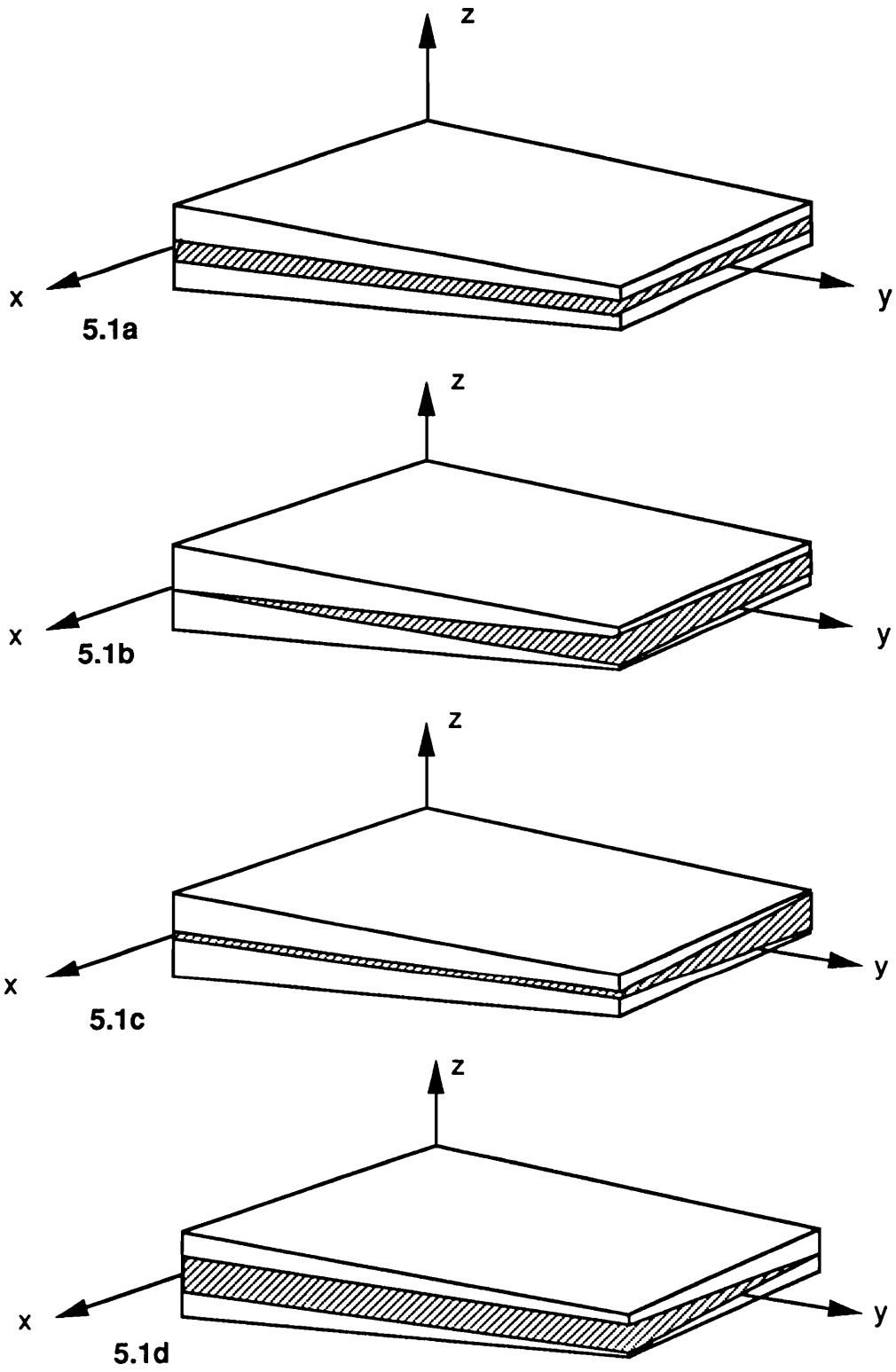

FIGURE 5.1 Tailoring Ply Distribution

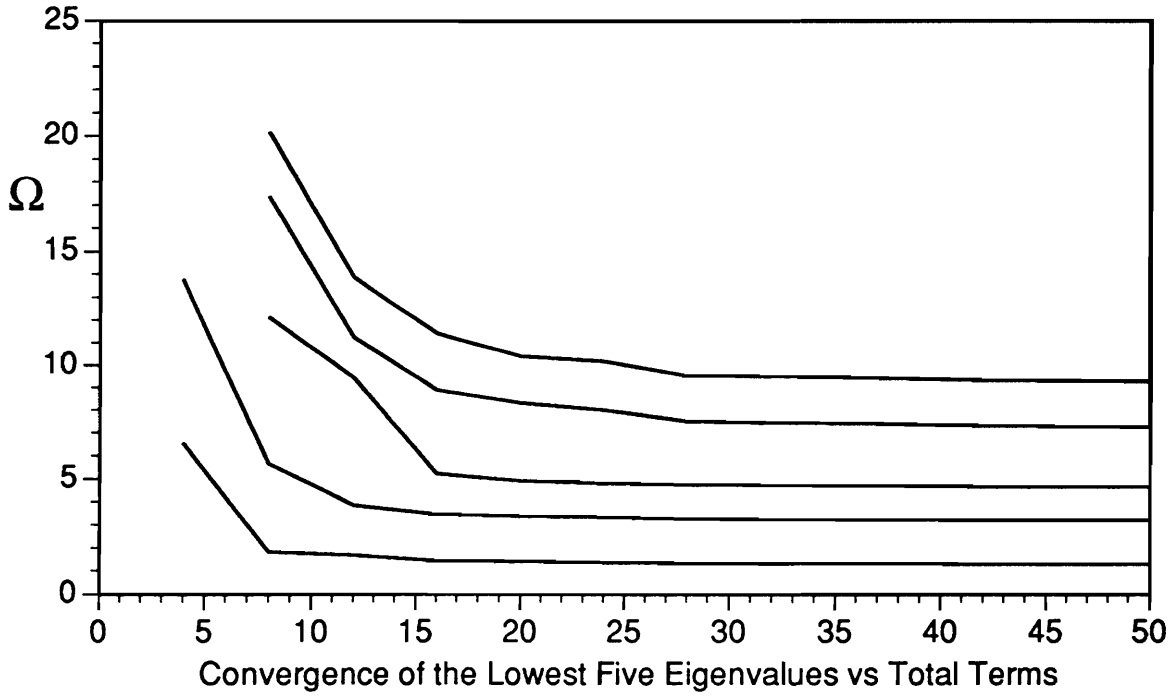

FIGURE 5.2 - Free Vibration Convergence for AN1

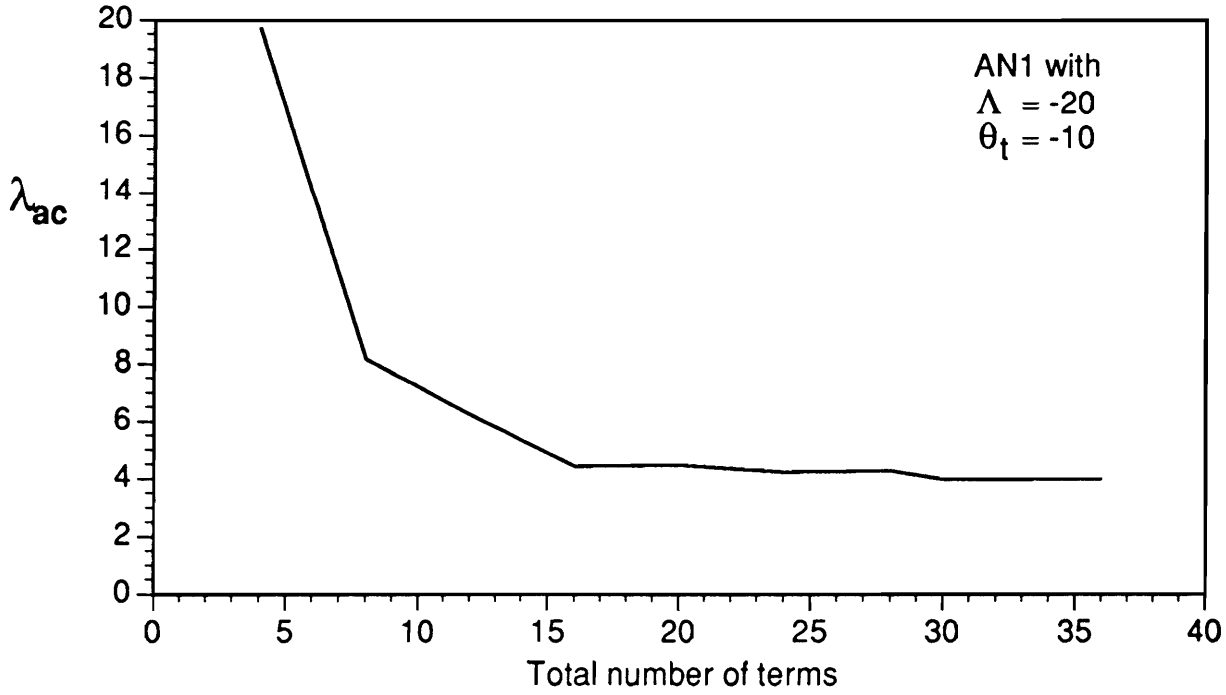

FIGURE 5.3 - Convergence of the Flutter Dynamic Pressure

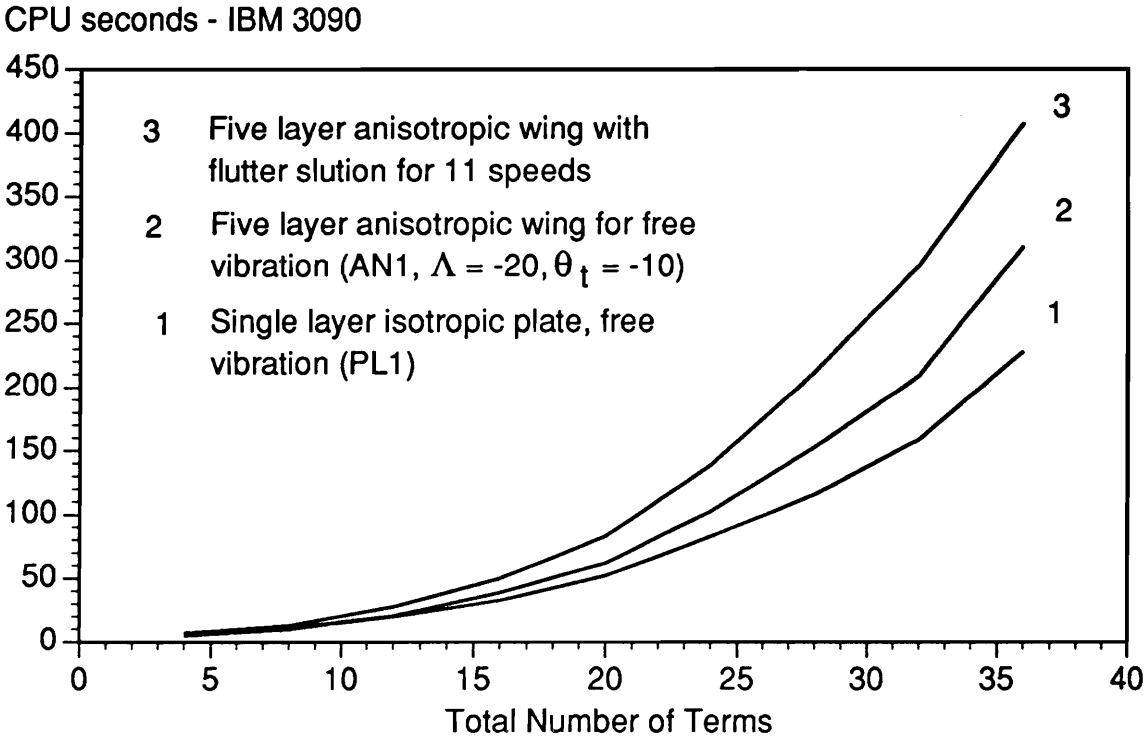

FIGURE 5.4 - Computing Cost Apportionment

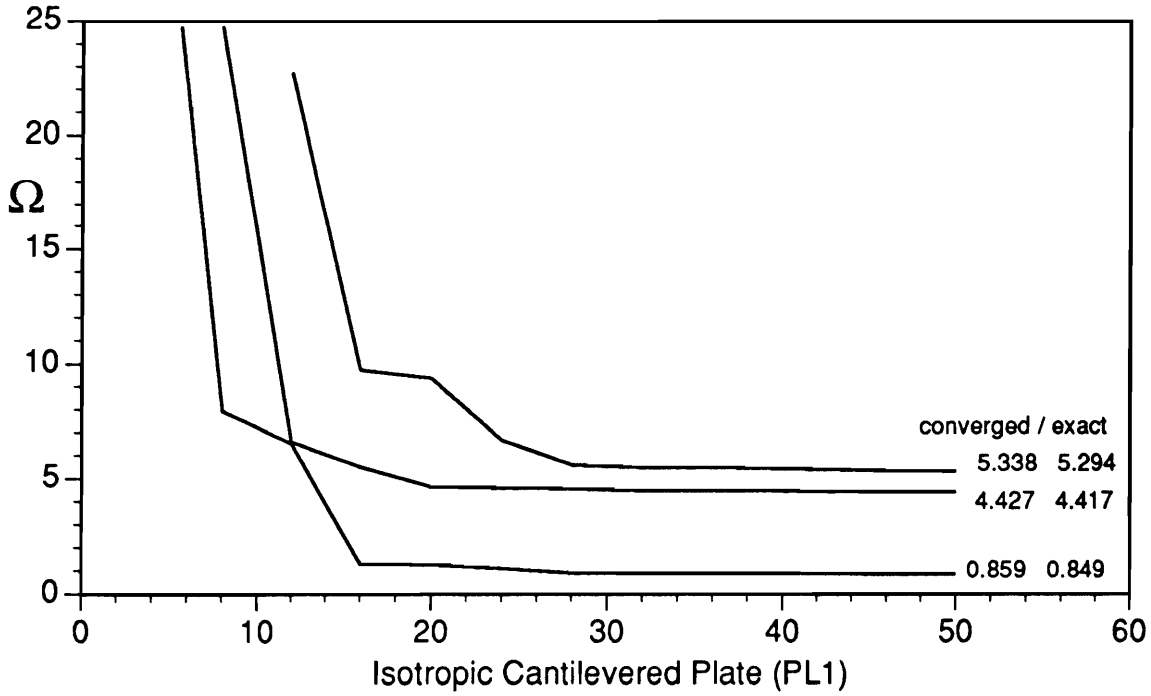

FIGURE 5.5 - Convergence to Known Values of Ω

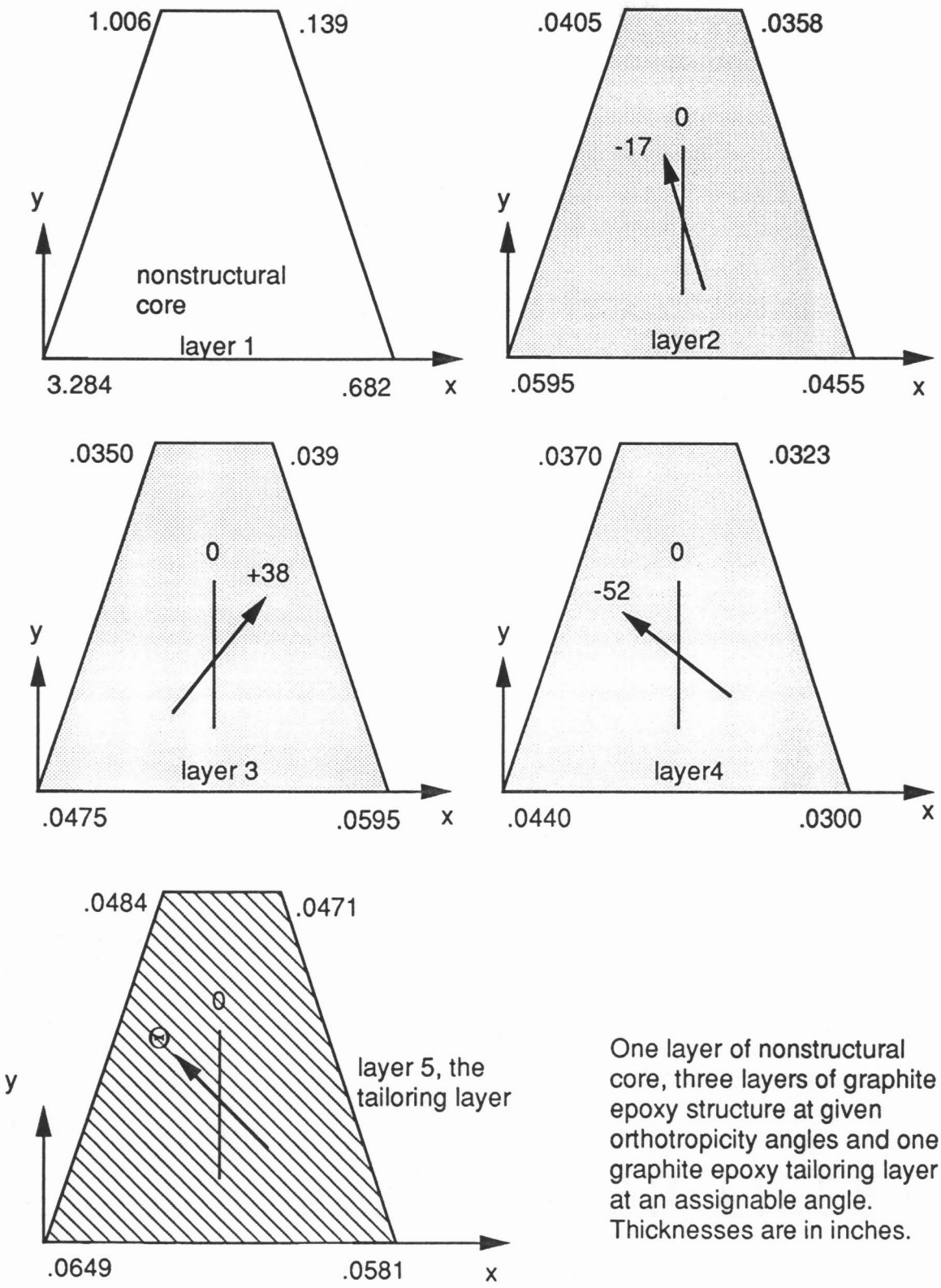

One layer of nonstructural core, three layers of graphite epoxy structure at given orthotropicity angles and one graphite epoxy tailoring layer at an assignable angle. Thicknesses are in inches.

FIGURE 5.6 - Layup of AnisotropicWing - AN1

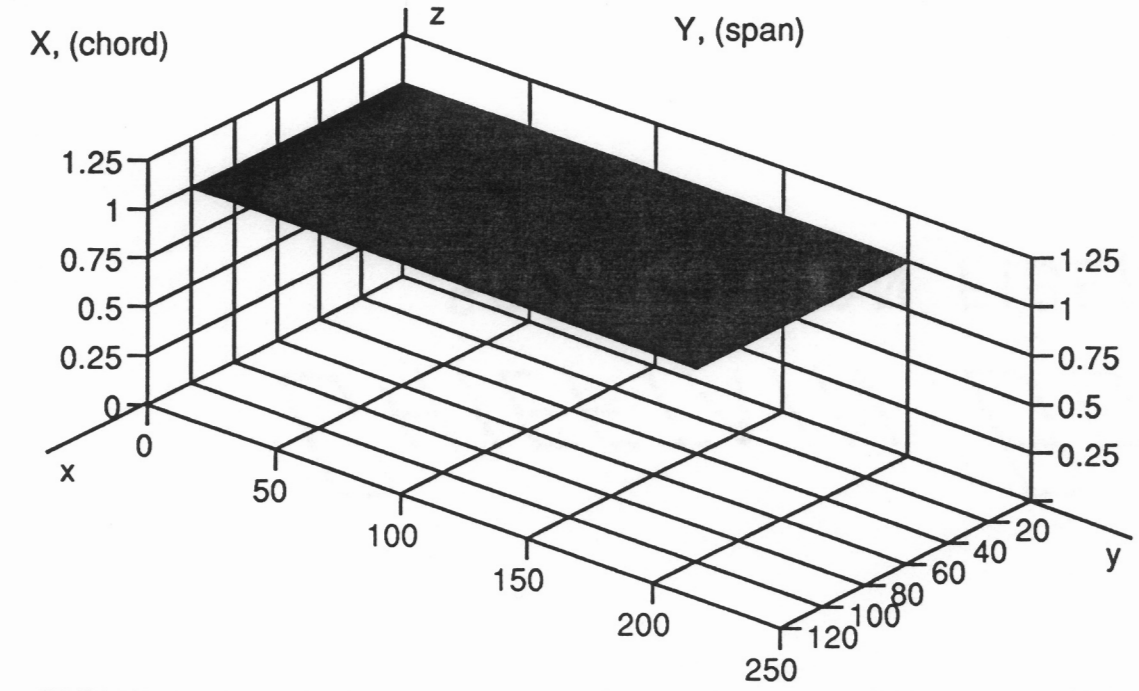

FIGURE 5.7 - First Mode, Rigid Body Plunge - Orthotropic Plate

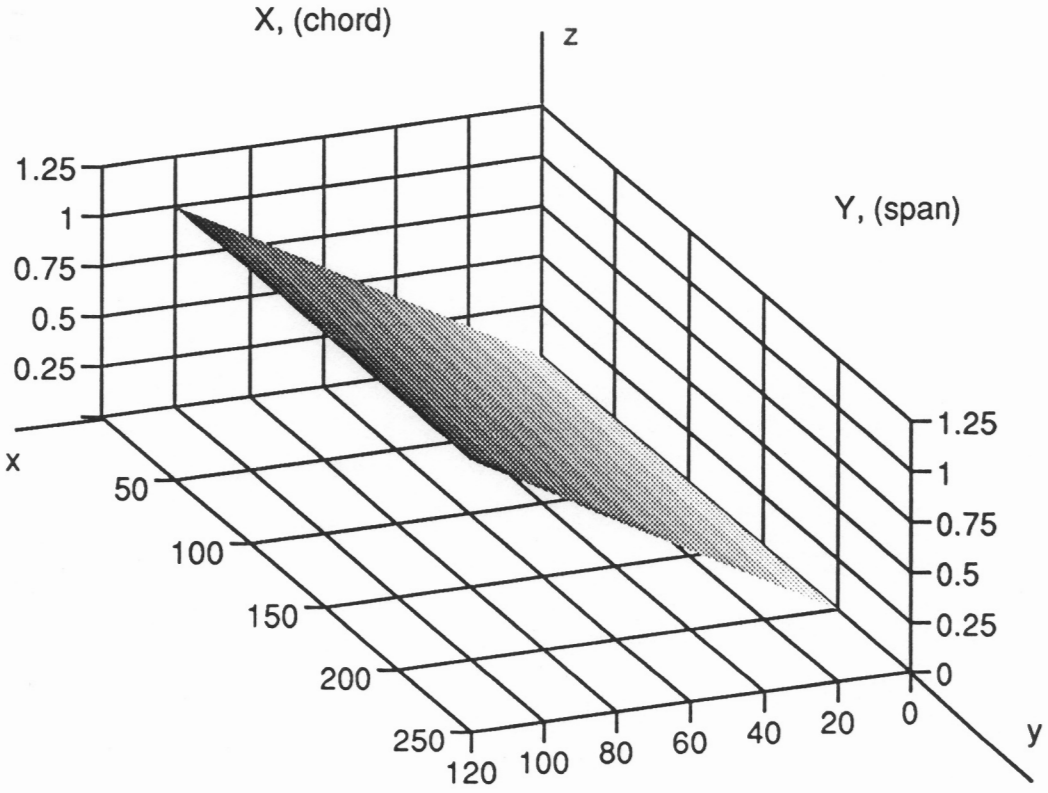

FIGURE 5.8 - Second Mode, Rigid Body Pitch- Orthotropic Plate

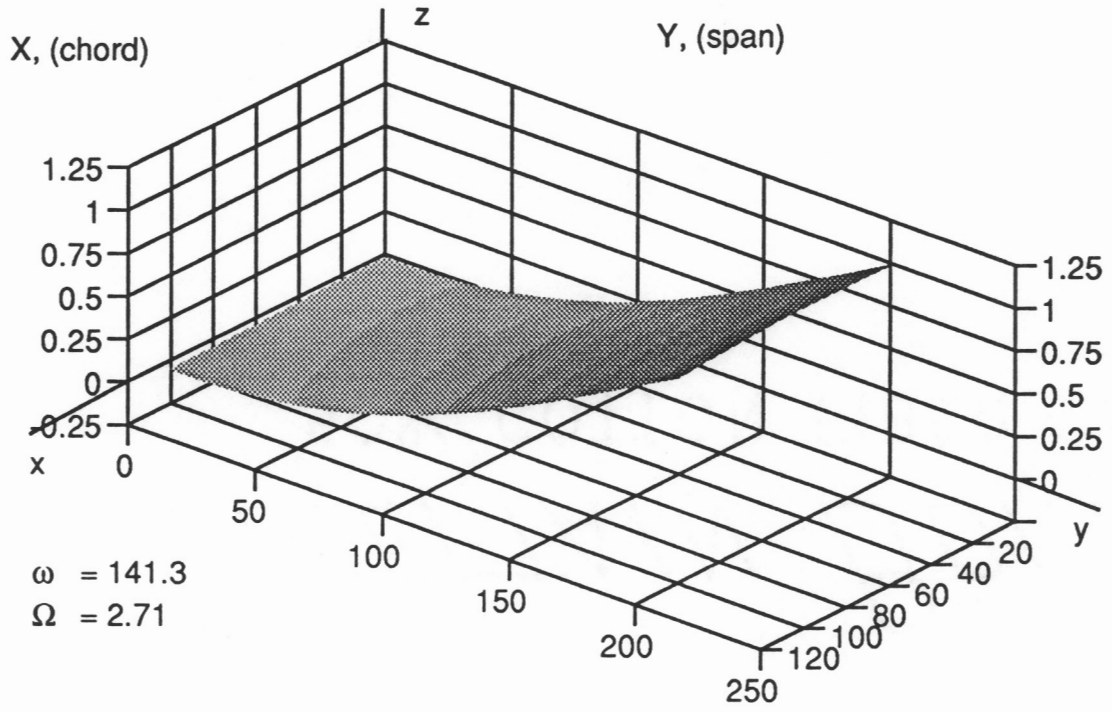

FIGURE 5.9 - Third Mode, 1st Bending - Orthotropic Plate

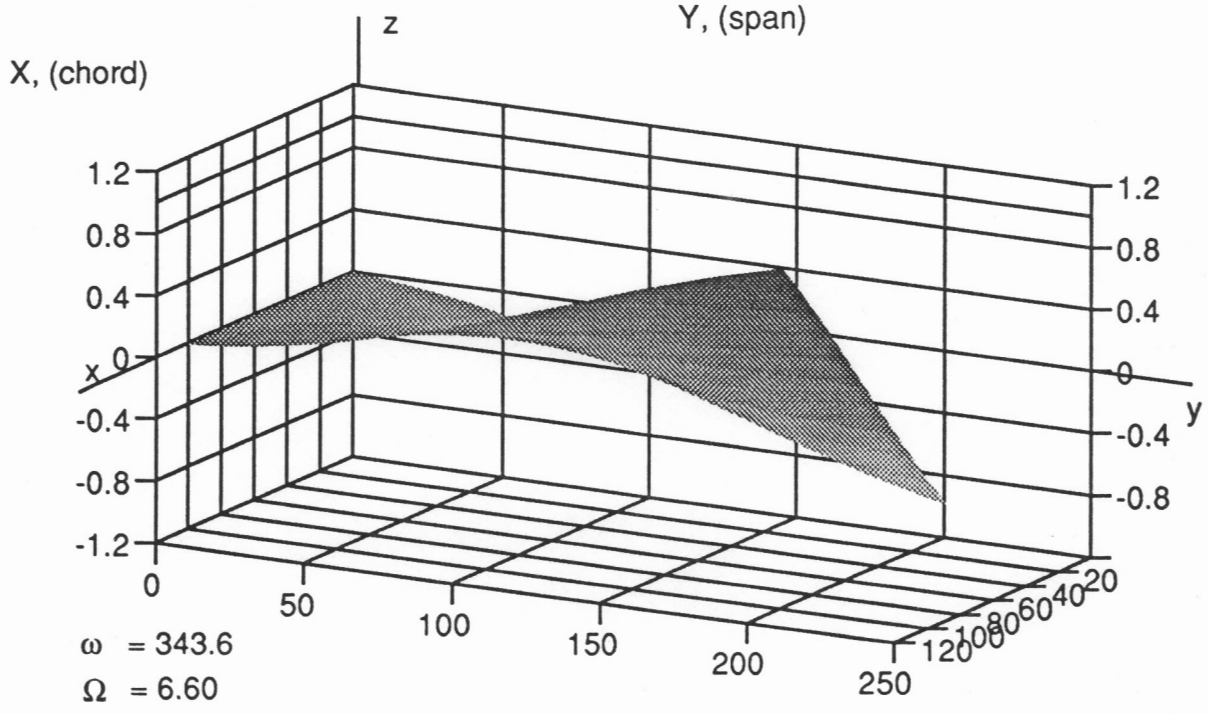

FIGURE 5.10 - Fourth Mode, 1st Torsion- Orthotropic Plate

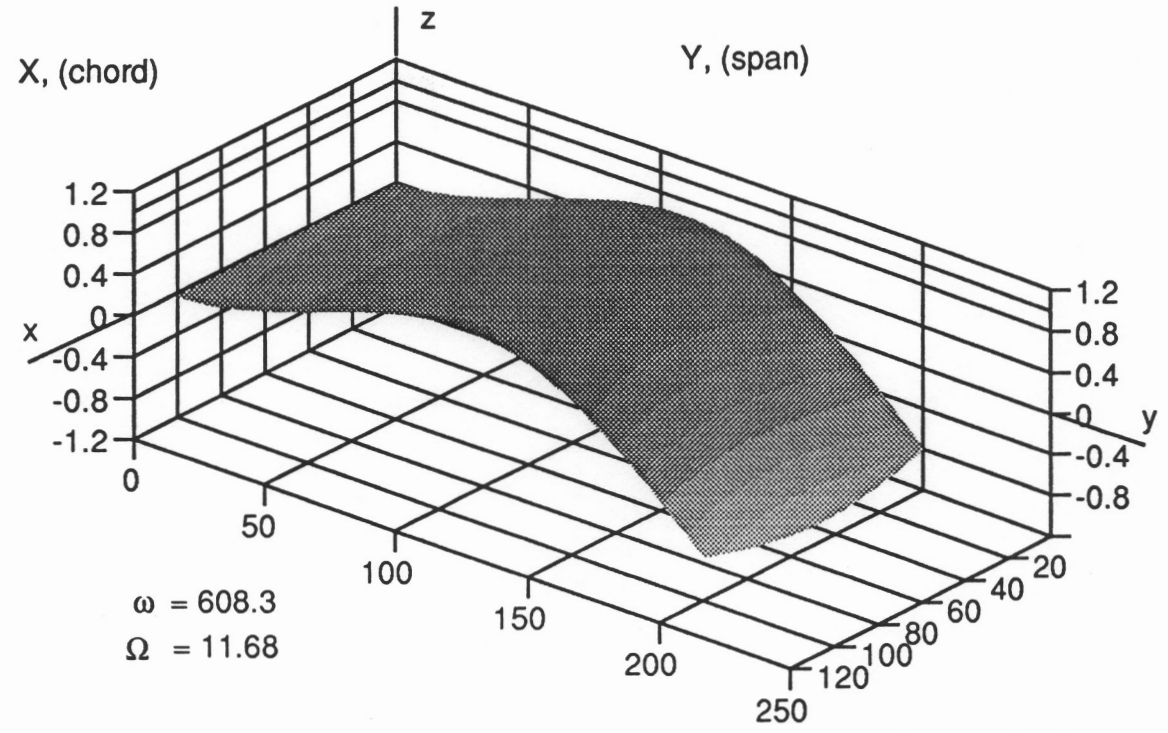

FIGURE 5.11 - Fifth Mode, 2nd Bending - Orthotropic Plate

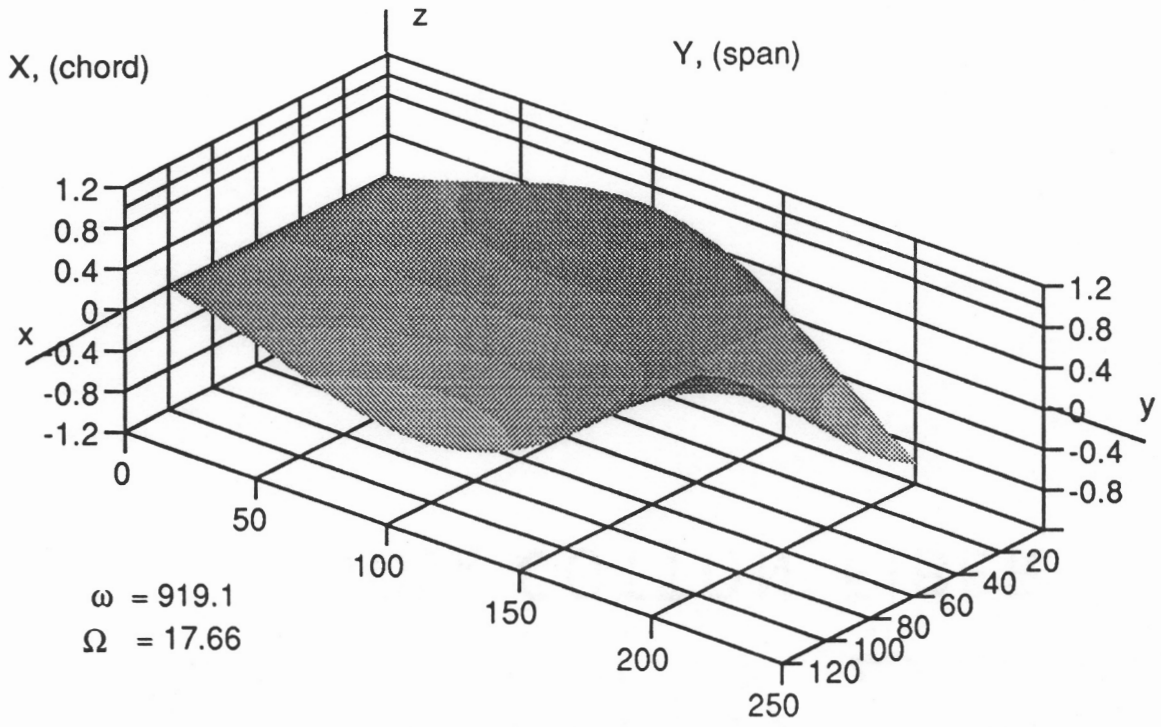

FIGURE 5.12 - Sixth Mode, 2nd Torsion - Orthotropic Plate

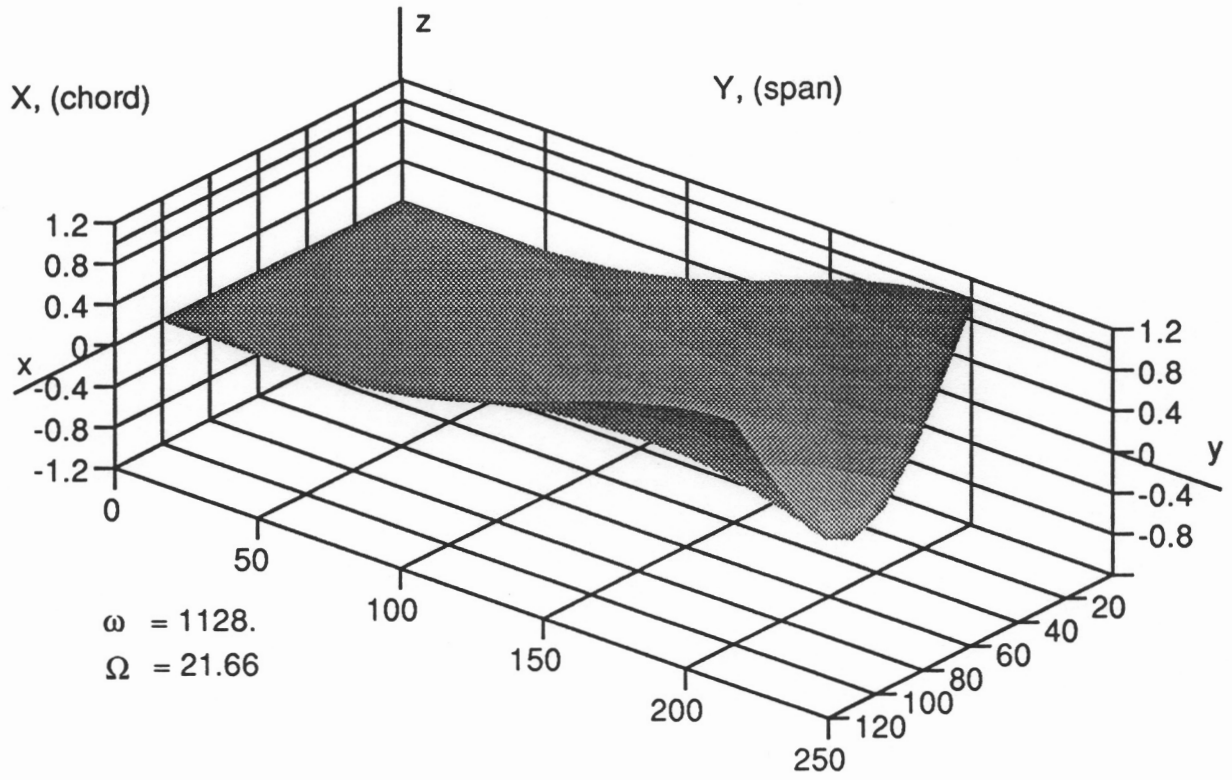

FIGURE 5.13- 7th Mode, 1st Chordwise Bending - Orthotropic Plate

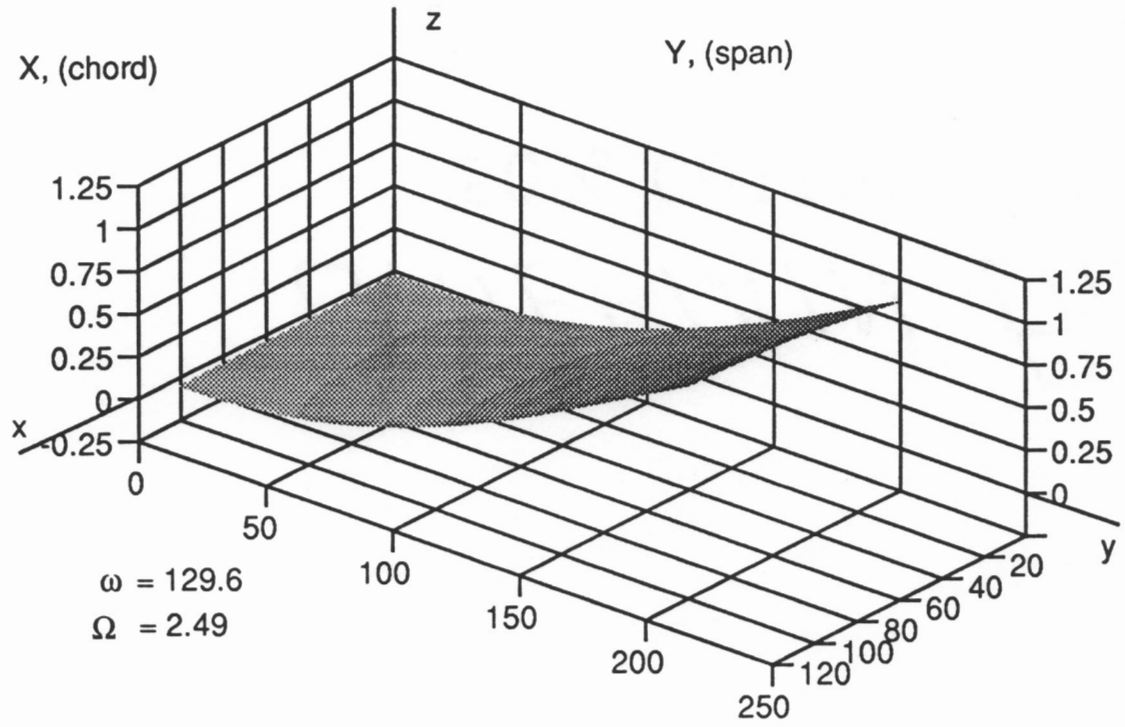

FIGURE 5.14 - Bending Mode, Tailoring Ply at -20 deg

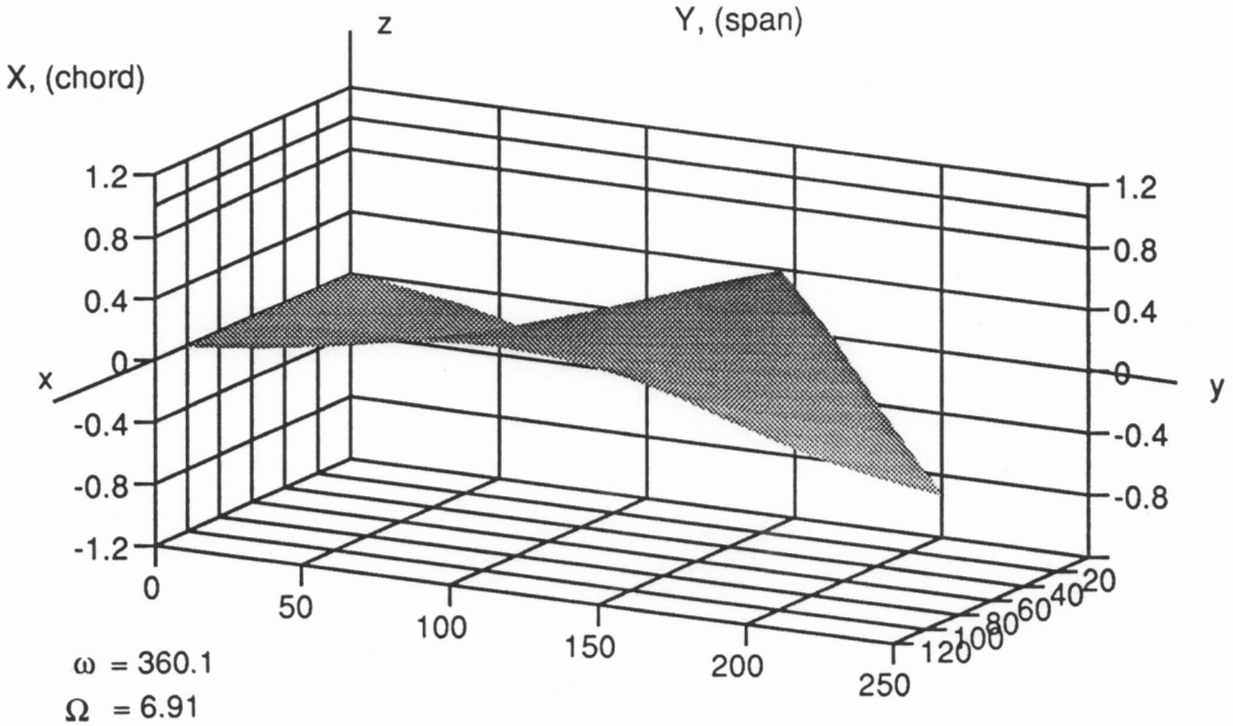

FIGURE 5.15 - Torsion Mode, Tailoring Ply at -20 deg

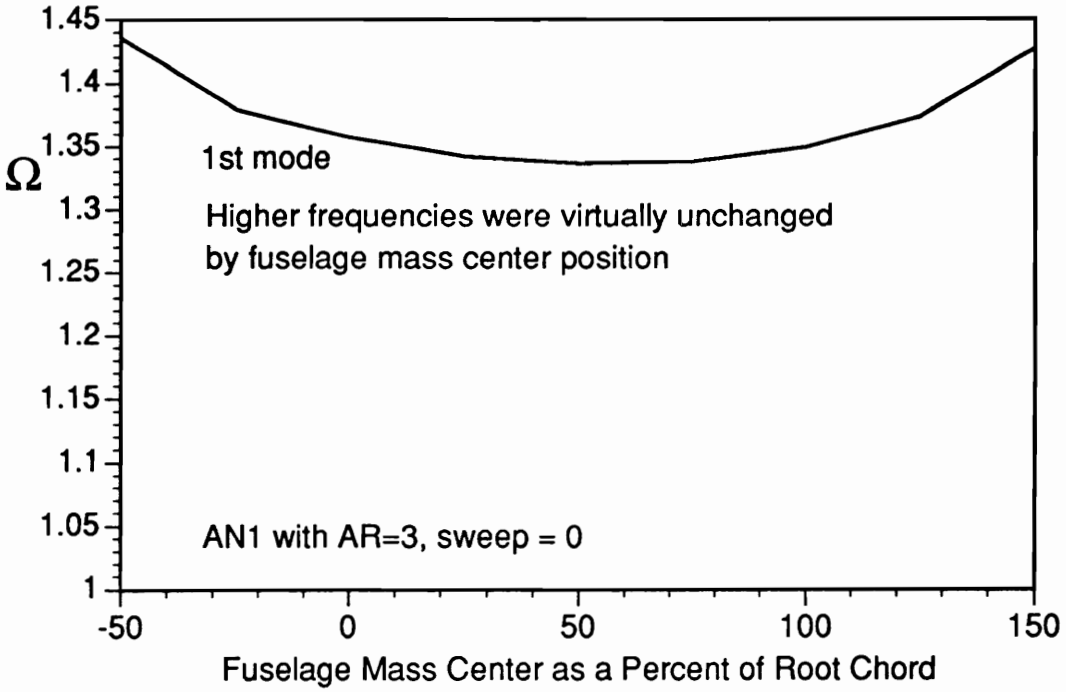

FIGURE 5.16 - Mass Center Position Effect on Frequency Results

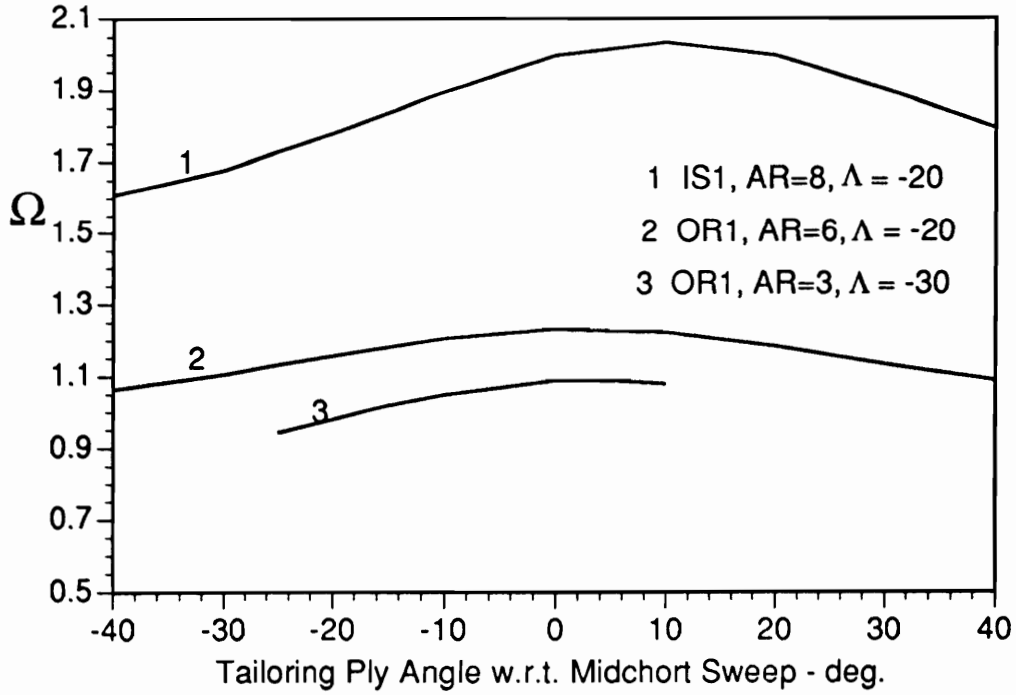

FIGURE 5.17 - Frequency Parameter vs Tailoring Ply Fiber Angle

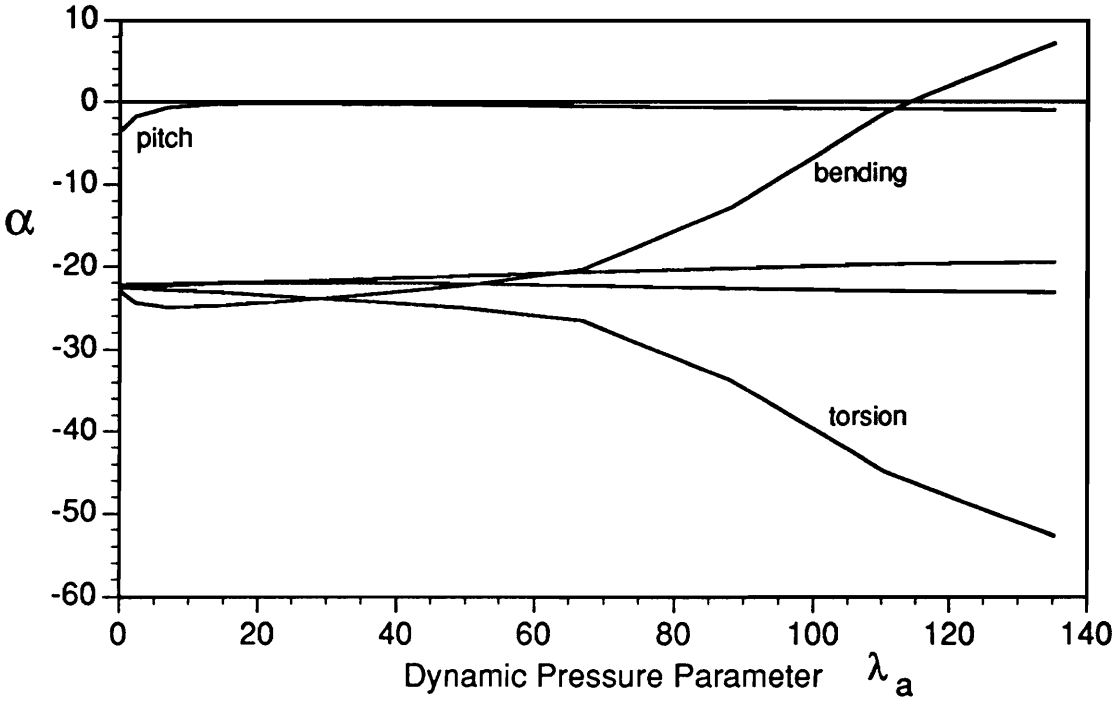

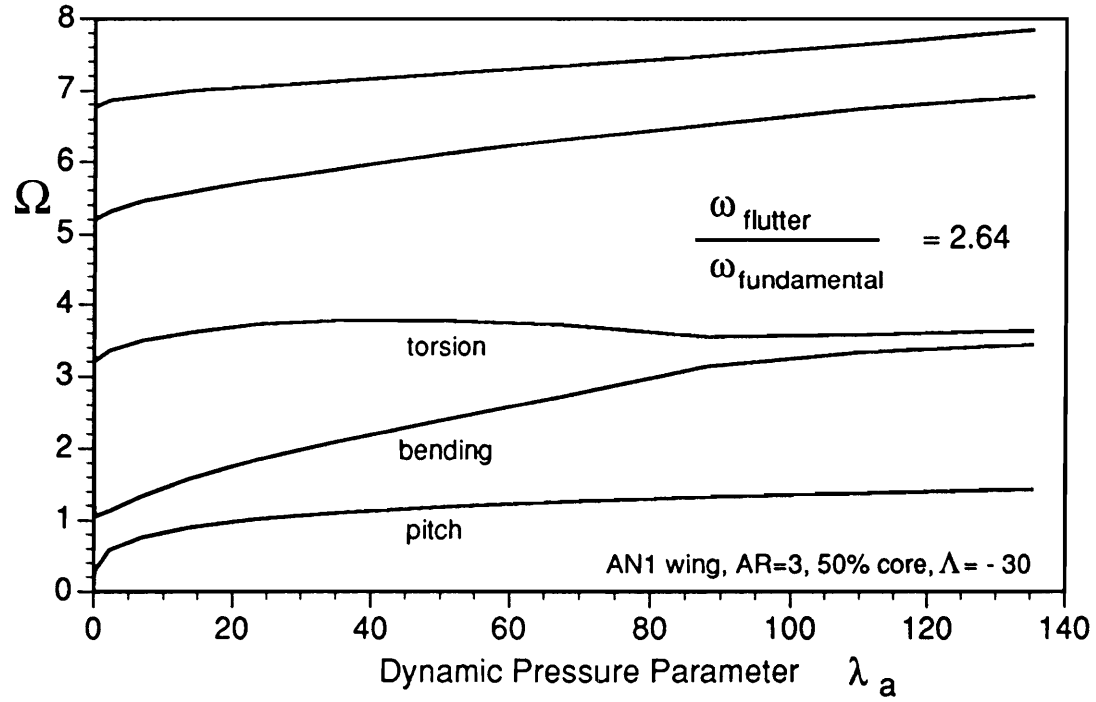

FIGURE 5.18 - A Bending-Torsion Flutter Case

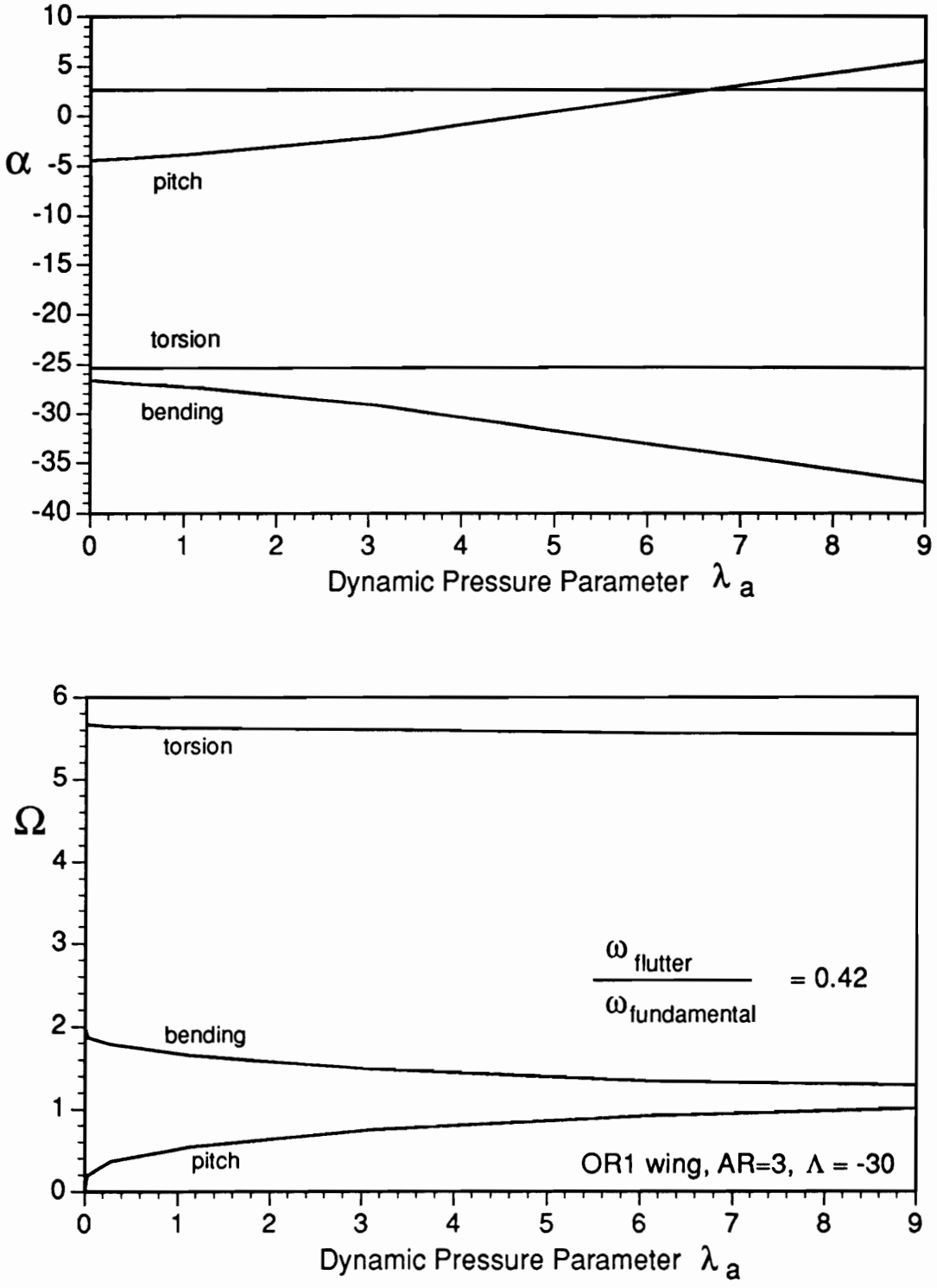

FIGURE 5.19 - A Body-Freedom Flutter Case

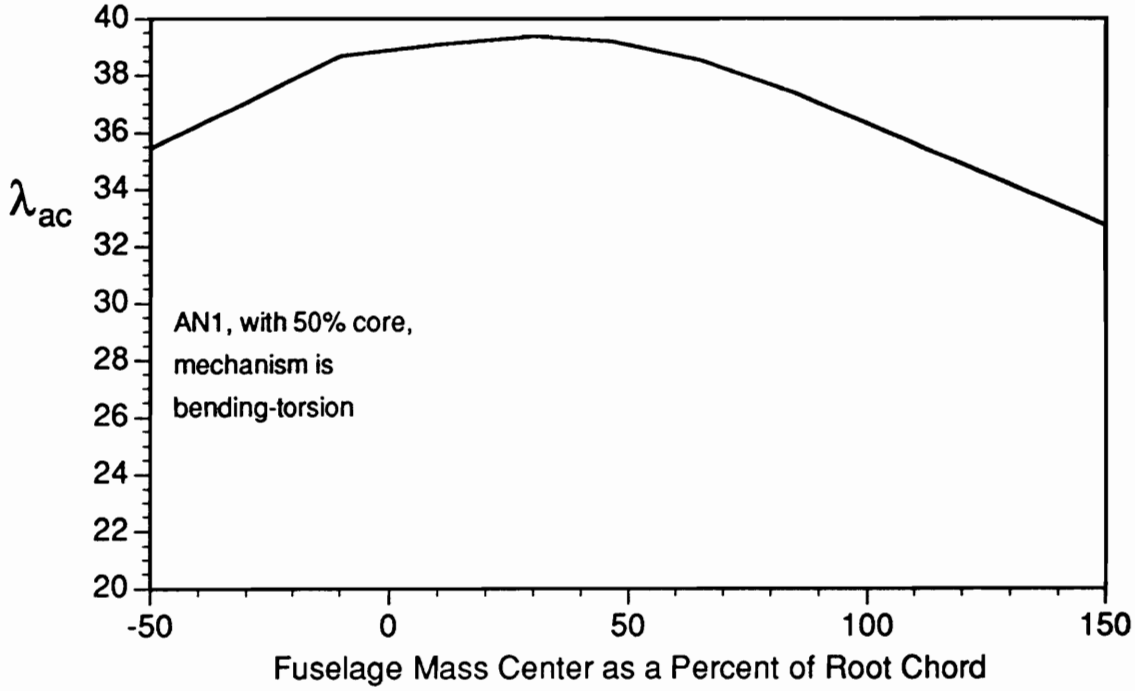

FIGURE 5.20 Mass Center Position Effect on Flutter Dynamic Pressure

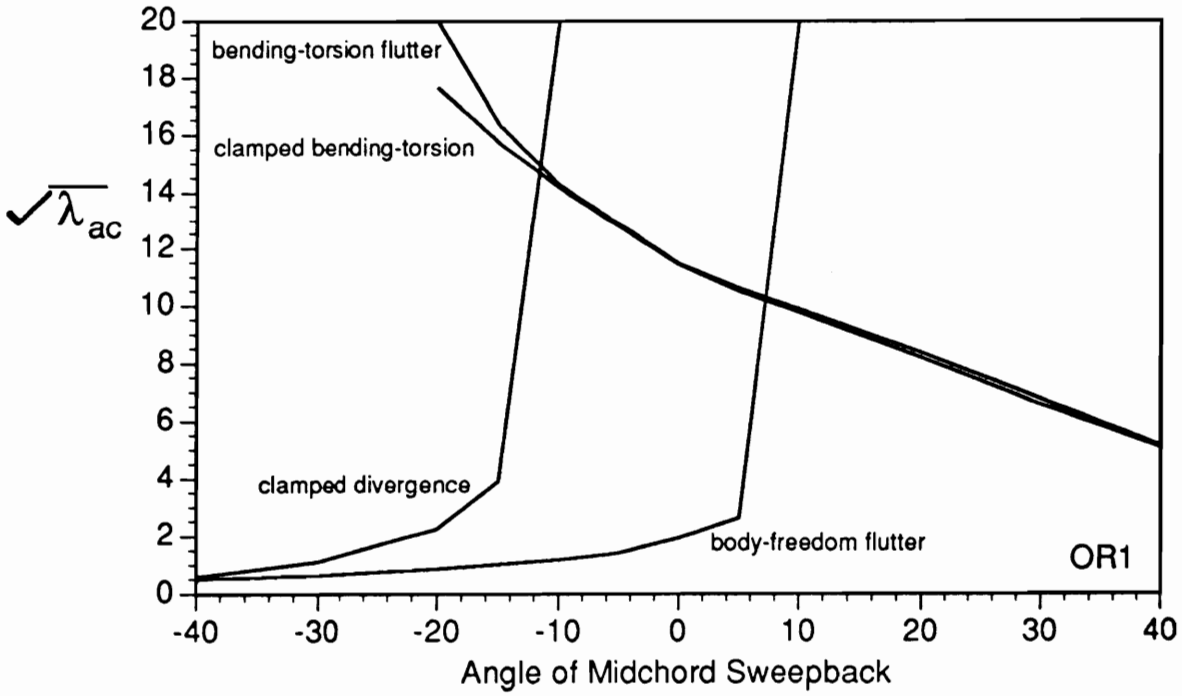

FIGURE 5.21 Wing Sweep Effect on Flutter Dynamic Pressure

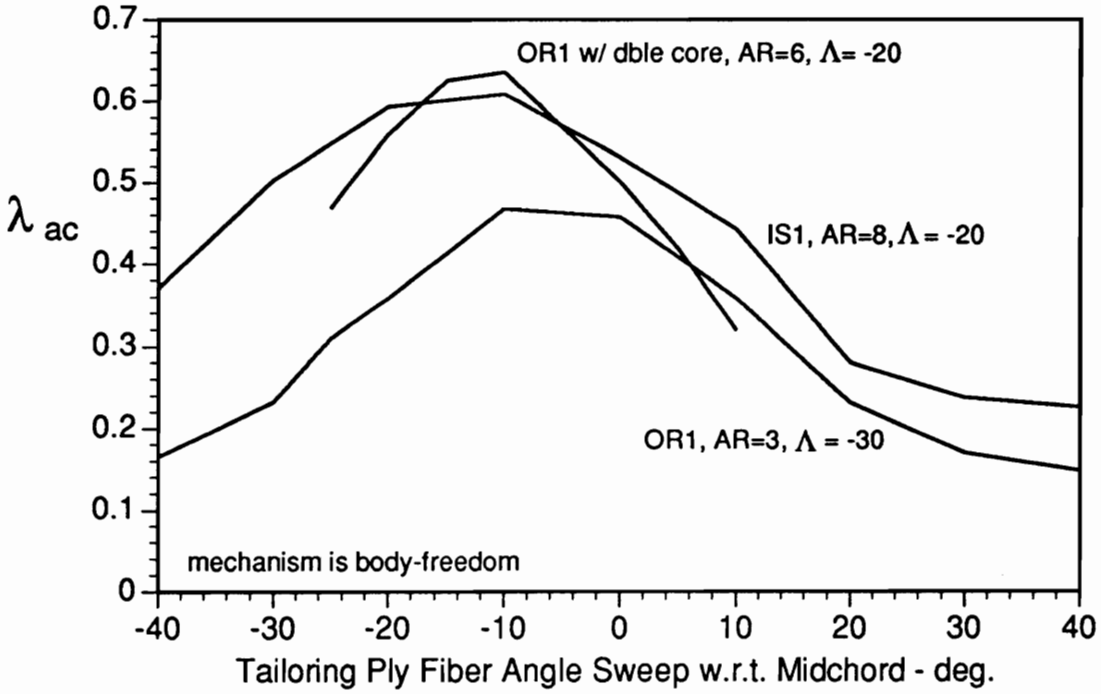

FIGURE 5.22 Tailoring Layer Angle Effect on Flutter Dynamic Pressure

CHAPTER VI

SUMMARY AND CONCLUSIONS

At the outset, the goal was to develop a structural model representing a modern aircraft wing sufficiently well that it could be used in a multidisciplinary optimization problem. Sharing equal weight with the requirement to be sufficiently sophisticated, is the requirement of a sufficiently simple model that an optimization routine in the loop is not precluded. This goal has been accomplished with the development of a plate model that accounts for shear deformation, variable layer thickness and orientation, fuselage degrees of freedom and chordwise flexibility. Consistent with conclusions reached by previous investigators, certain factors such as wing camber, unsymmetric ply stacking and rotatory inertia are sufficiently small for the problem at hand that they can be ignored.

The boundary value problem, consisting of the partial differential equations of motion and boundary conditions, was formulated by means of the extended Hamilton principle. The boundary value problem provides valuable insight into the requirements to be placed on the approximating functions. The algebraic eigenvalue problem was then formulated directly from the extended Hamilton principle. In solving the algebraic eigenvalue problem, the recently developed quasi-comparison functions were relied upon to guarantee rapid convergence.

The numerical results obtained by means of the current model confirmed various trends established by earlier investigators. The results demonstrate that there is a very wide array of inter-related parameters affecting the instability speed. The most clear outcome is a demonstration of the necessity of a formal optimization approach to bring consistency to the investigation of all the pertinent parameters.

The numerical results are limited to demonstration of the various features of the model and opening forays into regions of investigation previously closed to simpler models. Nevertheless, several previously unreported trends having significant bearing on the design of modern wings were revealed. These initial inquiries open the door to further research and refinement of the concept of composite tailoring. The results indicate that composite tailoring of forward swept wings may not be nearly as effective for modern low aspect ratio wings as for high aspect ratio wings. This is an important result which virtually mandates a structural model of at least the level of sophistication used here to accomplish optimal design of a low aspect ratio forward swept wing.

A second and also important new finding pertaining to two-dimensional models is the merit of tailoring ply distributions. Beyond finding the optimum angle of orientation of a tailoring ply, significant improvements in the flutter speed are left undiscovered if the distribution is not also subjected to scrutiny. The results presented here indicate that the tailoring plies are most effective when the distribution favors the leading edge and the wing root. This result is also unobtainable with more conventional models and points once again to the need of sufficient sophistication in modeling the pertinent physics. Optimization methods are dictated by the large number of interacting parameters, but such effort is wasted if the physical system is not modeled with sufficient accuracy.

REFERENCES

1. Grossman, B., Gurdal, Z., Struach, G. J., Eppard, W. M. and Haftka, R. T., "Integrated Aerodynamic / Structural Design of a Sailplane Wing," *Journal of Aircraft*, Vol. 25, No. 9, 1988, pp. 855-860.

2. Haftka, R. T., Grossman, B., Eppard, W. M. and Kao, P. J., "Efficient Optimization of Integrated Aerodynamic-Structural Design," *Proceedings of the International Conference on Inverse Design Concepts and Optimization in Engineering Sciences - II*, University Park, PA, Oct. 1987.

3. Haftka, R. T., Grossman, B., Kao, P. J., Polen, D.M. and Sobieszczanski-Sobieski, J., "Integrated Aerodynamic-Structural Design of a Forward-Swept Transport Wing," *Recent Advances in Multidisciplinary Analysis and Optimization*, NASA CP-3031, 1989, pp. 445-463.

4. Barthelemy, J. F. M. and Bergen, F. D., "Shape Sensitivity Analysis of Wing Static Aeroelastic Characteristics," *Journal of Aircraft*, Vol. 26, No. 8, 1989, pp. 712-717.

5. Kapania, R., Bergen, F. and Barthelemy, J., "Shape Sensitivity Analysis of Flutter Response of a Laminated Wing," *Proceedings of the 30th AIAA/ASME/ASCE/AHS/ASC Structures, Structural Dynamics and Materials Conference, Mobile, AL, AIAA Paper 89-1267*, April 1989.

6. Turner, M. J., "Optimization of Structures to Satisfy Flutter Requirements," *Proceedings of the AIAA Structural Dynamics and Aeroelasticity Specialists Conference*, New Orleans, LA, 1969, pp. 1-8.

7. Ashley, H., McIntosh, S. C. and Weatherill, W. H., "Optimization Under Aeroelastic Constraints," *Proceedings of the Symposium on Structural Optimization*, 1969, No. 36.

8. Krone, N. J., Jr., "Divergence Elimination with Advanced Composites," *The AIAA Aircraft Systems and Technology Meeting*, Los Angeles, CA, AIAA Paper 75-1009, Aug. 1975.

9. Weisshaar, T. A., "Divergence of Forward Swept Composite Wings," *Journal of Aircraft*, Vol. 17, 1980, pp. 442-448.

10. Weisshaar, T. A., "Aeroelastic Tailoring of Forward Swept Composite Wings," *Proceedings of the AIAA/ASME/ASCE/AHS 21st Structures, Structural Dynamics and Materials Conference*, Seattle, WA, May 1980, pp. 14-19.

11. Weisshaar, T. A. and Foist B. L., "Vibration Tailoring of Advanced Composite Lifting Surfaces," *Journal of Aircraft*, Vol. 22, No. 2, 1985, pp. 141-147.

12. Shirk, M. H., Hertz, T. J. and Weisshaar, T. A., "Aeroelastic Tailoring - Theory, Practice, and Promise," *Journal of Aircraft*, Vol. 23, No. 1, 1986, pp. 6-18.

13. Lynch, R. W. and Rogers, Q.A., "Aeroelastic Tailoring of Composite Materials to Improve Performance," *Proceedings of the 16th AIAA Structures, Structural Dynamics and Materials Conference*, Denver, Colorado, 1975, pp. 61-68.

14. Roger, K. E., Hodges, G. E. and Felt, L., "Active Flutter Suppression - A Flight Test Demonstration," *Journal of Aircraft*, Vol. 12, No. 6, 1975, pp. 551-556.

15. Horikawa, H. and Dowell, E. H., "An Elementary Explanation of the Flutter Mechanism with Active Feedback Controls," *Journal of Aircraft*, Vol. 16, No. 4, 1979, pp. 225-232.

16. Thompson, G. O. and Kass, G. J., "Active Flutter Suppression - An Emerging Technology," *Journal of Aircraft*, Vol. 9, No. 3, 1972, pp. 230-235.

17. Abel I., Perry, B. and Murrow, H. H., "Two Synthesis Techniques Applied to Flutter Suppression on a Flight Research Wing," *Journal of Guidance and Control*, Vol. 1, No. 5, 1978, pp. 340-346.

18. Newsom, J. R., "Control Law Synthesis for Active Flutter Suppression Using Optimal Control Theory," *Journal of Guidance and Control*, Vol. 2, No. 5, 1979, pp. 388-394.

19. Mahesh, J. K., Stone, C. R., Garrard, W. L. and Dunn, H. J., "Control Law Synthesis for Flutter Suppression Using Linear Quadratic Gaussian Theory," *Journal of Guidance and Control*, Vol. 4, No. 4, 1981, pp. 415-422.

20. Mukhopadhyay, V., Newsom, J. R. and Abel, I., "Reduced-Order Optimal Feedback Control Law Synthesis for Flutter Suppression," *Journal of Guidance, Control, and Dynamics*, Vol. 5, No. 4, 1982, pp. 389-395.

21. Newsom, J. R., Pototzky, A. S. and Abel, I., "Design of a Flutter Suppression System for an Experimental Drone Aircraft," *Journal of Aircraft*, Vol. 22, No. 5, 1985, pp. 380-386.

22. Meirovitch, L. and Silverberg, L. M., "Active Vibration Control of a Cantilever Wing," *Journal of Sound and Vibration*, Vol. 97, No. 3, 1984, pp. 489-498.

23. Nissim, E., "Flutter Suppression Using Active Controls Based on the Concept of Aerodynamic Energy," NASA TN D-6199, March 1971.

24. Chipman, R. R., Zislin, A. M. and Waters, C., "Control of Aeroelastic Divergence," *Journal of Aircraft*, Vol. 20, No. 12, 1983, pp. 1007-1013.

25. Noll, T. E., Eastep, F. E. and Calico, R. A., "Active Suppression of Aeroelastic

Instabilities on a Forward-Swept Wing," *Journal of Aircraft*, Vol. 21, No. 3, 1984, pp. 202-208.

26. Ghiringhelli, G. L., Lanz, M. and Mantegazza, P., "Active Flutter Suppression for a Wing Model," *Journal of Aircraft*, Vol. 27, No. 4, 1990, pp. 334-341.

27. Blair, M. and Weisshaar, T. A., "Swept Composite Wing Aeroelastic Divergence Experiments," *Journal of Aircraft*, Vol. 19, No. 11, 1982, pp. 1019-1024.

28. Sherrer, V. C., Hertz, T. J. and Shirk, M. H., "Wind Tunnel Demonstration of the Principle of Aeroelastic Tailoring Applied to Forward Swept Wings," *AIAA/ASME/ASCE/AHS 21st Structures, Structural Dynamics and Materials Conference*, AIAA Paper 80-0796, Seattle, WA, May 1980.

29. Wilkinson, K. and Rauch, F., "Predicted and Measured Divergence Speeds of an Advanced Composite Forward Swept Wing Model," AFWAL-TR-80-3059, July 1980.

30. Ellis, J. W. Dobbs, S. K. and Miller, G. D., "Structural Design and Wind Tunnel Testing of a Forward Swept Fighter Wing," AFWAL-TR-80-3073, July 1980.

31. Zeiler, T. A. and Weisshaar, T. A., "Integrated Aeroservoelastic Tailoring of Lifting Surfaces," *Journal of Aircraft*, Vol. 25, No. 1, 1988, pp. 76-83.

32. Isogai, K., "Direct Search Method to Aeroelastic Tailoring of a Composite Wing under Multiple Constraints," *Journal of Aircraft*, Vol. 26, No. 12, 1989, pp. 1076-1080.

33. Gupta, K. K., Brenner, M. J. and Voelker, L. S., "Integrated Aeroservoelastic Analysis Capability with X-29A Comparisons," *Journal of Aircraft*, Vol. 26, No. 1, 1989, pp. 84-90.

34. Livne, E., Schmit, L. A. and Friedmann, P.P., "Towards Integrated Multidisciplinary Synthesis of Actively Controlled Fiber Composite Wings," *Journal of Aircraft*, Vol. 27, No. 12, 1990, pp. 979-992.

35. Karpel, M., "Sensitivity Derivatives of Flutter Characteristics and Stability Margins for Aeroservoelastic Design," *Journal of Aircraft*, Vol. 27, No. 4, 1990, pp. 368-375.

36. Weisshaar, T. A., "The Influence of Aeroelasticity on Swept Composite Wings," AFFDL-TR-80-3137, Vol I, Nov., 1980.

37. Weisshaar, T. A. and Zeiler, T. A., "Dynamic Stability of Flexible Forward Swept Wing Aircraft," *Journal of Aircraft*, Vol. 20, No. 12, 1983, pp. 1014-1020.

38. Frazer, R. A. and Duncan, W. J., "Wing Flutter as Influenced by the Mobility of

the Fuselage," *British Aero. Research Council, R. & M. 1207*, 1929.

39. Broadbent, E. G., "Some Considerations of the Flutter Problems of High Speed Aircraft," *Proceedings of the Second International Aircraft Conference*, NY, 1949, pp. 556-581.

40. Gaukroger, D. R., "Wing Flutter" *AGARD Manual on Aeroelasticity*, 1960, Part V, Chapter 2.

41. Cunningham, H. J. and Lundstrom, R. R., "Description and Analysis of a Rocket-Vehicle Experiment on Flutter Involving Wing Deformation and Body Motions," NACA TN 311, Jan. 1955.

42. Weisshaar, T. A., Zeiler, T. A., Hertz, T. J. and Shirk, M. H., "Flutter of Forward Swept Wings, Analysis and Tests," *Proceedings of the AIAA/ASME/ASCE/AHS 23rd Structures, Structural Dynamics and Materials Conference*, New Orleans, LA, 1982, pp. 111-121.

43. Hertz, T. J., Shirk, M. H., Ricketts, R. H. and Weisshaar, T. A., "On the Track of Practical Forward-Swept Wings," *Astronautics and Aeronautics.*, Vol. 20, No. 1, 1982, pp. 40-52.

44. Lottati, L., "Flutter and Divergence Aeroelastic Characteristics for Composite Forward Swept Cantilevered Wings," *Journal of Aircraft*, Vol. 22, No. 11, 1985, pp. 1001-1007.

45. Livne, E., Schmidt, L. A. and Friedmann, P., "Design Oriented Structural Analysis for Fiber Composite Wings," *UCLA Report* UCLA-ENG-88-36, Nov. 1988.

46. Giles, G. L., "Equivalent Plate Analysis of Aircraft Wing Box Structures with General Planform Geometry," *Journal of Aircraft*, Vol. 23, No. 11, 1986, pp. 859-864.

47. Giles, G. L., "Further Generalization of an Equivalent Plate Representation for Aircraft Structural Analysis," *Journal of Aircraft*, Vol. 26, No. 1, 1989, pp. 67-74.

48. Jensen, D. W. and Crawley, E. F., "Frequency Determination Techniques for Cantilevered Plates with Bending-Torsion Coupling," *AIAA Journal*, Vol. 22, No. 3, 1984, pp. 415-420.

49. Bowlus, J. A., Palazotto, A. N. and Whitney, J. M., "Vibration of Symmetrically Laminated Rectangular Plates Considering Shear Deformation and Rotatory Inertia," *AIAA Journal*, Vol. 25, No. 11, 1987, pp. 1500-1511.

50. Reissner, E., "The Effect of Transverse Shear Deformation on the Bending of

Elastic Plates," *Journal of Applied Mechanics*, June, 1945, pp. A-69 - A-77.

51. Mindlin, R. D., "Influence of Rotatory Inertia and Shear on Flexural Motions of Isotropic, Elastic Plates," *Journal of Applied Mechanics*, March 1951, pp. 31-38.

52. Meirovitch, L. and Kwak, M. K., "Convergence of the Classical Rayleigh-Ritz Method and the Finite Element Method," *AIAA Journal*, Vol. 28, No. 8, 1990, pp. 1509-1516.

53. Bert, C. W., "Research on Dynamic Behavior of Composite and Sandwich Plates - IV," *The Shock and Vibration Digest*, Vol. 17, No. 11, 1985, pp. 3-15.

54. Leissa, A. W., *Vibration of Plates*, Scientific and Technical Information Division, Office of Technology Utilization, NASA, Washington, D.C.

55. Bisplinghoff, R. L. and Ashley, H., *Principles of Aeroelasticity*, Dover Publications, Inc., New York.

56. Jones, R. M., *Mechanics of Composite Materials*, Hemisphere Publishing Corporation, New York, 1975.

57. Ashton, J. E. and Whitney, J. M., *Theory of Laminated Plates*, Technomic Publishing Co., Inc., Stamford, Conn., 1970.

58. Averill, R. C., On the Behavior of Shear Deformable Plate Elements, Master Thesis, Engineering Mechanics, Virginia Polytechnic Institute and State University, July, 1989.

59. Frederick, D. and Chang, T. S., *Continuum Mechanics*, Scientific Publishers, Cambridge, MA, 1965.

60. Meirovitch, L., *Methods of Analytical Dynamics*, McGraw-Hill Book Co., New York, 1970.

61. Meirovitch, L. and Kwak, M. K., "Rayleigh-Ritz Based Substructure Synthesis for Flexible Multibody Systems," *AIAA Journal*, Vol. 29, No. 10, 1991, pp. 1709-1719.

62. Dowell, E. H., *A Modern Course in Aeroelasticity*, Kluwer Academic Publishers, The Netherlands, 1989.

63. Landahl, M. T., "Unsteady Flow Around Thin Wings at High Mach Numbers," *Journal of the Aeronautical Sciences*, Vol. 24, No. 1, 1957, pp. 33-38.

64. Ashley, H. and Zartarian, G., "Piston Theory - A New Aerodynamic Tool for the Aeroelastician," *Journal of the Aeronautical Sciences*, Vol. 23, No. 12, 1956, pp. 1109-1118.

65. Lighthill, M.J., "Oscillating Airfoils at High Mach Number," *Journal of the Aeronautical Sciences*, Vol. 20, No. 6, 1953, pp. 402-406.

66. Blevins, R.D., *Formulas for Natural Frequency and Modeshape*, Van Nostrand Reinhold, New York, 1979.

67. Rossettos, J.N. and Tong, P., "Finite-Element Analysis of Vibration and Flutter of Cantilever Anisotropic Plates,", *Journal of Applied Mechanics*, Vol. 41, No. 4, 1974, pp. 1075-1080.

68. McCullers, L.A., Naberhaus, J.A. and Bensinger, C.T., "Dynamic Characteristics of Advanced Filamentary Composite Structures, Vols. I and II," Air Force Flight Dynamics Laboratory, AFFDL-TR-73-111, Sept. 1975.

69. Lynch, R.W., Rogers, W.A. and Braymen, W.W., "Aeroelastic Tailoring of Advanced Composite Structures for Military Aircraft, Vols. I and II," Air Force Flight Dynamics Laboratory, AFFDL-TR-76-100, April 1977.

70. Miller, G. D., Wykes, J. H. and Brosnan, M. J., "Rigid-Body Structural Mode Coupling on a Forward Swept Wing Aircraft," *Journal of Aircraft*, Vol. 20, No. 8, 1983, pp. 696-702.

71. Meirovitch, L., *Computational Methods in Structural Dynamics*, Sijthoff & Noordhoff, The Netherlands, 1980.

72. Librescu, L., *Elastostatics and Kinetics of Anisotropic and Heterogeneous Shell-Type Structures*, Noordhoff International Publishing, The Netherlands, 1977.

73 Hayes, W. O., "Hypersonic Similitude", *Quart. Appl. Math.*, Vol. 5, p. 105, 1947.

VITA

The author was born to Marvin R. and Mildred C. Seitz on November 20, 1955 in Topeka, Kansas. He received the degree of Bachelor of Science in Mechanical Engineering from Wichita State University of Wichita, Kansas in December 1977. The author was married to Mary Angelee Smith in May of 1978. The first six years of his professional experience were with various engineering consulting companies engaged in seismic analysis of nuclear power plant systems. He became a registered professional engineer in the state of North Carolina in 1982. He became engaged as a structural dynamics engineer at Beech Aircraft Corporation in 1983, where he was engaged in testing and analysis of aircraft for the following six years. During this tenure he was admitted to the graduate school at Wichita State University from which he received the degree of Master of Science in Aeronautical Engineering in May 1987. In August 1989 he entered Virginia Polytechnic Institute and State University and has been working towards the degree of Doctor of Philosophy in Engineering Mechanics.